

PURDUE UNIVERSITY
GRADUATE SCHOOL
Thesis/Dissertation Acceptance

This is to certify that the thesis/dissertation prepared

By David Farrel Mase

Entitled

A Coupled Modeling and Observational Approach to Understanding Oxygen-18 in Atmospheric Nitrate

For the degree of Master of Science

Is approved by the final examining committee:

Gabe Bowen

Chair

Greg Michalski

Chad T. Jafvert

To the best of my knowledge and as understood by the student in the *Research Integrity and Copyright Disclaimer (Graduate School Form 20)*, this thesis/dissertation adheres to the provisions of Purdue University's "Policy on Integrity in Research" and the use of copyrighted material.

Approved by Major Professor(s): Greg Michalski

Approved by: Jon M. Harbor

Head of the Graduate Program

12/01/2010

Date

**PURDUE UNIVERSITY
GRADUATE SCHOOL**

Research Integrity and Copyright Disclaimer

Title of Thesis/Dissertation:

A Coupled Modeling and Observational Approach to Understanding Oxygen-18 in Atmospheric Nitrate

For the degree of Master of Science

I certify that in the preparation of this thesis, I have observed the provisions of *Purdue University Executive Memorandum No. C-22*, September 6, 1991, *Policy on Integrity in Research*.*

Further, I certify that this work is free of plagiarism and all materials appearing in this thesis/dissertation have been properly quoted and attributed.

I certify that all copyrighted material incorporated into this thesis/dissertation is in compliance with the United States' copyright law and that I have received written permission from the copyright owners for my use of their work, which is beyond the scope of the law. I agree to indemnify and save harmless Purdue University from any and all claims that may be asserted or that may arise from any copyright violation.

David Farrel Mase

Printed Name and Signature of Candidate

12/01/2010

Date (month/day/year)

*Located at http://www.purdue.edu/policies/pages/teach_res_outreach/c_22.html

A COUPLED MODELING AND OBSERVATIONAL APPROACH TO
UNDERSTANDING OXYGEN-18 IN ATMOSPHERIC NITRATE

A Thesis

Submitted to the Faculty

of

Purdue University

by

David F. Mase

In Partial Fulfillment of the
Requirements for the Degree

of

Master of Science

December 2010

Purdue University

West Lafayette, Indiana

UMI Number: 1490679

All rights reserved

INFORMATION TO ALL USERS

The quality of this reproduction is dependent upon the quality of the copy submitted.

In the unlikely event that the author did not send a complete manuscript and there are missing pages, these will be noted. Also, if material had to be removed, a note will indicate the deletion.



UMI 1490679

Copyright 2011 by ProQuest LLC.

All rights reserved. This edition of the work is protected against unauthorized copying under Title 17, United States Code.



ProQuest LLC
789 East Eisenhower Parkway
P.O. Box 1346
Ann Arbor, MI 48106-1346

To my friends and family:
Thank you for the support.

ACKNOWLEDGMENTS

I would like to thank the following people and organizations who helped with the outcome of the work presented here (in no particular order): Dr. Greg Michalski, my supervisor, provided the tools (both literal and intellectual) needed to complete the work presented within this thesis. Without his guidance (and occasional motivational nudge), there's a chance I would still be struggling to understand stable isotopes as I was when I first arrived at Purdue. My committee members, Drs. Gabe Bowen and Chad Jafvert, for thoughtful discussion and questions which helped to shape this work. Lindsey Crawley, for her help with the operation of the denitrifier method discussed in Chapter 4. Vicky Sehrawat for his effort and aid with the setup and operation of the model discussed in Chapter 3. Lisa Wagner of the Indiana Department of Environmental Management for the archived air quality data from the Gary, Indiana site. The National Atmospheric Deposition Program for supplying the precipitation samples and associated data used in this study. Dr. Mike Baldwin for his help with extracting North American Regional Reanalysis data useful for this study. I would also like to thank the organizations that helped to fund the work presented in this thesis: The Purdue Research Foundation and the National Science Foundation.

PREFACE

The work presented here is the result of approximately two years of data collection and analysis. Before this work was completed, the body of information on the topic of stable isotopes of oxygen from nitrate was steadily growing, but not without occasionally cloudy interpretations as to what the meaning of specific isotope values. That is the primary motivation behind the work presented here. We want to provide a means for a researcher to make better interpretations of their oxygen isotope values from atmospheric nitrate based on a straightforward modeling technique which takes into account air quality, spatial location, and time of the year. Based on these parameters, photolysis constants are calculated, as are mole fractions for specific HNO₃-producing pathways in the atmosphere, and this data is combined to output a $\delta^{18}\text{O}$ value for atmospheric nitrate.

While this model is not perfect, it can help with interpretations of $\delta^{18}\text{O}$ values from atmospheric nitrate by examining the chemistry behind the model calculations. If a measured $\delta^{18}\text{O}$ value of atmospheric nitrate is lower on one day compared to the next, the model can be used to help determine why. Each pathway of HNO₃ formation in the atmosphere and its output can be examined, in addition to the mole fractions calculated by the RACM (Stockwell et al., 1997) model. The coupling of these tools, and being able to see how they work, will help a researcher see (at least in an idealized mathematical sense) what the dominant HNO₃-producing pathway is for that specific day. Perhaps the dominant pathway is different for the following day. That is one possible explanation for why values between the two days are different, and it helps to guide interpretations of these values so that we are trying to understand why the pathway dominant pathway changed. Was it because the air quality for that day was different? Perhaps solar radiation

was high so photolysis was more greatly affecting results. With access to the model parameters this model becomes a powerful tool for better understanding $\delta^{18}\text{O}$ values from atmospheric nitrate.

Further, the model presented in this thesis will help researchers understand the effect of atmospheric liquid H_2O on $\delta^{18}\text{O}$ values of atmospheric nitrate, and to see how that effect compares with the effect of atmospheric chemistry. Further, the coupling of the RACM model with this mass balance approach allows researchers to thoroughly understand where $\delta^{18}\text{O}$ contributions to overall HNO_3 are occurring and where they are not. Better interpretations of $\delta^{18}\text{O}$ values from atmospheric nitrate lead to a better understanding of atmospheric dynamics and how isotopes can help with the scientific community's understanding of atmospheric chemistry.

TABLE OF CONTENTS

	Page
LIST OF TABLES	ix
LIST OF FIGURES	x
ABSTRACT	xiii
CHAPTER 1. INTRODUCTION	1
1.1. Introduction	1
1.2. Stable Isotope Theory	5
1.3. $\delta^{15}\text{N}$ in Atmospheric Nitrate	6
1.4. Stable Isotopes of Oxygen	8
1.5. Understanding the Atmospheric NO_3^- budget	9
CHAPTER 2. ION CHROMATOGRAPHY INSTRUMENTATION FOR NITRATE SEPARATION	11
2.1. Technical Note	11
2.2. Introduction	11
2.3. Ion Chromatography	13
2.3.1. Ion Chromatography Instrument	13
2.3.2. Analytical Mode	15
2.3.3. Preparative Mode	15
2.3.4. Fraction Collection	16
2.4. Results and Discussion	17
2.4.1. Anion Concentration Analysis	17
2.4.2. Collection Efficiency	18

	Page
2.4.3. Isotopic Viability.....	20
2.5. Conclusion.....	21
CHAPTER 3. MODELING $\delta^{18}\text{O}$ IN ATMOSPHERIC NITRATE.....	22
3.1. Technical Note.....	22
3.2. Introduction	22
3.3. Methods	26
3.3.1. Fitting the model to atmospheric HNO_3 production pathways	28
3.3.2. $\delta^{18}\text{O}$ of atmospheric NO_x	28
3.3.3. $\delta^{18}\text{O}$ of Liquid Water	30
3.3.4. Atmospheric O_2	31
3.3.5. OH Radical.....	32
3.3.6. Atmospheric O_3	33
3.3.7. Total HNO_3	35
3.4. Results and Discussion	35
3.4.1. $\delta^{18}\text{O}$ of $\text{H}_2\text{O}_{(\text{liquid})}$	36
3.4.2. $\delta^{18}\text{O}$ of the OH radical	37
3.4.3. $\delta^{18}\text{O}$ of Tropospheric O_3	39
3.4.4. Modeling HNO_3 production pathway R3.1.....	43
3.4.5. Modeling HNO_3 production pathway R3.2.....	44
3.4.6. Modeling HNO_3 production pathway R3.3.....	45
3.4.7. Total HNO_3	47
3.5. Conclusions and Future Considerations	48
CHAPTER 4. AN APPLICATION OF THE MODELING APPROACH TO A SITE IN NORTHWESTERN INDIANA.....	50
4.1. Technical Note.....	50
4.2. Introduction	50

	Page
4.3. Methods	53
4.3.1. Study Location: Indiana Dunes National Lakeshore, IN, USA	53
4.3.2. Sample Collection and Preparation	55
4.3.3. Isotope Analysis of NO ₃ ⁻ using the Denitrifier Method	56
4.3.4. A Simple Mass Balance for the Prediction of δ ¹⁸ O	57
4.4. Results	58
4.4.1. Sample Data	58
4.4.2. Model Predictions	61
4.5. Discussion	67
4.5.1. Comparison of Modeled δ ¹⁸ O Values to Observed Results	68
4.5.2. HYSPLIT Analysis	75
4.6. Conclusions and Future Considerations	77
LIST OF REFERENCES	80
APPENDICES	
Appendix A.	88
Appendix B.	90
Appendix C.	108

LIST OF TABLES

Table	Page
Table 1.1: 2005 EPA NO _x emissions inventory for total US.....	2
Table 2.1: Measurement of the Hoffman standard compared to that of the collected NO ₃ ⁻ fraction (n=7).	21
Table 4.1: 2005 EPA emissions inventory for areas near NADP site IN34 (emissions in tons NO _x /year).....	54
Table 4.2: Isotopic Standard Composition and δ Values (‰)	57
Appendix Table	
Table A.1: EPA Source Sector Descriptions	88
Table B.1: Events and times for timed fraction collection	93

LIST OF FIGURES

Figure	Page
Figure 1.1: Atmospheric Nitrogen Cycle (from Alexander et al., 2009).....	4
Figure 1.2: Dual isotope approach for the determination of a source from NO ₃ ⁻ (from Kendall et al., 2008).	9
Figure 2.1: IC instrumentation. Components: eluant degassing module (1), suppressors (2), electronically actuated control valves (3), conductivity detector (4), the anion exchange columns (5), PeakSimple Relay Board (6), mobile phase pump (7), sample pump (8).	14
Figure 2.2: The Spectrum Chromatography CF-1 Peak Separation Instrument.	16
Figure 2.3: Comparison of bulk analysis and fraction collected from 15ml of a 300nM Hoffman isotopic standard solution.	19
Figure 3.1: A sample of studies which have measured δ ¹⁸ O in atmospheric NO ₃ ⁻	25
Figure 3.2: Spatial trends of the δ ¹⁸ O _(Liquid H₂O) dataset for the months of January and July.	37
Figure 3.3: Spatial trends of the δ ¹⁸ O _(OH) dataset for the months of January and July based on equilibrium calculations.	39
Figure 3.4: Variation of δ ¹⁸ O with altitude, with P and T separated.	40
Figure 3.5: Variation of δ ¹⁸ O in O ₃ with altitude with T and P coupled.	41
Figure 3.6: Spatial trends of the δ ¹⁸ O _(O₃) dataset for the months of January and July.....	42
Figure 3.7. Comparison of predicted and observed δ ¹⁸ O values for O ₃ relative to VSMOW at La Jolla, CA. (data from Johnston and Thiemens, 1997).	43
Figure 3.8: Spatial trends of the δ ¹⁸ O _(NO₂+OH) dataset for the month of January based purely on equilibrium fractionations for the δ ¹⁸ O of OH.....	44
Figure 3.9: Spatial trends of the δ ¹⁸ O _(N₂O₅+surface) dataset for the month of January	45

Figure	Page
Figure 3.10: Spatial trends of $\delta^{18}\text{O}_{(\text{NO}_3+\text{VOC})}$ shown as the $\delta^{18}\text{O}_{(\text{NO}_3)}$ dataset for the month of January	46
Figure 3.11: Spatial trends of the $\delta^{18}\text{O}_{(\text{total HNO}_3)}$ dataset for the month of January based on equilibrium fractionations for the $\delta^{18}\text{O}$ of OH.....	47
Figure 4.1: Location map of the Indiana Dunes National Lakeshore NADP site IN34 ...	53
Figure 4.2: Monthly averaged results for NO_3^- in precipitation collected at the Indiana Dunes National Lakeshore in 2001	59
Figure 4.3: Monthly-averaged isotopic results for NO_3^- in precipitation collected at the Indiana Dunes National Lakeshore in 2002	60
Figure 4.4: Monthly-averaged isotopic results for NO_3^- in precipitation collected at the Indiana Dunes National Lakeshore in 2003	60
Figure 4.5: Predicted $\delta^{18}\text{O}$ of the OH radical based on equilibrium isotopic fractionation	61
Figure 4.6: Predicted $\delta^{18}\text{O}$ of tropospheric O_3 based on temperature and pressure	62
Figure 4.7: Predicted $\delta^{18}\text{O}$ of HNO_3 from HNO_3 production pathway R4.1	62
Figure 4.8: Predicted $\delta^{18}\text{O}$ of HNO_3 from HNO_3 production pathway R4.2.....	63
Figure 4.9: Predicted $\delta^{18}\text{O}$ of HNO_3 from HNO_3 production pathway R4.3.....	63
Figure 4.10: Mole fraction of R4.1 for the $\delta^{18}\text{O}$ of total HNO_3	64
Figure 4.11: Mole fraction of R4.2 for the $\delta^{18}\text{O}$ of total HNO_3	65
Figure 4.12: Mole fraction of R4.3 for the $\delta^{18}\text{O}$ of total HNO_3	65
Figure 4.13: Modeled prediction of $\delta^{18}\text{O}$ of total HNO_3	67
Figure 4.14: Comparison of modeled and observed $\delta^{18}\text{O}$ values in NO_3^- for 2001.....	69
Figure 4.15: Comparison of modeled and observed $\delta^{18}\text{O}$ in NO_3^- values for 2002.....	69
Figure 4.16: Comparison of modeled and observed $\delta^{18}\text{O}$ values in NO_3^- for 2003.....	70
Figure 4.17: $\delta^{18}\text{O}$ values for both measured and predicted NO_3^- in precipitation, utilizing the correction factor calculated from Savarino and Thiemens (1999) for 2001.	71
Figure 4.18: $\delta^{18}\text{O}$ values for both measured and predicted NO_3^- in precipitation, utilizing the correction factor calculated from Savarino and Thiemens (1999) for 2002.	71

Figure	Page
Figure 4.19: $\delta^{18}\text{O}$ values for both measured and predicted NO_3^- in precipitation, utilizing the correction factor calculated from Savarino and Thiemens (1999) for 2003.	72
Figure 4.20. Monthly-averaged model calculations for $\delta^{18}\text{O}$ of total HNO_3 in 2001 with the O_3 correction of +15‰ (equilibrium $\delta^{18}\text{O}$ OH values used).....	73
Figure 4.21. Monthly-averaged model calculations for $\delta^{18}\text{O}$ of total HNO_3 in 2002 with the O_3 correction of +15‰ (equilibrium $\delta^{18}\text{O}$ OH values used).....	74
Figure 4.22: Monthly-averaged model calculations for $\delta^{18}\text{O}$ of total HNO_3 in 2003 with the O_3 correction of +15‰ (equilibrium $\delta^{18}\text{O}$ OH values used).....	74
Figure 4.23: HYSPLIT Back Trajectory projected air mass provenance compared to $\delta^{15}\text{N}$ values for precipitation samples collected at the Indiana Dunes National Lakeshore	76
Figure 4.24: HYSPLIT Back Trajectory projected air mass provenance compared to $\delta^{18}\text{O}$ values for precipitation samples collected at the Indiana Dunes National Lakeshore	76
 Appendix Figure	
Figure B.1.: Example anion resin affinities for specific anions (from Bio-Rad AG1 Resin Manual).	90
Figure B.2: Schematic of Tube Rack used with CF-1 Collector	94
Figure B.3: Schematic of 10-port Alltech SelectPro Valve as set up with our preparative IC system.....	97
Figure B.4: Pressure regulator for argon tank.....	99
Figure B.5: Relay selection in the PeakSimple (SRI) software	100
Figure B.6: Valco 6-port valve (manual).....	101
Figure B.7: Gilson Autosampler controller	102
Figure B.8: Autosampler Queue with multiple samples in PeakSimple.....	103
Figure B.9: Edit file window in PeakSimple software. Event file space is marked.	104
Figure C.1: Coordinate System Tab in ArcMap	109
Figure C.2: Create New Shapefile popup window (image from http://www.u-s-c.org).	110
Figure C.3: Shapefile laid over a dataset for all of N. America. When extracted, the data beneath the shapefile will be preserved as a new dataset.....	112
Figure C.4: ‘Extract by Mask’ input box	113

ABSTRACT

Mase, David F. M.S., Purdue University, December 2010. A Coupled Modeling and Observational Approach to Understanding Oxygen-18 in Atmospheric Nitrate. Major Professor: Greg Michalski.

$\delta^{15}\text{N}$ and $\delta^{18}\text{O}$ values of atmospheric nitrate are fairly well documented in the literature. Some research has suggested $\delta^{15}\text{N}$ in atmospheric nitrate is an indicator of NO_x source in the atmosphere, where $\delta^{18}\text{O}$ of atmospheric nitrate tends to be an indicator of atmospheric oxidation. $\delta^{18}\text{O}$ in particular however is not as well understood as it can be. Many papers suggest that $\delta^{18}\text{O}$ values in atmospheric NO_3^- , and variations therein, indicate specific HNO_3 production pathways or other such atmospheric chemistry, though most of these assessments are qualitative. Presented here is the first coupled modeling and observational approach to fully understanding $\delta^{15}\text{N}$ and $\delta^{18}\text{O}$ values in atmospheric nitrate. A model for the prediction of $\delta^{18}\text{O}$ in atmospheric HNO_3 has been developed which utilizes mass-balance relationships to estimate $\delta^{18}\text{O}$ values in atmospheric HNO_3 . Precipitation samples collected by the National Atmospheric Deposition Program at the Indiana Dunes National Lakeshore between 2001 and 2003 are analyzed for $\delta^{15}\text{N}$ and $\delta^{18}\text{O}$. These measured values are compared with the first predictions of $\delta^{18}\text{O}$ in atmospheric NO_3^- to help to quantitatively determine the specific atmospheric chemistry behind the trends. This first attempt at a model which predicts $\delta^{18}\text{O}$ of atmospheric HNO_3 does not produce completely accurate results, however it shows potential. The shortfalls of the model exist primarily in its underestimation of $\delta^{18}\text{O}$ values of atmospheric HNO_3 when compared to the measured samples from the Indiana Dunes National Lakeshore. A correction to some components of the estimation help to rectify some of this underestimation, although predicted values still deviate from those measured. The RACM

model (Stockwell et al., 1997), which is coupled with this isotopic mass-balance model, predicts the contribution of each major HNO₃ production pathway however the calculations of RACM are based on air quality data that was incomplete for this study location. Ultimately the accuracy of the model depends on accurate and complete known datasets for calculation. Despite not showing absolute accuracy in the prediction of $\delta^{18}\text{O}$ values of HNO₃, this model shows tremendous potential in helping to better understand the chemical reactions which control the $\delta^{18}\text{O}$ of atmospheric HNO₃.

CHAPTER 1. INTRODUCTION

1.1. Introduction

The global nitrogen cycle has been greatly affected by anthropogenic inputs, including an increase in reactive nitrogen arising from the use of fossil fuels, agriculture, and industrial processes (e.g., Galloway et al., 2004). Many of these anthropogenic sources emit nitrogen to the atmosphere, which causes an abundance of potential problems for both the environment and human health. Nitrogen oxides (NO_x : nitric oxide (NO) and nitrogen dioxide (NO_2)) are a highly reactive form of nitrogen, and in the troposphere anthropogenic sources dominate the NO_x emission inventories (Jaegle et al., 2005). Since NO_x emissions are closely correlated with acid deposition as well as aerosol formation (Zhang et al., 2003) and associated climate forcing (e.g., Seinfeld and Pandis, 2006), understanding specific sources of NO_x in the atmosphere has become increasingly relevant.

Potential anthropogenic sources of NO_x emissions to the atmosphere include industrial sources such as manufacturing, power plants, emissions from vehicle exhaust systems, and agricultural emissions resulting from increased fertilization. A 2005 US Environmental Protection Agency (EPA) emissions inventory of anthropogenic NO_x sources for the entire United States is shown in Table 1.1. The prevalence of each of these anthropogenic sources will vary with place and time. For example, a metropolitan area may show high NO_x emissions from manufacturing industries, vehicle exhaust, and power production, where a rural region will likely experience fewer industrial emissions (though automobile exhaust may effect these areas) and a greater prevalence of agricultural emissions. Over different time scales, the dominant source(s) of NO_x emissions may change as well. During the winter months NO_x emissions from power

generation facilities may increase due to an increase in the need to heat/light dwellings, but during the transition from warm to cold and vice versa, power production is generally reduced due to people not needing to heat or cool their living quarters. Naturally, the reduced need for power generation during these times of the year shift NO_x emissions dominance to other sources.

Table 1.1: 2005 EPA NO_x emissions inventory for total US
(A detailed description of each source sector is available in Appendix A)

Source Sector	Total Emissions (Tons NO_x)
On Road Vehicles	6,491,821
Non Road Equipment	4,162,872
Electricity Generation	3,783,659
Fossil Fuel Combustion	2,384,297
Industrial Processes	1,163,635
Waste Disposal	155,415
Fires	94,372
Residential Wood Combustion	38,324
Solvent Use	6,400
Miscellaneous	3,644
Fertilizer & Livestock	2,098

In addition to spatial and temporal variations in anthropogenic emissions of NO_x, the effect of biogenic emissions of NO_x can also vary spatially and temporally. Biogenic NO_x emissions come primarily from nitrification and denitrification processes, although quantifying the relative importance of specific biogenic NO_x sources has been difficult. Estimates of the dominate sources of biogenic NO_x contribution show agriculture, grasslands, and tropical rainforests accounting for 41%, 35%, and 16% of the annual

biogenic NO_x budget, respectively (Yienger and Levy, 1995). In rural areas where industrial processes are not particularly prevalent, biogenic emissions of NO_x may show increased prevalence relative to urban settings. Even in these locations however, NO_x emissions inventories tend to show that anthropogenic sources of NO_x have notable presence. Additionally, seasonal changes can alter biogenic emissions depending on the activity of microorganisms and how they respond to changes in temperature.

NO_x in the atmosphere is ultimately deposited to the surface of the Earth via either dry or wet deposition. Before this can occur, reactions in the atmosphere oxidize NO_x into either nitrate (NO_3^-) aerosols or nitric acid (HNO_3) (e.g., Finlayson-Pitts and Pitts, 2000). Nitrate from the atmosphere is a significant source of N to ecosystems (Galloway et al., 2004). Atmospheric deposition of HNO_3 is a common contributor to acid rain, and therefore N deposition can cause considerable acidification of soils, which can lead to deforestation and/or significant crop damage (e.g, Likens et al., 2003; Fenn et al., 2008). Additionally, overabundant N deposition can lead to an overgrowth of algae in aquatic ecosystems (Paerl et al., 2000), starving these systems of oxygen and leading to completely anoxic conditions (Anderson, 1989). Because of these concerns the need to better understand sources of NO_x in the atmosphere, the chemical reactions which convert it into HNO_3 in the atmosphere, and nitrate deposition is very important.

As briefly discussed above, NO_x is converted to HNO_3 through multiple chemical pathways in the atmosphere (Figure 1.1). The prevalence of these HNO_3 -forming reactions depends on the stage of the Earth's diurnal cycle. During the day, oxygen atoms exchange between ozone (O_3 , R1.5) and NO_x through repeated photochemical cycling (R1.1 and 1.4). Then OH radicals (R1.2 and 1.3) cause the oxidation of NO_2 to HNO_3 (R.6) (Seinfeld and Pandis, 2006).





A different suite of reactions resulting in the formation of HNO_3 occur at night. At night, O_3 oxidizes NO_2 to produce the nitrate radical (NO_3 , R1.7). NO_3 then oxidizes to dinitrogen pentoxide (N_2O_5 , R1.8), which is then hydrolyzed into HNO_3 (R1.9) (Seinfeld and Pandis, 2006).

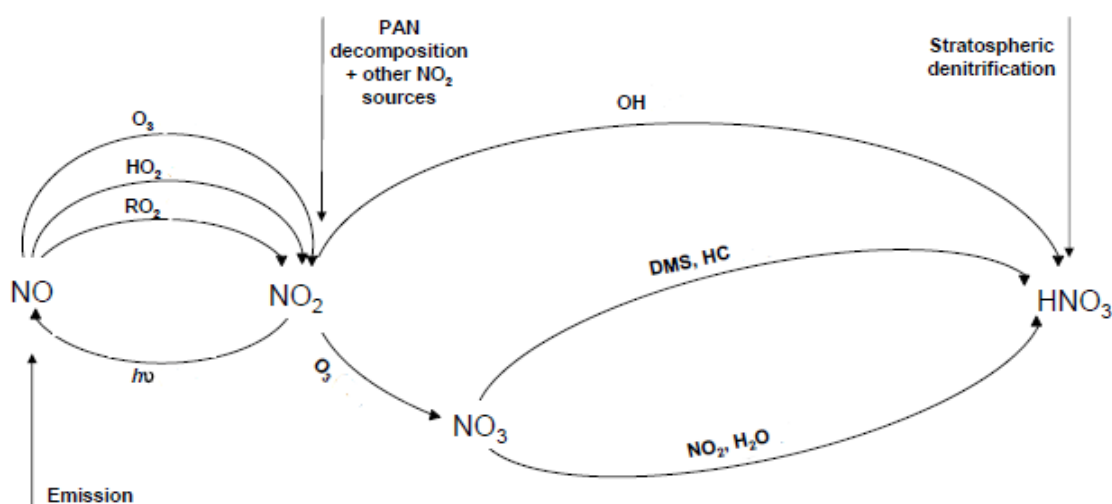
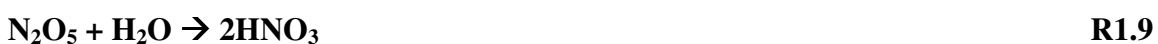


Figure 1.1: Atmospheric Nitrogen Cycle (from Alexander et al., 2009)

The increasing use of fossil fuels and subsequent acid deposition has prompted renewed interest in the study of nitrates derived from the atmosphere. Two primary questions driving research into this topic involve both the identification of the source of the NO_x emissions in the atmosphere, and the identification and understanding of chemical transformations of NO_x in the atmosphere. In order to address these nitrate

source and transformation questions, we utilize the stable isotopes ^{15}N , ^{18}O , and ^{17}O in precipitation (the most abundant form of HNO_3 wet deposition) samples.

1.2. Stable Isotope Theory

Neutral elements on the periodic table have equal numbers of protons and electrons. The atomic number of an element is indicated by the number of protons in a single atom of that element, so that any nucleus containing 7 protons belongs to a nitrogen atom (which is considered part of a neutral atom with 7 electrons to balance the charge of the protons). The atomic mass of an element, which is the sum of the masses of protons, neutrons, and electrons in an atom, can vary despite the consistency in number of protons. Variations in atomic mass from a neutral state atom are due to a greater number of neutrons. If the number of neutrons is not sufficient for the stability threshold of a nucleus, the repulsive forces of the protons in the nucleus (which are insulated by the neutrons) dominate and therefore the atom decays radioactively (Choppin et al., 1995). There are, however, atoms which remain stable with multiple nuclear configurations (i.e., number of neutrons), and these are called stable isotopes. For stable isotopes, standard chemical notation denotes an element (A), its atomic number (n), and its atomic mass (m) as m_pA , so the stable isotopes of oxygen would be $^{16}_8\text{O}$, $^{17}_8\text{O}$, and $^{18}_8\text{O}$. In geochemical studies it is common to drop the unchanging atomic number for simplicity (e.g., ^{16}O , ^{17}O , ^{18}O).

Stable isotopes are quantified as abundance ratios between isotopes of the same element through delta notation, as per Equation 1.1:

$$\delta = \{[R_{(sample)}/R_{(standard)}] - 1\} * 1000 \quad \text{E1.1}$$

where $R_{(sample)}$ is the ratio of the less abundant to more abundant isotope in a sample (e.g., $^{15}\text{N}/^{14}\text{N}$), and $R_{(standard)}$ is the ratio of the less abundant to more abundant isotope in a reference standard. The resulting value is an isotopic abundance of a sample relative to the abundance of the same isotope in the accepted standard. Relative abundances for isotope analyses are easier to use than absolute abundances due to the generally small

differences in absolute abundances between stable isotopes. The use of a ratio makes more apparent the differences in isotopic abundances between multiple samples as well. Isotope ratio abundances are given in parts per thousand or permil (‰) relative to the reference standard used in the calculation. For N, this reference standard is air N₂, and for O this reference standard is Vienna Standard Mean Ocean Water (VSMOW).

1.3. $\delta^{15}\text{N}$ in Atmospheric Nitrate

There are conflicting interpretations in regard to whether atmospheric nitrate $\delta^{15}\text{N}$ variations are due to changes in NO_x source or a consequence of shifts in NO_x photochemistry (Elliott et al., 2007; Elliott et al., 2009; Freyer, 1991). The $\delta^{15}\text{N}$ of NO_x can vary greatly between anthropogenic and natural sources, which amplifies confusion over the contribution of source vs. atmospheric chemistry. A limited number of measurements show values of $\delta^{15}\text{N}$ in NO_x from the combustion of coal from +6 to +13‰ (Heaton, 1990; Kiga et al., 2000). NO_x generated from vehicle emissions, roadside denuders, and roadside vegetation have $\delta^{15}\text{N}$ values of +3.7, +5.7, and +3.8‰, respectively (Ammann et al., 1999; Moore, 1977; Pearson et al., 2000). Natural sources of atmospheric NO_x, such as nitrogen fixation by lightning are limited to laboratory studies on electric discharges (simulating lightning) that have shown a range in $\delta^{15}\text{N}$ values from -0.5 to +1.4‰ (Hoering, 1957). There are no data on $\delta^{15}\text{N}$ of NO emitted by the nitrification-denitrification process, which is a serious shortcoming if $\delta^{15}\text{N}$ is to be used as a tracer of NO_x source. Despite the lack of specific $\delta^{15}\text{N}$ values for natural sources of NO_x, a number of studies (Ammann et al., 1999; Moore, 1977; Freyer, 1991; Russell et al., 1998) have shown comparisons of $\delta^{15}\text{N}$ values at polluted and pristine areas, to find that $\delta^{15}\text{N}$ values tend to be lower in pristine sites (relative to polluted sites). Additionally, comparisons between seasons show generally lower $\delta^{15}\text{N}$ values during the spring and summer (relative to other seasons) (e.g., Elliott et al., 2007; Elliott et al., 2009; Hastings et al., 2003). These comparisons suggest that biogenic activity forms isotopically depleted NO_x (with regard to ¹⁵N) which is emitted in abundance during the warmer months when biologic growth is active.

More recently, studies in the Midwestern United States show strong correlations between electric generating unit (EGU) NO_x and $\delta^{15}\text{N}$ when sampled from ~500 to 600km of the source area (Elliott et al., 2007). This is consistent with the output from the EPA's Regional Acid Deposition Model (RADM) (Paerl et al., 2002). Based on these and other strong correlations ($\delta^{15}\text{N}$ and EGU emissions within source areas of 80-800km, for example), Elliott et al. suggest that $\delta^{15}\text{N}$ can be used as a tracer for emissions source despite transformations and fractionations which may occur during regional transport.

Regional observations shown by Elliott et al. (2007) indicate that $\delta^{15}\text{N}$ can be used as a source tracer of wet NO_3^- , and as a fate tracer of NO_x emissions in the environment. Therefore, $\delta^{15}\text{N}$ in precipitation NO_3^- can be used to monitor progress toward NO_x source reduction goals. In the Midwestern U.S., NO_3^- deposition is dominated by inputs of NO_x from stationary sources such as power plants. Accurate NO_x fate/ NO_3^- source determinations by $\delta^{15}\text{N}$ are promising, but the presence of possible fractionations, and interfering atmospheric compounds such as NO_y ($\text{NO}_x + \text{HNO}_3$) are greater than previously thought, and could interfere with atmospheric nitrate $\delta^{15}\text{N}$ values and interpretations. These uncertainties show that improvements to the current methods of assessing NO_3^- deposition from the atmosphere are needed to better understand the environmental and ecological impacts of atmospheric NO_3^- deposition.

Contrasting Elliott et al., Freyer (1991) has shown that for certain locations in Germany (Julich and Ahrensburg) and France (Le Conquet), $\delta^{15}\text{N}$ variations in precipitation nitrate are likely a result of atmospheric chemistry rather than differences in source contributions. Specific evidence for this case comes from primarily the seasonal variations in precipitation $\delta^{15}\text{N}$. Also analyzed in Freyer (1991) was nitric acid vapor, which showed little variation in $\delta^{15}\text{N}$ signature. Freyer suggests that this may be due to seasonal effects being masked by dissociation of the NH_4NO_3 aerosol during warmer months. Freyer (1991) acknowledges that source contributions frequently do affect $\delta^{15}\text{N}$ signatures in samples, however there are other potentially more important factors that Freyer considers: 1) The temperature-dependent isotopic exchange equilibria between

atmospheric nitrogen species, and 2) seasonal-dependent changes in the method of nitrate formation.

Freyer (1991) and Elliott et al. (2007) both comment on the fact that more data and study is needed to fully identify the source and chemical relationships responsible for the variations observed in atmospheric nitrate $\delta^{15}\text{N}$. In Freyer's case, the focus is on chemical changes since he discounts the attribution of stationary source emissions due to a lack of significant data from his sites. Elliott et al.'s data focuses on stationary source contribution, since the chemical contributions to isotope variation in the atmosphere was not found to be significant in their data. Naturally the conflicting views between Freyer (1991) and Elliott et al. (2007) call to question the real cause of $\delta^{15}\text{N}$ variations in atmospheric samples.

1.4. Stable Isotopes of Oxygen

In addition to ^{15}N , the oxygen isotopes ^{18}O and ^{17}O are measured in atmospheric NO_3^- . A commonly used isotopic technique for source and chemical pathway determination of NO_3^- is the coupling of ^{18}O with ^{15}N . This is called a dual-isotope approach, which greatly helps to narrow down the source of atmospheric nitrate based on the values of $\delta^{15}\text{N}$ and $\delta^{18}\text{O}$ in nitrate samples. An example of the utility of a dual isotope approach is shown in Figure 1.2. The most recent tabulation of $\delta^{18}\text{O}$ values (relative to Standard Mean Ocean Water, or SMOW) in atmospheric nitrate shows a range of 18 to 110‰ for precipitation across multiple studies (Burns et al., 2002; Campbell et al., 2002; Elliott et al., 2009; Hales et al., 2007; Hastings et al., 2003; Savarino et al., 2007; Spoelstra et al., 2001; Buda et al., 2009).

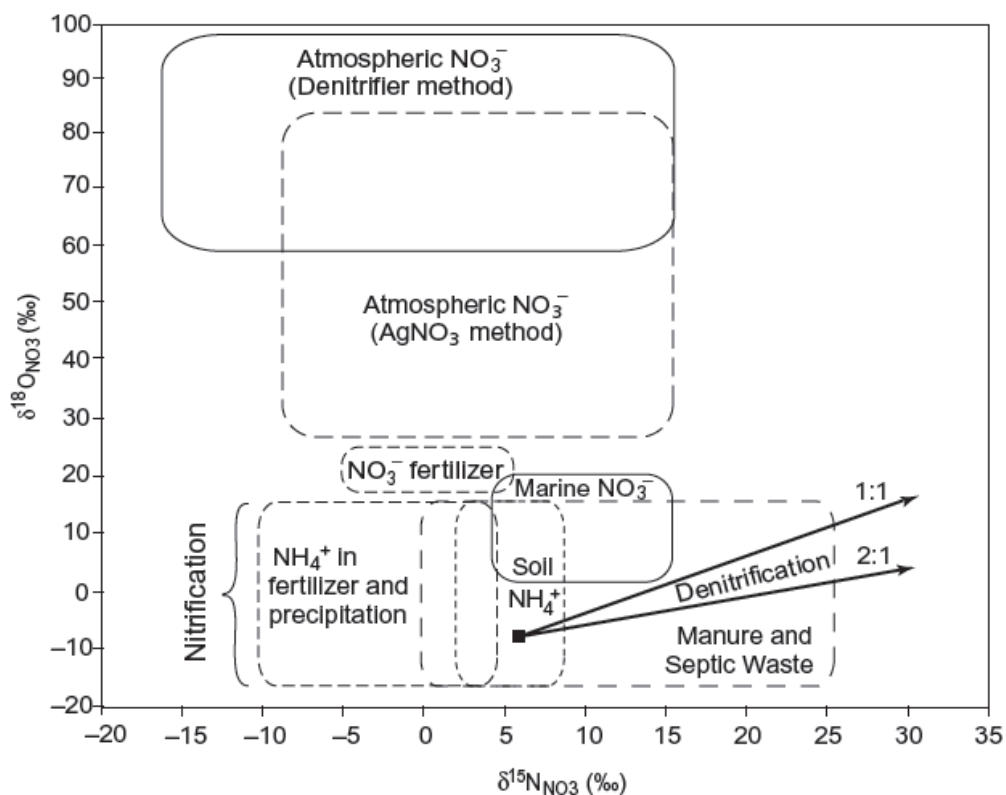


Figure 1.2: Dual isotope approach for the determination of a source from NO_3^- (from Kendall et al., 2008).

1.5. Understanding the Atmospheric NO_3^- - budget

Understanding the relative importance of specific oxidation pathways for NO_x in the formation of atmospheric nitrate is very important for a comprehensive understanding of the atmospheric nitrate budget, both regionally and globally. Modeling efforts (i.e., Alexander et al., 2009) for the global transport of the oxygen isotopic composition of atmospheric NO_3^- are useful for comparisons with observational data to interpret results from analysis and to understand/improve on the accuracy of the model. Alexander et al. (2009) utilize the GEOS-Chem global 3D model of coupled aerosol-oxidant chemistry (Park et al., 2004) to simulate nitrate $\Delta^{17}\text{O}$ values. Within the model, with all sources of NO_x are accounted for (anthropogenic emissions are taken from the Global Emission Inventory Activity) (Benkovitz et al., 1996).

The biggest challenge when modeling $\Delta^{17}\text{O}$ for NO_3^- is the uncertainty regarding the variability in $\Delta^{17}\text{O}$ for ozone, as discussed in Alexander et al., (2009). In this and other models of $\Delta^{17}\text{O}$ in atmospheric NO_3^- (Michalski et al., 2003; Michalski et al., 2004; Savarino et al., 2007), the $\Delta^{17}\text{O}$ in nitrate depends largely on the importance of O_3 in NO_x cycling. If O_3 is present and active in the cycling of NO_x , then the $\Delta^{17}\text{O}$ signal will be transferred to the resulting NO_3^- . The same is true for $\delta^{18}\text{O}$, indicating that atmospheric chemistry is largely responsible for $\delta^{18}\text{O}$ values in atmospheric NO_3^- .

Little modeling has been attempted for the $\delta^{18}\text{O}$ of atmospheric NO_3^- . Further, interpretations of the spatial variance of $\delta^{18}\text{O}$ are lacking a true quantitative understanding. $\delta^{18}\text{O}$ varies greatly in some locations, and yet a quantitative explanation as to why does not exist. Similar to the $\Delta^{17}\text{O}$ modeling studies, $\delta^{18}\text{O}$ values may be explained by multiple pathways in the atmospheric NO_x oxidation cycle. This thesis aims to unravel the mystery behind variations in $\delta^{18}\text{O}$ values throughout the contiguous United States. This is accomplished by applying a mass-balance modeling approach for the prediction of $\delta^{18}\text{O}$ values based on the mixing relationships of species in the HNO_3 production pathways (R1.1-1.3). This modeling effort is coupled with isotopic analysis applied to precipitation samples collected by the National Atmospheric Deposition Program through the years 2001, 2002, and 2003 in the Midwestern United States. It is hoped that the information obtained through the work presented here will be used to better understand the N budget in the atmosphere above the Midwestern United States. Following this introduction is a detailed description of the methods used to measure and compare both observed results from precipitation to predicted results from a model based on isotopic mass-balance relationships. Resulting from this will be a new method for the interpretation of atmospheric NO_3^- data, and new ideas as to why isotope values measured from atmospheric nitrate in precipitation vary in time and space as observed and modeled.

CHAPTER 2. ION CHROMATOGRAPHY INSTRUMENTATION FOR NITRATE SEPARATION

2.1. Technical Note

This chapter details the development of a preparative ion chromatography system that I developed over the summer of 2009. The system is used to prepare samples discussed in Chapter 4. Material in this chapter is not a prerequisite for understanding the data and interpretations presented in Chapters 3 and 4.

2.2. Introduction

As discussed in Chapter 1, isotope values of atmospheric NO_3^- are important for the determination of source and transformation pathways of NO_x in the atmosphere. Samples of atmospheric NO_3^- are collected as either dry (aerosol/denuder samples) or wet (precipitation samples) deposition. These types of samples usually contain common anions other than NO_3^- , such as NO_2^- , Cl^- and SO_4^{2-} . This presents some difficulty, as multiple anions in a sample may cause interference in isotope measurements when using certain methods. For example, isotopic analysis of NO_3^- in the presence of NO_2^- using the bacterial reduction method can cause measured oxygen isotope values for NO_3^- to be lower than expected (Casciotti et al., 2007).

Isotopes of SO_4^{2-} also help with understanding the source and transformation of SO_2 which is an important component of H_2SO_4 in the atmosphere. Many methods designed to analyze NO_3^- in a sample containing both NO_3^- and SO_4^{2-} make it impossible to accurately measure SO_4^{2-} after the NO_3^- analysis. This is due to either the destruction of the sulfate anion during nitrate analysis (pyrolysis techniques; e.g., Silva et al., 2000)

or adding contaminants to the sulfate solution (denitrifier method; e.g., Casciotti et al., 2002). Additionally, depending on the analytical method (TC/EA, laser fluorination), isotopic analysis of oxygen in nitrate in the presence of sulfate, or vice versa, can result in interference and incorrect oxygen isotope values (Michalski et al., 2008; Böhlke et al., 2003). In order to prevent issues associated with samples containing both NO_3^- and SO_4^{2-} , it is important to be able to isolate these different ions in samples.

There are several approaches to isolate and purify ions from sample solutions, consisting of chemical means, physical means, or a combination of both. NO_2^- can be removed from a solution via the addition of ascorbic acid (Granger et al., 2006), which allows for more accurate isotopic analysis of isotopes in NO_3^- . However, this prohibits determining concentrations or isotope abundances of the nitrite. A chemical method for isolation and purification of nitrate for isotopic analysis uses BaCl_2 to precipitate SO_4^{2-} out of a solution. The solution is then passed through a cation exchange resin and subsequently reacted with Ag_2O to produce AgNO_3 that can be analyzed for isotopes by thermal decomposition (Silva et al., 2000; Michalski et al., 2004). While this method successfully isolates NO_3^- from a sample, the BaSO_4 precipitate is not suitable for oxygen isotopic analysis due to the coprecipitation of a trace amount of NO_3^- (Michalski et al., 2008; Böhlke et al., 2008). Additionally, small amounts of BaSO_4 are difficult to isolate for $\delta^{34}\text{S}$ or $\delta^{18}\text{O}$ analysis. A disadvantage of the AgNO_3 method is the relatively large amount of NO_3^- needed to successfully guarantee conversion to AgNO_3 (~10-50 μmol) which limits analysis to the rare systems where large amounts of nitrate are present. When limited to sub-micromole amounts of nitrate in a sample, the bacterial reduction method (Sigman et al., 2001; Casciotti et al., 2002) is ideal. However, the bacterial solution contaminates the residual sulfate and makes its isolation impractical. Utilization of anion exchange resins in ion chromatography where different anions can be collected as they are separated by the chromatography and then analyzed for isotopes using various methods overcomes these limitations. The purpose of this chapter is to describe the development of an automated, preparative IC system that was interfaced to a fraction collector for the purpose of isolating NO_2^- , NO_3^- , and SO_4^{2-} from sample solutions.

2.3. Ion Chromatography

Ion chromatography (IC) is a method that separates ions in a solution based on their size and charge. Ions in a sample are pumped through an ion-exchange column, absorbed onto a resin within the column based on their affinity, and then desorbed back into solution via a mobile phase. The desorbing of ions back into solution does not occur simultaneously, and therefore the ions are separated as the mobile phase passes through the anion exchange column. Anions are detected by changes in the solution's conductivity, and the elution time can be correlated with specific anions. The IC instrumentation in the PSI lab was modified to operate in two 'modes:' analytical and preparative. The purpose of analytical mode is to measure concentrations of specific ions in a sample solution. This is accomplished by referencing the conductivity of the sample to that of standards mixed to known concentrations. In analytical mode samples with very low anion concentrations can be measured and only a small amount of the total solution is analyzed (~100 μ L). However, the analytical mode is destructive in that the anions in a sample solution are sent to a waste container after analysis. The purpose of the preparative mode of the IC system is to isolate and collect all of the anions in the total sample as well as determine the anion concentration. The differences between these modes are the method of mobile phase suppression, number of columns used, the use of a sample loop, and the incorporation of a fraction collector.

2.3.1. Ion Chromatography Instrument

The IC instrument consists of two pumps (one for sample, and one for the mobile phase), two suppressors, three anion separation columns, one eluant degassing module, an autosampler, a fraction collector, and one conductivity detector (Figure 2.1). The mobile phase pump is a dual-head pump (Alltech Model 626) and the pump for the sample is a single head (Alltech Model 426). In both modes the samples are placed in an autosampler (Gilson) capable of holding either 176 15mL tubes or 56 50mL tubes. The anion separation columns (4mm Dionex AS14) are designed to separate inorganic anions, including fluoride, chloride, nitrite, bromide, nitrate, phosphate, and sulfate based on

their affinity for the column resin (Figure B.1, Appendix B). Each column is protected by one guard column (Dionex AG14) which acts as a trap for both highly-retained components and particulate matter in the sample. The eluant degassing module (Alltech) generates a small vacuum to remove gas dissolved in the mobile phase before it flows to the analytical columns. This ensures that no bubbles will form in the mobile phase which can cause pump malfunction and interfere with conductivity. The mobile phase is a 0.0018M/0.0017M solution of $\text{NaHCO}_3/\text{Na}_2\text{CO}_3$, respectively, in two 2L bottles that are connected to the mobile phase pump. After the mobile phase elutes the anions from the column, it passes through a chemical suppressor (4mm Dionex AMMS300) that exchanges H^+ for the mobile phases's Na^+ . This converts the $\text{NaHCO}_3/\text{Na}_2\text{CO}_3$ into CO_2 which suppresses the mobile phase's contribution to conductivity. After suppression, the mobile phase passes through the conductivity detector (Alltech), which measures the conductivity of the sample. The entire instrumentation setup is regulated by a relay board (SRI) and controlled with the PeakSimple (SRI) software. Details on the use of both analytical and preparative modes, system parameters, and software hints can be found in Appendix B.

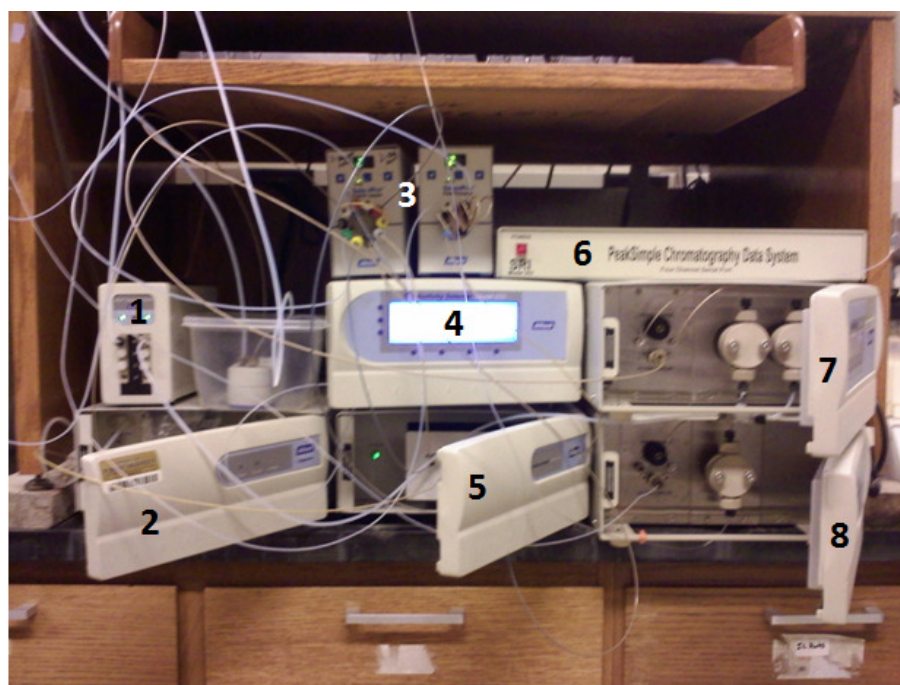


Figure 2.1: IC instrumentation. Components: eluant degassing module (1), suppressors (2), electronically actuated control valves (3), conductivity detector (4), the anion exchange columns (5), PeakSimple Relay Board (6), mobile phase pump (7), sample pump (8).

2.3.2. Analytical Mode

In the analytical mode of IC operation, only a portion of the sample is used in the determination of anion concentrations. The sample pump pulls the sample solution from its tube (in the autosampler), and pushes it via a 6-port valve through a sample loop of a known volume (standard procedure uses a 100 μ L loop, but they can range from 1 to 1000 μ L or higher). The analytical mode only uses one anion column (Dionex AS14), which is protected by a single guard column (Dionex AG14). The 6-port valve is switched and the mobile phase carries the sample solution from the loop to the column, where the anions are separated based on their affinity for the anion resin in the column. The mobile phase elutes the anions, undergoes suppression, and finally the anions are detected by conductivity as a function of retention time. To determine concentrations, a set of calibrated standards are run along with samples. The software integrates the area under the time versus conductivity intensity curve (hereafter referred to as the “peak area”), which can be transformed into a specific concentration of anion. Each analytical sample takes only ~15 minutes to run.

2.3.3. Preparative Mode

In the preparative mode of IC operation, the entire volume of a sample is pumped onto a column and its individual anion fractions are collected. A key difference in the preparative mode is that the entire sample volume is pumped directly onto an analytical column through a 10-port valve using an Alltech model 426 pump. The 10-port valve is switched and the mobile phase (0.0018M/0.0017M NaHCO₃/Na₂CO₃) is pumped continuously at 2 mL/min until the end of a sample run. The anions are separated based on affinity for the column resin. The mobile phase elutes the ions, undergoes suppression, and finally the anions are detected by conductivity as a function of retention time. After detection of conductivity, the eluted anions flow to a fraction collector instead of going to waste. Running a sample in preparative mode takes ~30-45 minutes depending on the volume to be pumped.

2.3.4. Fraction Collection

In order to collect individual anion peaks using automation, a fraction collector is interfaced to the IC system. The fraction collector (Spectrum Chromatography Model CF-1; Figure 2.2) is capable of collecting 174 individual sample fractions (peaks) in 5 ml vials. A three-way valve on the back of the fraction collector is connected to the IC's conductivity detector by a 36" x 1/16" OD piece of Teflon tubing. The three-way valve controls flow between the IC system, the fraction collector and the waste container. In "collect mode" the valve directs the flow into one of the fraction tubes and in "bypass mode" to the waste container. Collect mode is activated by either programmed timing windows or the detection of peaks in conductivity levels. The system can be configured to collect the Cl^- , NO_2^- , NO_3^- , and SO_4^{2-} fractions from a sample.

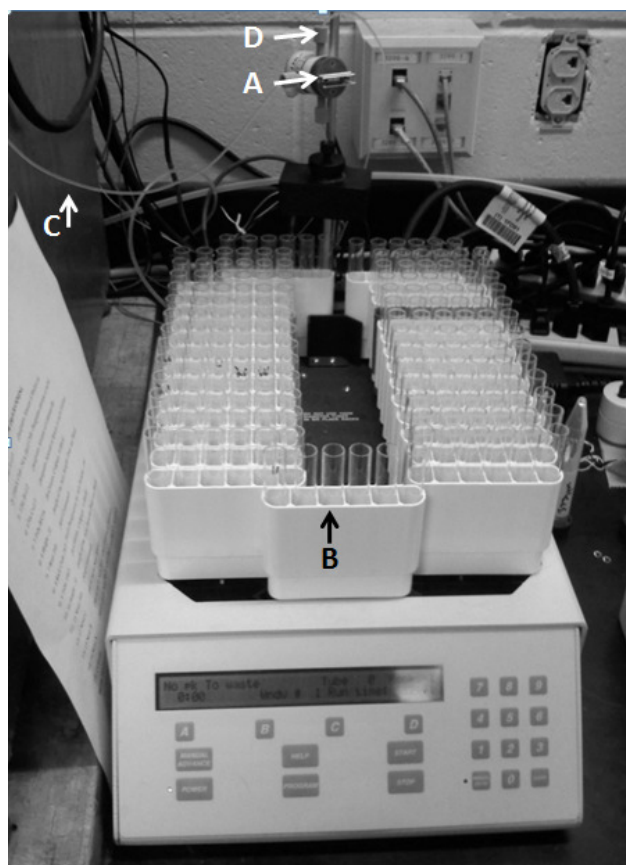


Figure 2.2: The Spectrum Chromatography CF-1 Peak Separation Instrument. A is the 3-port valve, B is a vial in the vial rack, C is the tube coming from the conductivity detector, and D is the outlet to waste from the fraction collector valve.

2.4. Results and Discussion

In preparative mode, the objective is to accurately determine anion concentrations, ensure good fraction collection efficiency, and retain the isotopic integrity of anions isolated from the original solution. The collection efficiency means the entire peak eluted from the IC is collected, and isotopic integrity means that no isotopic fractionation occurred during the separation and collection process. Ideally, the fraction of nitrate collected will contain 300nM of nitrate; enough for triplicate isotope analysis using the bacterial methods described in Chapter 4 of this thesis. Therefore a set of standard solutions were mixed to contain 300nM of nitrate, chloride, and sulfate. The nitrate used in these standards was a calibrated isotopic standard (Hoffman). For peak retention and concentration calibration, a second set of chloride, nitrate, and sulfate concentration standards were used.

2.4.1. Anion Concentration Analysis

The concentration standards were used to determine the maximum amount of anions that could be successfully split into fractions, and to test the ability of the preparative mode to precisely determine anion concentrations. Standard concentrations were mixed to cover a wide range: 50ppb, 100ppb, 200ppb, 500ppb, 1ppm, 5ppm, 10ppm, 100ppm, and 300ppm. This ensures that at low concentrations the anion conductivity peaks could be detected and at high concentrations the column would not become saturated and fail to effectively separate the anions. 15mL of each standard solution was pumped onto the columns and separated. This corresponds to ~12-2400nMol of nitrate across this range of concentrations. At these concentrations, all fractions were separated without peak overlap, even when the peak height is off scale. Further, the low concentrations were detected and show that this preparative technique can be used for determining concentrations in samples containing low anion abundances.

2.4.2. Collection Efficiency

In order to test collection efficiency, a series of control experiments were carried out. 15mL of a 1ppm IC concentration standard (NaCl, KNO₃, Na₂SO₄; ~242 nMol NO₃⁻) was separated and collected with the fraction collector. Only the NO₃⁻ fraction was then run through preparative mode a second time. The first attempt at this saw significant loss of NO₃⁻ concentrations, but with further testing it was found that this is a result of mobile phase presence in the collected fraction. Therefore, before the anion concentrations in any fraction can be measured, the fraction needs to be passed through H⁺ cation exchange resin (Bio-Rad) to remove any additional mobile phase in the fraction. Without passing the fraction through the cation exchange resin, the column resin treats the fraction like mobile phase and the sample fails to exchange, resulting in poorly defined results at best. The fraction collector's efficiency in the collection of NO₃⁻ is determined by comparing the peak area from an initial separation to the peak area of the fraction (peak) collected (Figure 2.3). The collection efficiency (initial sample peak area/collected fraction peak area) was determined to be 90% +/- 3%; (n=40).

Less than 100% yield may be the result of retention within the column, or issues regarding pumping efficiency. If solids are incorporated into the IC instrumentation due to improper sample handling and preparation, these solids greatly reduce the efficiency of the sample pump and result in a less-than-optimal amount of sample being injected into the IC instrument for separation. Additionally, the autosampler needle is only capable of collecting all except 1-2 mL per sample tube. However slight the amount, this unused sample will reduce the yield of the collection NO₃⁻ fraction. Further, yield discrepancies may be the result of inaccurate peak timing. The two columns used for the fraction separation and collection each have slightly different retention times for NO₃⁻. In one column, the NO₃⁻ peak elutes between 5.8 minutes and 9.2 minutes, where the other has NO₃⁻ eluting between 5.1 minutes and 8.2 minutes. The difference in elution time is easily corrected for by simply utilizing one consistent collection window for NO₃⁻ that spans the elution time of NO₃⁻ in both columns: 5.1 minutes to 9.2 minutes. Since the elution times of the columns do not change over several straight days of sample analysis,

the use of this collection window allows for accurate collection of NO_3^- on our automated instrument.

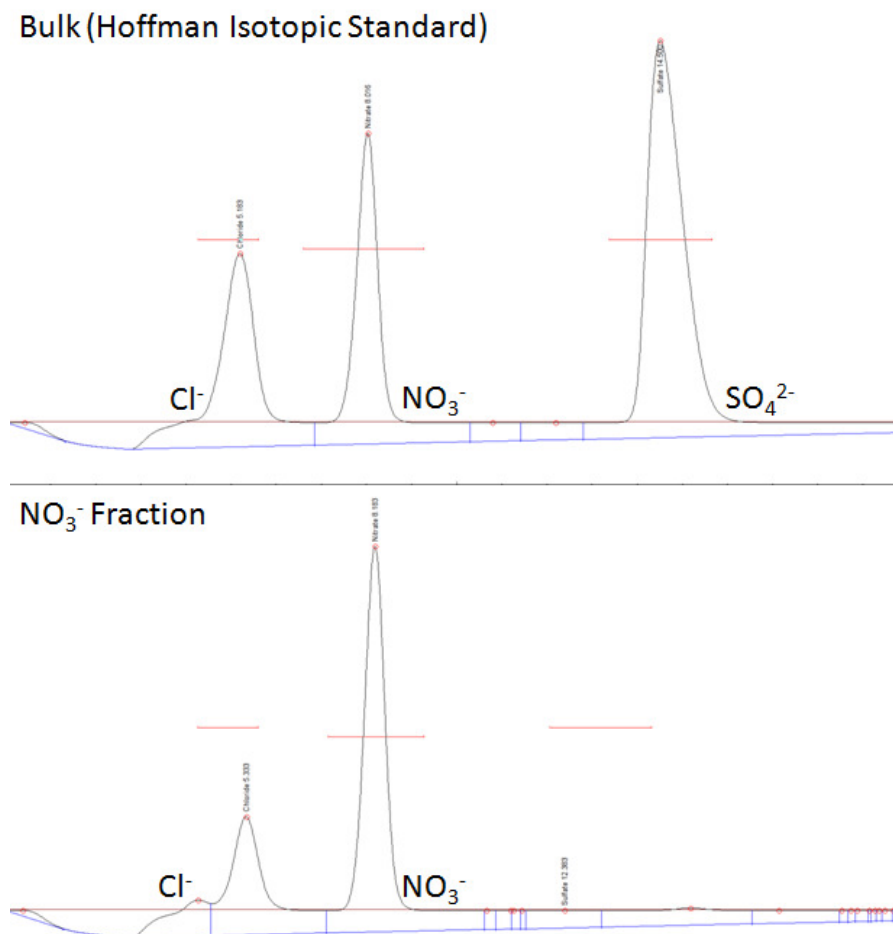


Figure 2.3: Comparison of bulk analysis and fraction collected from 15ml of a 300nM Hoffman isotopic standard solution.

The NO_3^- fraction contains some chloride (Figure 2.3), due to some difficulty with setting up the timing of peak separation on the fraction collector. Since Cl^- does not interfere with NO_3^- isotopic analysis however, collecting both Cl^- and NO_3^- helped to widen the timing window for the collection of the NO_3^- fraction to ensure that as much of NO_3^- as possible is collected. If NO_2^- were in our samples, this would be an unacceptable method of anion isolation, as can NO_2^- interfere with NO_3^- isotope analysis.

2.4.3. Isotopic Viability

To test that the separation and fraction collection procedure does not affect the isotopic composition of NO_3^- , a series of control experiments were carried out. Standards with 300nM of NO_3^- were used to determine the isotopic viability of this method. An NO_3^- isotopic reference (Hoffman brand Chilean fertilizer KNO_3) was used for the NO_3^- component of the standard. This reference NO_3^- has been calibrated relative to VSMOW and atmospheric air N_2 (Table 2.1). A bulk standard solution was mixed so that 100nMol of each Cl^- , NO_3^- , and SO_4^{2-} would be present in 1mL of solution. These solutions were mixed to mimic the typical sample solutions which would be separated using this method. 3mL of this bulk standard was diluted to 15mL, which produced 300nMol of Hoffman NO_3^- which was separated using the preparative IC technique.

The NO_3^- fraction recovered using the preparative method was analyzed utilizing the denitrifier method (Sigman et al., 2001; Casciotti et al., 2002) for $\delta^{18}\text{O}$ and $\delta^{15}\text{N}$ values. Table 2.1 compares the isotope values of our calibrated lab standards to the isotope values measured from the collected NO_3^- fraction across multiple trials. The denitrifier method analyses for the standards prior to separation show an average value of +39.9‰ for $\delta^{18}\text{O}$ and -5.1‰ for $\delta^{15}\text{N}$. For the separated NO_3^- fractions (excluding a single outlier), the average values are 38.9‰ for $\delta^{18}\text{O}$ and -4.9‰ for $\delta^{15}\text{N}$. Based on our analyses, the similarity of the values between bulk standard and collection NO_3^- fraction indicates that there are no significant fractionations which occur during the separation process. This means that the IC separation and collection of corresponding fractions is a valid method for isolating the NO_3^- fraction of a sample for isotope analysis.

Table 2.1: Measurement of the Hoffman standard compared to that of the collected NO_3^- fraction (n=7).

	Standard Isotope Measurement		Value from NO_3^- fraction	
	$\delta^{18}\text{O}$	$\delta^{15}\text{N}$	$\delta^{18}\text{O}$	$\delta^{15}\text{N}$
Mean:	39.9	-5.1	38.9	-4.9
St.Dev:	1.1	1.3	0.7	0.9

2.5. Conclusion

The isolation and collection of fractions of specific anions is helpful in isotopic analysis in that it avoids interference between anions measured using some isotopic methods and it solves the issue of losing certain anions (such as SO_4^{2-}) through the analysis of others (NO_3^-). The success of such a method depends on the researcher's ability to test the yield of the fraction collected, and test the fraction for isotopic relevance through isotopic standard measurement. When successfully implemented, fraction collection of NO_3^- from a sample is a relatively simple way to easily isolate specific anions for isotopic analysis.

CHAPTER 3. MODELING $\delta^{18}\text{O}$ IN ATMOSPHERIC NITRATE

3.1. Technical Note

This chapter details the development of an isotopic mass balance model for the prediction of $\delta^{18}\text{O}$ in atmospheric HNO_3 . Material in this chapter is meant to stand on its own, and will help with understanding the data and interpretations presented in Chapter 4.

3.2. Introduction

The oxidation of nitrogen compounds in the atmosphere is a very important mechanism in atmospheric chemistry. NO_x ($\text{NO}_2 + \text{NO}$) is emitted primarily as a by-product of combustion, and in recent times anthropogenic NO_x inputs from fossil fuel combustion have been dominating the global atmospheric NO_x budget (Galloway et al., 2004; Galloway, 1998). NO_x is also emitted by natural processes such as biogenic emissions via nitrification-denitrification and fixation through lightning (Galloway, 2004). NO_x is ultimately oxidized in the atmosphere to nitric acid, which frequently causes a significant decrease in the pH of precipitation (Rodhe et al., 2002, Galloway, 1995) or “acid rain.” Acid rain can acidify soils and cause significant damage to vegetation such as crops and forests (e.g., Likens et al., 2003). Nitric acid also reacts with ammonia or alkaline aerosol particles, forming new aerosols or altering the chemical composition and size of the existing aerosols (Zhang et al., 2000). Changes in aerosol composition and size can affect albedo and feeds back into climate change (e.g., Seinfeld and Pandis, 2006). Atmospheric nitrate ($\text{HNO}_{3(\text{g})}$, $\text{NO}_3^-_{(\text{s})}$, $\text{NO}_3^-_{(\text{aq})}$) is ultimately removed from the atmosphere by dry and wet deposition and transported to various ecosystems where it is utilized as a source of bioavailable N (Galloway, 2004). High rates of N deposition, however, can negatively impact ecosystems. In aquatic systems rampant

growth of algae spurred by N can starve ecosystems of oxygen (anoxia) (Rabalais, 2002). Excess N deposition can also reduce plant diversity in terrestrial ecosystems, by forcing out plants that cannot survive in systems with such high N (Bobbink et al., 2010; Fenn et al., 2008). Therefore, identifying the sources of and mechanisms that transform NO_x into atmospheric nitrate is important to understanding the natural and anthropogenic nitrogen cycles on local, regional, and global scales.

Stable isotopes are very useful as tracers of chemical sources and atmospheric chemistry, and may be useful for understanding the transformation of NO_x into atmospheric nitrate. For atmospheric nitrate, the stable isotopes of interest are ^{14}N and ^{15}N for nitrogen and ^{16}O , ^{17}O , and ^{18}O for oxygen. Changes in isotope abundances are reported in standard delta (δ) notation, expressed in parts per thousand (permil: ‰), which is the difference of the between ratio of heavy to light isotopes in a sample and that of a standard reference material and normalized to the reference ratio. The standard reference material for nitrogen is atmospheric air N_2 and Vienna Standard Mean Ocean Water (VSMOW) for oxygen. It has been suggested that $\delta^{15}\text{N}$ variations in nitrate can be used to trace sources of atmospheric NO_x (e.g., Elliott et al., 2009). ^{17}O variations have been used extensively to identify oxidation of NO_x in the atmosphere by ozone (e.g., Michalski et al., 2002; Michalski et al., 2003). The variation in $\delta^{18}\text{O}$ values of atmospheric nitrate has been measured in multiple studies with the vast majority being from precipitation samples (e.g., Hastings et al., 2003; Savarino et al., 2007; Moravec et al., 2010).

Despite the abundance of studies that report measured $\delta^{18}\text{O}$ values in atmospheric nitrate, inferences as to the chemical or physical mechanisms that cause spatial and temporal $\delta^{18}\text{O}$ variations are rare and qualitative. Some studies have suggested that ^{18}O can be used to trace atmospheric alteration of NO_x -derived compounds (e.g., Hastings et al., 2003; Elliott et al., 2009). This is similar to ^{17}O , but ^{17}O has strictly been used for tracing NO_x oxidation by ozone in the atmosphere. Variations in $\delta^{18}\text{O}$ values of atmospheric water may also be noticeable in atmospheric HNO_3 , as water is a known component of HNO_3 production (N_2O_5 hydrolysis; Finlayson-Pitts and Pitts, 2006). This

role of water in the production of HNO_3 may affect the $\delta^{18}\text{O}$ of HNO_3 , yet no previous studies have attempted to quantify the role $\delta^{18}\text{O}$ values of water play in the $\delta^{18}\text{O}$ of atmospheric HNO_3 . To further investigate these possibilities, an approach coupling recorded atmospheric nitrate $\delta^{18}\text{O}$ data and predictive modeling of NO_x oxidation in the atmosphere would be very useful.

Atmospheric nitrate $\delta^{18}\text{O}$ values vary in space and time (Figure 3.1) (e.g., Burns and Kendall, 2002; Hastings et al., 2003; Spoelstra et al., 2001). Atmospheric nitrate $\delta^{18}\text{O}$ values are consistently higher in winter compared to summer. This suggests a dependency of $\delta^{18}\text{O}$ in atmospheric nitrate on either temperature or photolysis lifetime, as these both change with season. At high latitudes, atmospheric nitrate $\delta^{18}\text{O}$ values are consistently higher when compared to lower latitudes, while also showing a seasonal trend. This is further evidence of a dependency of atmospheric nitrate $\delta^{18}\text{O}$ values on temperature or photolysis lifetime, since these also vary with latitude. Some exceptions to these trends are observed in Turkey Lakes Ontario (Spoelstra et al. 2001) and central PA (Buda and DeWalle, 2009). It may be the lower than expected $\delta^{18}\text{O}$ values recorded in these locations were due to analytical error (Revesz and Böhlke, 2002), however it has recently been shown (Xue et al., 2010) that the AgNO_3 method (Silva et al., 2000) used in these studies produces results as valid as those from the denitrifier method (Sigman et al., 2001). These exceptions may be due to high aerosol and gaseous pollutant levels, which could possibly lead to lower $\delta^{18}\text{O}$ values for atmospheric nitrate. This suggests photochemical mechanisms other than temperature and photolysis lifetime may be important in changing $\delta^{18}\text{O}$ values in atmospheric nitrate. Despite the abundance atmospheric nitrate $\delta^{18}\text{O}$ data available, a quantitative assessment of the cause of these discrepancies has not been attempted.

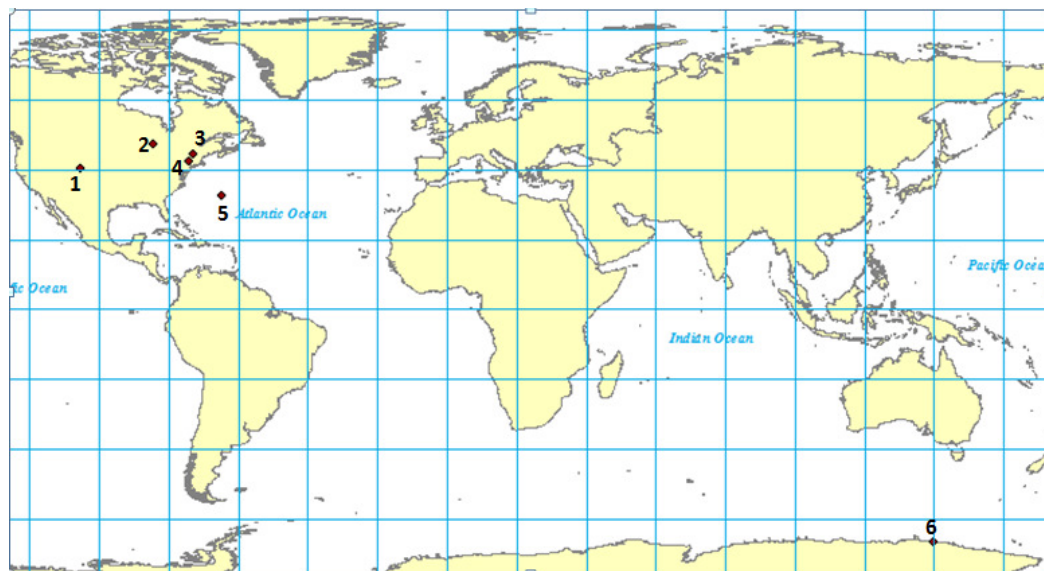


Figure 3.1: A sample of studies which have measured $\delta^{18}\text{O}$ in atmospheric NO_3^- . Each number represents an individual location and study: 1. The Loch Vale watershed, Colorado (Campbell et al., 2002; approx. $\delta^{18}\text{O}$ values: +40 to +65‰). 2. The turkey lakes watershed, Ontario (Spoelstra et al., 2001; approx. $\delta^{18}\text{O}$ values: +39 to +60‰). 3. Brush brook, Vermont (Hales et al., 2007; approx. $\delta^{18}\text{O}$ values: +31 to +57‰). 4. The Catskill Mountains of New York (Burns and Kendall, 2002; approx. $\delta^{18}\text{O}$ values: +38 to +58‰). 5. Bermuda (Hastings et al., 2003; approx. $\delta^{18}\text{O}$ values: +64 to +80‰). 6. Coastal Antarctica (Savarino et al., 2006; approx. $\delta^{18}\text{O}$ values: +60 to +110‰).

Seasonal and spatial trends in $\delta^{18}\text{O}$ data give rise to the following key questions: What causes these spatial and regional trends in $\delta^{18}\text{O}$ of atmospheric NO_3^- ? Can these trends be reproduced in a model to better help interpret changes in $\delta^{18}\text{O}$ values? Attempts to model isotopic variations in $\Delta^{17}\text{O}$ in atmospheric nitrate (e.g., Michalski et al., 2003; Michalski et al., 2004, Alexander et al., 2009) have used a theoretical isotopic mass-balance approach to obtain reasonably accurate isotope values when compared to measured data. The lack of such a model for $\delta^{18}\text{O}$ may be due to difficulties associated with assessing kinetic isotope effects, equilibrium isotope effects, or $\delta^{18}\text{O}$ values of oxygen sources such as water. Our objective in this chapter is to introduce a relatively

simple model utilizing mass-balance and kinetic or equilibrium isotope effects to model the $\delta^{18}\text{O}$ of atmospheric NO_3^- .

3.3. Methods

We have developed a simple model that uses isotopic mass-balance and kinetic/equilibrium isotope fractionation factors to predict $\delta^{18}\text{O}$ in atmospheric nitrate. The mass-balance approach assesses the $\delta^{18}\text{O}$ values of oxygen-containing compounds that participate in the oxidation of NO_x to NO_3^- . Isotope effects (both kinetic and equilibrium) are the cause of $\delta^{18}\text{O}$ variations. Unfortunately, accurate modeling of both kinetic and equilibrium isotope effects is difficult, especially when many fractionation factors in the NO_x system are unknown.

In an isotopic mass-balance model for $\delta^{18}\text{O}$ of atmospheric nitrate, each oxygen component in the mixture has a $\delta^{18}\text{O}$ value and a mole fraction associated with it. The $\delta^{18}\text{O}$ value of a given compound is either measured or calculated, and the mole fraction is either calculated based on stoichiometry (inspection), experimentally determined, or inferred from measurements. In a stepwise oxidation process, such as the oxidation NO into NO_3^- , the mole fraction (x_i) is the number oxygen atoms contributed from each specific oxidant (i) relative to the total oxygen in the product. The $\delta^{18}\text{O}$ of the product is then given by the general isotopic mass balance equation:

$$\delta^{18}\text{O}_{\text{product}} = \sum x_i \delta^{18}\text{O}_{\text{reactant } i} \quad (\text{E3.1})$$

Isotopic mass balance (E3.1) for $\delta^{18}\text{O}$ is simplified when there are only two $\delta^{18}\text{O}$ sources contributing to the final product:

$$X \delta^{18}\text{O}_x + (1-X) \delta^{18}\text{O}_{x-1} = \delta^{18}\text{O}_{(\text{final})} \quad (\text{E3.2})$$

In E3.2, X is the mole fraction of a specific oxygen source, and $1-X$ is the mole fraction of the second oxygen source. In the present study, there are more than two

components in our total mass balance, but each of these can be simplified as a series of two-component mass balance functions (discussed below).

In addition to the effects of general isotope mass balance, the isotopic composition of a compound will be influenced by kinetic and equilibrium fractionation factors (α), which can be expressed as an enrichment factor (ϵ). ϵ is equal to $1000(\ln \alpha)$ (Criss, 1999). Adding ϵ to the isotope mass balance yields:

$$\delta^{18}\text{O}_{\text{product}} = \sum X_i \delta^{18}\text{O}_{\text{reactant } i} + \sum \epsilon_{\text{reaction } i} \quad (\text{E3.3})$$

where $\sum \epsilon_{\text{reaction } i}$ is the sum of the enrichment/depletion of $\delta^{18}\text{O}$ due to the kinetic or equilibrium isotope effect for reaction ‘i’. These isotope enrichment factors are highly dependent on temperature. Many of the equilibrium and kinetic enrichment factors in the photochemical oxidation of NO_x are unknown. Those that are known, such as the kinetic isotope effect in ozone formation (discussed below), have temperature and pressure dependencies. Likewise, equilibrium enrichment factors, such as the equilibrium between gas and liquid water (discussed below) are a function of temperature. The proposed model utilizes the known equilibrium and kinetic fractionation factors to determine the contribution of different compounds to the product nitrate $\delta^{18}\text{O}$ value. Our model is simplified in that unknown kinetic and equilibrium fractionation factors are assumed to be 1. We believe these are negligible as detailed in the discussion section.

The $\delta^{18}\text{O}$ values of atmospheric NO_3^- will also be influenced by atmospheric loss processes. In the atmosphere, the two primary loss mechanisms for atmospheric nitrate are wet and dry deposition. These are first-order loss processes, which alter $\delta^{18}\text{O}$ values of the residual nitrate following Rayleigh distillation behavior:

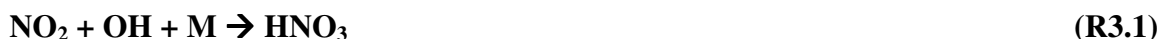
$$\delta^{18}\text{O}_{\text{remaining}} = \delta^{18}\text{O}_{\text{initial}} - \epsilon \ln[f(t)] \quad (\text{E3.4})$$

Where $\delta^{18}\text{O}_{\text{remaining}}$ is the $\delta^{18}\text{O}$ value of the remaining NO_3^- in the atmosphere, $\delta^{18}\text{O}_{\text{initial}}$ is the starting $\delta^{18}\text{O}$ value of atmospheric nitrate, and ϵ is the enrichment factor. The change in $\delta^{18}\text{O}$ remaining is a function of the natural log of the fraction remaining,

which for first-order processes is a function of time ($\ln[f(t)]$), (Criss, 1999). Here we ignore isotope effects due to loss processes, as specific enrichment factors for the loss processes have not been calculated or experimentally determined.

3.3.1. Fitting the model to atmospheric HNO₃ production pathways

Nitric acid is formed in the atmosphere through the following reaction pathways:



Reaction R3.1, where M is a third body, is considered the dominant HNO₃ production pathway (Seinfeld and Pandis, 2006). R3.2 is a hydrolysis reaction where N₂O₅ reacts with H₂O absorbed on an aerosol surface to produce HNO₃ and is considered the second most important atmospheric nitrate source (Deneter and Crutzen, 1993; Brown et al., 2006). Finally, R3.3 is an oxidation reaction where NO₃ radicals abstract hydrogen atoms from volatile organic compounds (VOC) to produce HNO₃. In our simplified model, we are ignoring any kinetic isotope effect associated with R3.1, 3.2 or 3.3. This is justified as nearly all of the N-oxides are converted to HNO₃ over relatively short time scales (Seinfeld and Pandis, 2006). The application of our mass balance approach to reactions R3.1, 3.2, and 3.3 is detailed below.

3.3.2. δ¹⁸O of atmospheric NO_x

The first step in atmospheric nitrate production is the oxidation of NO into NO₂, which can occur by either ozone or peroxy radicals (R3.4, 3.5, 3.6). Of these two pathways, O₃ oxidation (R3.4) is dominant, as the oxidation of NO by peroxy radicals (R3.5, 3.6) is relatively small (Finlayson-Pitts and Pitts, 2000). Sometimes this is not the case, however, such as in events of high atmospheric NO_x saturation (Jaegle et al., 2001). The majority of peroxy radicals are produced when other radicals such as H, CH₃, and R (an organic radical) combine with atmospheric O₂ (R3.5).



NO is regenerated when NO₂ is photolyzed by light at wavelengths less than 420nm (R3.7). Under daytime conditions at mid-latitudes, photolysis of NO₂ occurs roughly once every 3 minutes (Seinfeld and Pandis, 2006). This allows for multiple cycles of R3.4, 3.7, and 3.8 to occur and rapid cycling between NO_x and atmospheric O₂ allows oxygen equilibration via reactions R 3.5, 3.6, and 3.8.

Peroxy radical moieties are derived from atmospheric O₂, with O₃ as the other predominant oxidant of NO_x to NO₂. Therefore, in terms of isotopic mass balance we can reduce the production of NO₂ to two components: atmospheric O₃ and O₂.

$$\delta^{18}\text{O NO}_2 = X \delta^{18}\text{O}_{(\text{O}_3)} + (1-X) \delta^{18}\text{O}_{(\text{O}_2)} \quad (\text{E3.5})$$

Where X is the fraction of NO_x oxidized into NO₂ by O₃, and $1-X$ is the remaining fraction that is oxidized by peroxy radicals.

The next step in atmospheric HNO₃ production is the production of higher oxides of nitrogen such as the nitrate radical (NO₃, R3.9 below). The mass balance calculation for atmospheric NO₃ production, after substituting E3.5 for δ¹⁸O of NO₂ is:



$$\delta^{18}\text{O NO}_3 = 2/3 [X \delta^{18}\text{O}_{(\text{O}_3)} + (1-X) \delta^{18}\text{O}_{(\text{O}_2)}] + 1/3 (\delta^{18}\text{O}_{(\text{O}_3)}) \quad (\text{E3.6})$$

The second most prevalent HNO₃ production pathway is hydrolysis of N₂O₅ (R3.2) (Deneter and Crutzen, 1993). N₂O₅ forms from the reaction of two radicals: NO₂ and NO₃. This reaction is a simple combination reaction, and therefore in the isotope

mass balance model we simply combine E3.6 and E3.5 and have a $\delta^{18}\text{O}$ mass balance equation in terms of only atmospheric O_3 and O_2 :



$$\delta^{18}\text{O}_{\text{N}_2\text{O}_5} = 4/5[(X \delta^{18}\text{O}_{(\text{O}_3)} + (1-X) \delta^{18}\text{O}_{(\text{O}_2)})] + 1/5 [\delta^{18}\text{O}_{(\text{O}_3)}] \quad (\text{E3.7})$$

Based on these considerations, we can rewrite R3.1 through R3.3 in terms of isotopic mass balance:

$$\underline{\text{NO}_2 + \text{OH}}: 2/3[X \delta^{18}\text{O}_{(\text{O}_3)} + (1-X) \delta^{18}\text{O}_{(\text{O}_2)}] + 1/3 (\delta^{18}\text{O}_{(\text{OH})}) \quad (\text{E3.8})$$

$$\underline{\text{NO}_3 + \text{VOC}}: 2/3 [X \delta^{18}\text{O}_{(\text{O}_3)} + (1-X) \delta^{18}\text{O}_{(\text{O}_2)}] + 1/3 (\delta^{18}\text{O}_{(\text{O}_3)}) \quad (\text{E3.9})$$

$$\underline{\text{N}_2\text{O}_5 + \text{H}_2\text{O}}: 5/6\{4/5 [X \delta^{18}\text{O}_{(\text{O}_3)} + (1-X) \delta^{18}\text{O}_{(\text{O}_2)}] + 1/5 [\delta^{18}\text{O}_{(\text{O}_3)}]\} + 1/6(\delta^{18}\text{O}_{(\text{H}_2\text{O})}) \\ = 2/3[X \delta^{18}\text{O}_{(\text{O}_3)} + (1-X) \delta^{18}\text{O}_{(\text{O}_2)}] + 1/6[\delta^{18}\text{O}_{(\text{O}_3)}] + 1/6(\delta^{18}\text{O}_{(\text{H}_2\text{O})}) \quad (\text{E3.10})$$

For E3.8, the $\delta^{18}\text{O}$ value of the product HNO_3 is the result of an isotope mass balance between the $\delta^{18}\text{O}$ values of NO_2 and the OH radical. For E3.9, NO_3 reacts with VOC in the atmosphere to produce HNO_3 . Since this is a hydrogen abstraction, it is assumed that VOC are not responsible for any oxygen transfer, therefore, the $\delta^{18}\text{O}$ of R3.3 is the same as the $\delta^{18}\text{O}$ of NO_3 (E6). In E3.10 NO_2 and NO_3 combine to form N_2O_5 , which is then hydrolyzed to HNO_3 on a wetted aerosol surface. As a result, $\delta^{18}\text{O}$ value of HNO_3 produced from this pathway is a result of mass balance between NO_2 , NO_3 , and H_2O . The three atmospheric nitrate production pathways (E3.8, 3.9, and 3.10) have only four variables: $\delta^{18}\text{O}_{(\text{H}_2\text{O liquid})}$, $\delta^{18}\text{O}_{(\text{OH})}$, $\delta^{18}\text{O}_{(\text{O}_3)}$, and $\delta^{18}\text{O}_{(\text{O}_2)}$ which need to have been measured or inferred in order to solve the mass balance equation.

3.3.3. $\delta^{18}\text{O}$ of Liquid Water

The $\delta^{18}\text{O}$ of liquid water factors into our mass balance approach in two ways: as $\delta^{18}\text{O}$ of liquid water in E3.10, and as a component of $\delta^{18}\text{O}$ values of OH in E3.8 (explained in more detail below: Section “OH Radical”). The presence of liquid water in our mass balance makes the temporal and spatial variations of liquid water $\delta^{18}\text{O}$ important in that they will affect the $\delta^{18}\text{O}$ of the product HNO_3 . There is an abundance of

available data on $\delta^{18}\text{O}$ values of atmospheric liquid water from the Global Network of Isotopes in Precipitation (GNIP; IAEA/WMO, 2001), which is a part of the International Atomic Energy Agency (IAEA). While the GNIP $\delta^{18}\text{O}$ database is quite large, the samples are from a relatively limited number of sites. Therefore, in order to estimate the $\delta^{18}\text{O}$ values of liquid water for areas that are not included in the sampling network, mathematical estimations, or interpolations are needed. Bowen and Ravenaugh (2003) have modified a method from Bowen and Wilkinson (2002) to interpolate water $\delta^{18}\text{O}$ data between sampling points. The effect of temperature on $\delta^{18}\text{O}$ of liquid water is described as a function of the sampling stations' latitude and altitude. The effect of transportation is based on regional patterns of water vapor source/delivery (wind). These two parameters are fitted using non-linear least squares and used to predict continuous spatial $\delta^{18}\text{O}$ values for liquid water. These data are available at 10' Arc raster format and complete spatial datasets can be found on the <http://www.waterisotopes.org> website. The $\delta^{18}\text{O}$ of liquid water in our model uses predicted $\delta^{18}\text{O}$ data from the WaterIsotopes website, for the contiguous United States.

3.3.4. Atmospheric O_2

Atmospheric O_2 enters into our mass-balance by reacting with peroxy radicals as per reactions R3.5 and R3.6. O_2 gas is the main oxygen component of the atmosphere, and its $\delta^{18}\text{O}$ values are reflected in all other atmospheric oxygen containing compounds. Dole (1975) showed that atmospheric O_2 has a consistent $\delta^{18}\text{O}$ value of 23.2‰ (relative to SMOW) and is due to the balance between photosynthesis and respiration (Dole, 1975). There is little spatial or temporal variation of the $\delta^{18}\text{O}$ value for atmospheric O_2 in the troposphere, however small cyclical variations (+/- 0.2) have been recorded over the past ~100,000 years (Bender et al, 1985; Bender et al., 1994). A mass balance model that incorporated fractionations due to photosynthesis, respiration, and other minor contributions (Beerling, 1999) estimated the Dole Effect should produce atmospheric O_2 with a $\delta^{18}\text{O}$ value of 23.2‰, which is very close to the most recent observed value of 23.9‰ (Barkan and Luz, 2005) and this value is used in the present model.

3.3.5. OH Radical

The OH radical is used in our isotope mass balance model due to the gas-phase reaction that forms HNO₃ (R3.1). OH is formed when and O¹D atom that is derived from ozone photolysis reacts with water vapor (R3.11):



Since OH is highly reactive and has a very low steady state abundance (10^5 - 10^6 molecules/cm³, Seinfeld and Pandis, 2006), no direct measurements of its isotopic composition in the atmosphere have been made. Considering isotope mass conservation, the $\delta^{18}\text{O}$ of OH should be a mix between $\delta^{18}\text{O}_{(\text{ozone})}$ and $\delta^{18}\text{O}_{(\text{atmospheric water vapor})}$. However, OH achieves isotopic equilibrium with water vapor through the exchange reaction R13 (Dubey et al., 1997). As a result of this exchange the $\delta^{18}\text{O}$ value of OH is a function of the $\delta^{18}\text{O}$ of water vapor in a given air mass and in the fractionation factor for the equilibrium reaction (E11):



$$\mathbf{\delta^{18}O_{(OH)} = \delta^{18}O_{(\text{water vapor})} + \epsilon_{R13}} \quad \mathbf{(E3.11)}$$

Variations in $\delta^{18}\text{O}$ values of water vapor relative to liquid water is temperature dependent and have been quantified experimentally (Horita and Wesolowski, 1994; Majoube, 1971):

$$\mathbf{\delta^{18}O_{(\text{water vapor})} = \delta^{18}O_{(\text{liquid water})} + \epsilon_{E13}} \quad \mathbf{(E3.12)}$$

$$\mathbf{\epsilon_{(\%)} = 1000 \ln \alpha = -7.685 + 6.7123 (10^3/T) - 1.6664 (10^6/T^2) + 0.35041 (10^9/T^3)} \quad \mathbf{(E3.13)}$$

In E3.12, the $\delta^{18}\text{O}$ of water vapor is dependent on the $\delta^{18}\text{O}$ of liquid water plus an enrichment factor, ϵ . This enrichment factor is calculated based on E3.13. We have regressed E3.13 from data in Horita and Wesolowski (1994) to yield the following linear temperature dependent equation for the water vapor enrichment factor

$$\mathbf{\epsilon_{(\%)} = 0.1056T - 40.632} \quad \mathbf{(E3.14)}$$

Based on E3.14, at 298K water vapor is depleted relative to liquid H₂O by approximately 9.2‰.

The equilibrium enrichment factor for exchange between OH and water vapor has not been measured but it can be calculated. Water molecule isotopologue vibrational frequencies (Herzberg, 1966) and the OH radical's fundamental frequency (Dousmanis et al., 1955) are known. Applying the reduced mass, simple harmonic oscillator approximation yields the ¹⁸OH vibrational frequency. From these frequencies the reduced partition functions of OH and water isotopologues can be solved as a function of temperature (Urey, 1947) and a temperature dependent enrichment factor formula for the OH-H₂O exchange reaction is::

$$\epsilon_{(‰)} = 1000 \ln \alpha = 0.1884T - 99.297 \quad (\text{E3.15})$$

This enrichment factor equation predicts the $\delta^{18}\text{O}$ of OH will be depleted 43‰ relative to atmospheric water vapor (at 298K). Simplifying the resulting equation for $\delta^{18}\text{O}$ of OH in terms of our known data ($\delta^{18}\text{O}_{(\text{H}_2\text{O})}$ and temperature) yields:

$$\delta^{18}\text{O}_{(\text{OH})} = \delta^{18}\text{O}_{(\text{Liquid Water})} + 0.294T - 139.929 \quad (\text{E3.16})$$

3.3.6. Atmospheric O₃

Atmospheric O₃ is a part of the mass balance approach for the approximation of $\delta^{18}\text{O}$ in atmospheric HNO₃ in that O₃ plays a large role in R3.4 and R3.8. During ozone formation (R3.4 and R3.8), isotope effects as large as +170‰ have been observed in atmospheric O₃ (e.g., Krankowsky and Mauersbuerger, 1996; Mauersberger et al., 1993). The $\delta^{18}\text{O}$ value for O₃ has been shown to have a dependency on the pressure and temperature of O₃ formation (e.g., Morton et al., 1990; Thiemens and Jackson, 1990; Gao and Marcus, 2007). While many previous studies have examined oxygen isotopes in ozone from both pressure-dependency (e.g., Thiemens and Jackson, 1990) and temperature-dependency (e.g., Morton et al., 1990) viewpoints, there have been no attempts to derive an equation which calculates the $\delta^{18}\text{O}$ of ozone based on *both*

temperature and pressure over an extended range. For pressures typical of the troposphere, a regression of data reported in Morton et al. (1990) yields the pressure-dependency Equation E3.17. This equation corrects the $\delta^{18}\text{O}$ value to be relative to VSMOW by adding +23.2‰ to produce the factor of 135.62.

$$\delta^{18}\text{O}_{(\text{ozone})} = -0.0299\text{P} + 135.62 \quad (\text{E3.17})$$

where P is pressure in torr. These results were obtained at a temperature of 321K. For temperature, data also from Morton et al. was regressed to yield the O_3 temperature-dependency Equation E3.18:

$$\delta^{18}\text{O}_{(\text{ozone})} = 0.52\text{T} - 45 \quad (\text{E3.18})$$

where T is temperature in degrees K. These results were obtained at a pressure of 50 torr.

The calculation of $\delta^{18}\text{O}$ of ozone is based on pressure (E3.17) and then corrected for the change of $\delta^{18}\text{O}$ in O_3 due to the temperature difference described above (321-T in E3.19). We assume the temperature at the surface of the Earth is 298 K. We then correct for the experimental temperature difference by subtracting the temperature calculated by the dry adiabatic lapse rate from the reference temperature of 321K. The result is a $\delta^{18}\text{O}$ value, which needs to be corrected for isotope effects associated with the transfer of oxygen from the terminal atom of O_3 in the calculation of NO_2/NO_3 (Savarino et al., 2008). This correction accounts for the transfer of $\delta^{18}\text{O}$ when O_3 reacts with NO_x to form NO_2 and NO_3 . Based on calculations in Savarino et al. (2008), this correction factor is 0.83. Including this correction, the final equation for the $\delta^{18}\text{O}$ of atmospheric ozone is (E3.20):

$$\delta^{18}\text{O}_{(\text{ozone})} = 0.83 * \{(-0.0299\text{P} + 135.62) - [0.52 * (321 - \text{T})]\} \quad (\text{E3.19})$$

Using this equation, at a temperature of 298 K and a pressure of 760 torr, the resulting $\delta^{18}\text{O}$ value of ozone is ~83.8‰.

Since the calculation of $\delta^{18}\text{O}$ of O_3 relies on pressure and temperature data to predict $\delta^{18}\text{O}$ of O_3 with reasonable accuracy, datasets for pressure and temperature are needed. To accomplish this, data was taken from the National Oceanic and Atmospheric Administration (NOAA) National Operational Model Archive & Distribution System (NOMADS). For this study, North American Regional Reanalysis Data (NARR) was used. This data (three hour resolution) was averaged to daily average temperature and pressure for the purpose of calculations of $\delta^{18}\text{O}$ of HNO_3 .

3.3.7. Total HNO_3

Using these estimates of the main oxygen source incorporated into atmospheric nitrate during NO_x oxidation, the $\delta^{18}\text{O}$ of atmospheric HNO_3 can be estimated based on mass balance. The mass-balance approach yields a master mass-balance equation for the total $\delta^{18}\text{O}$ of atmospheric HNO_3 :

$$\delta^{18}\text{O}_{(\text{HNO}_3)} = \beta(\text{E3.8}) + \chi(\text{E3.9}) + \zeta(\text{E3.10}) \quad (\text{E3.20})$$

where β is the mole fraction of the $\text{NO}_2 + \text{OH} \rightarrow \text{HNO}_3$ production pathway, χ is the mole fraction of the $\text{NO}_3 + \text{VOC}$ pathway, and ζ is the mole fraction of the N_2O_5 aerosol surface pathway. These fractions are determined based on air quality data used in conjunction with a photochemical box model based on the Regional Atmospheric Chemistry Mechanism (RACM), (Stockwell et al, 1997). This model calculates each of these fractions once per hour during the duration of a model simulation, and then averages them for the specified window. Through this model we account for changes in each pathway during the course of a day.

3.4. Results and Discussion

The predicted $\delta^{18}\text{O}$ values of atmosphere HNO_3 are reliant on three variables throughout the mass balance approach described here: the $\delta^{18}\text{O}$ of $\text{H}_2\text{O}_{(\text{liquid})}$ in the

atmosphere, the $\delta^{18}\text{O}$ of the OH radical, and the $\delta^{18}\text{O}$ of tropospheric O_3 . This section will focus primarily on these variables in the discussion of the model described here.

3.4.1. $\delta^{18}\text{O}$ of $\text{H}_2\text{O}_{(\text{liquid})}$

The $\delta^{18}\text{O}$ of atmospheric liquid water is data obtained from the waterisotopes.org (<http://www.waterisotopes.org>) website. This data is presented as monthly long-term averages. Figure 3.2 shows the spatial resolution of this dataset for the continuous United States in the winter and summer. Generally, the $\delta^{18}\text{O}$ of liquid water is correlated with temperature, and therefore the spatial pattern of the $\delta^{18}\text{O}$ of liquid water in the atmosphere is similar to spatial patterns expected with temperature. Altitude also greatly effects $\delta^{18}\text{O}$ of atmospheric liquid water, and as a result values are lower at higher altitudes. The effect of changing seasons leads to lower values in the summer months and higher values in the winter months due to temperature changes. As air masses move from the coastal regions (Pacific or Gulf Coasts of the US), vapor molecules containing heavy isotopes preferentially condense and rain out. This is usually modeled as a Rayleigh-type process (Bowen and Ravenaugh, 2003). The spatial trends during both seasons are similar, except in the summer the values tend to be much higher.

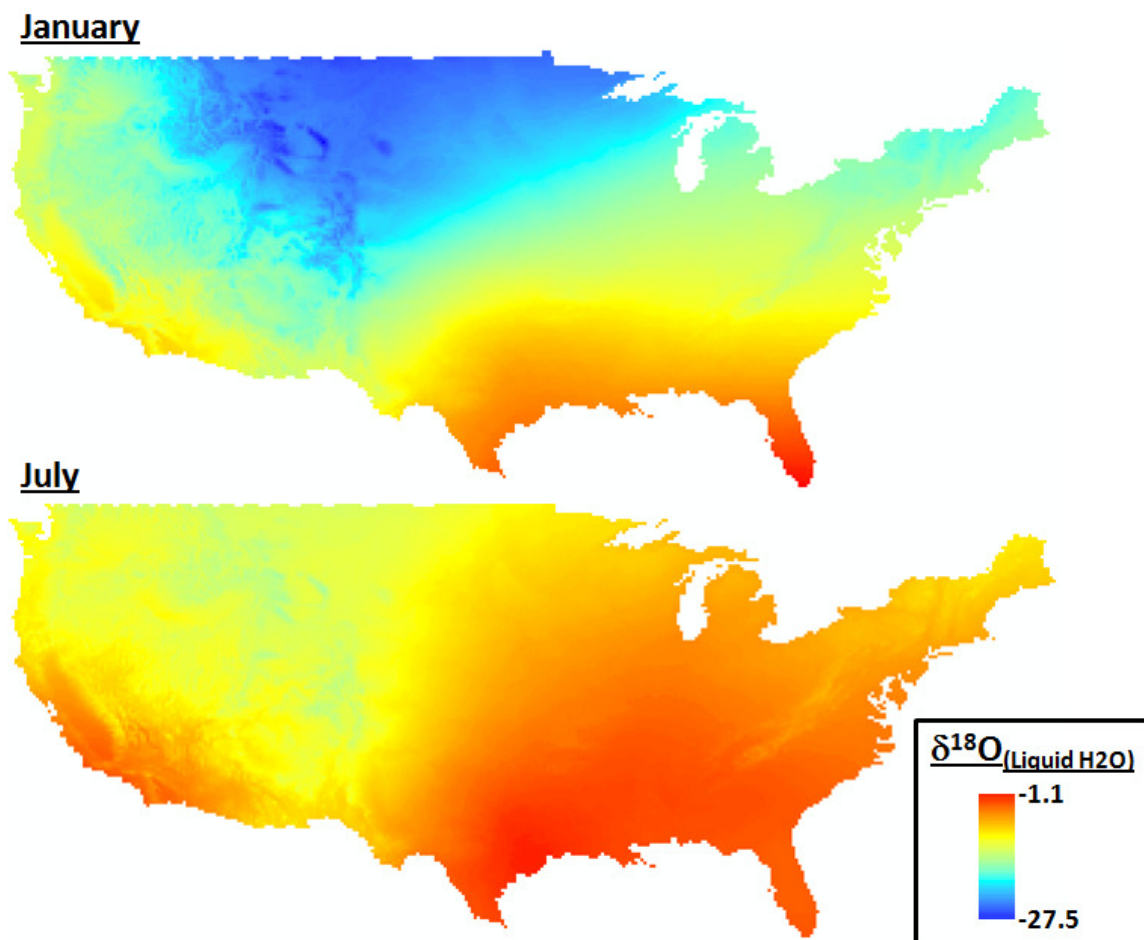


Figure 3.2: Spatial trends of the $\delta^{18}\text{O}_{(\text{Liquid H}_2\text{O})}$ dataset for the months of January and July.

3.4.2. $\delta^{18}\text{O}$ of the OH radical

As discussed above in section 3.2.5, the $\delta^{18}\text{O}$ of OH radical can be calculated based on fractionation factors between liquid water and water vapor in the atmosphere, followed by fractionation factors between atmospheric water vapor and the OH radical. The calculation used in this model is based on the equilibrium fractionation relationships between OH and water in the atmosphere, but there are other components of this isotopic system that need to be understood to accurately model $\delta^{18}\text{O}$ of OH in the atmosphere. Figure 3.3 shows the continuous United States' $\delta^{18}\text{O}$ of OH values calculated based on equilibrium fractionations for the winter and summer. These predicted $\delta^{18}\text{O}$ values range

from approximately -52.6 to -89.5‰ over the course of a year. Since the $\delta^{18}\text{O}$ of the OH radical has not yet been measured or determined experimentally, it is difficult to say if this range of values is accurate. Other factors which could have an effect on the $\delta^{18}\text{O}$ of OH in the atmosphere are kinetic isotope effects (which usually produce enrichments of ^{18}O on the order of approximately +100‰ as per Dubey et al., 1997) during the formation of the OH radical. Likely the true value of $\delta^{18}\text{O}$ from OH in the atmosphere is between the equilibrium range and the kinetic isotope approximation. OH radicals can react to form HO_x and subsequently H_2O_2 in the atmosphere. Previous measurements of $\delta^{18}\text{O}$ in atmospheric H_2O_2 show a range between +21.9 and +52.9 for the winter months (Savarino and Thiemens, 1999), which are values that would be expected between the calculated equilibrium OH radical $\delta^{18}\text{O}$ values and those predicted based on kinetic isotope effects from Dubey et al. (1997). It is possible that the $\delta^{18}\text{O}$ of H_2O_2 can be used to correct $\delta^{18}\text{O}$ values of OH calculated based solely on equilibrium fractionations, however the correction factor is greater than +120‰ and as a result is not used in our initial predictions as to the spatial arrangement of $\delta^{18}\text{O}$ values for the continuous United States.

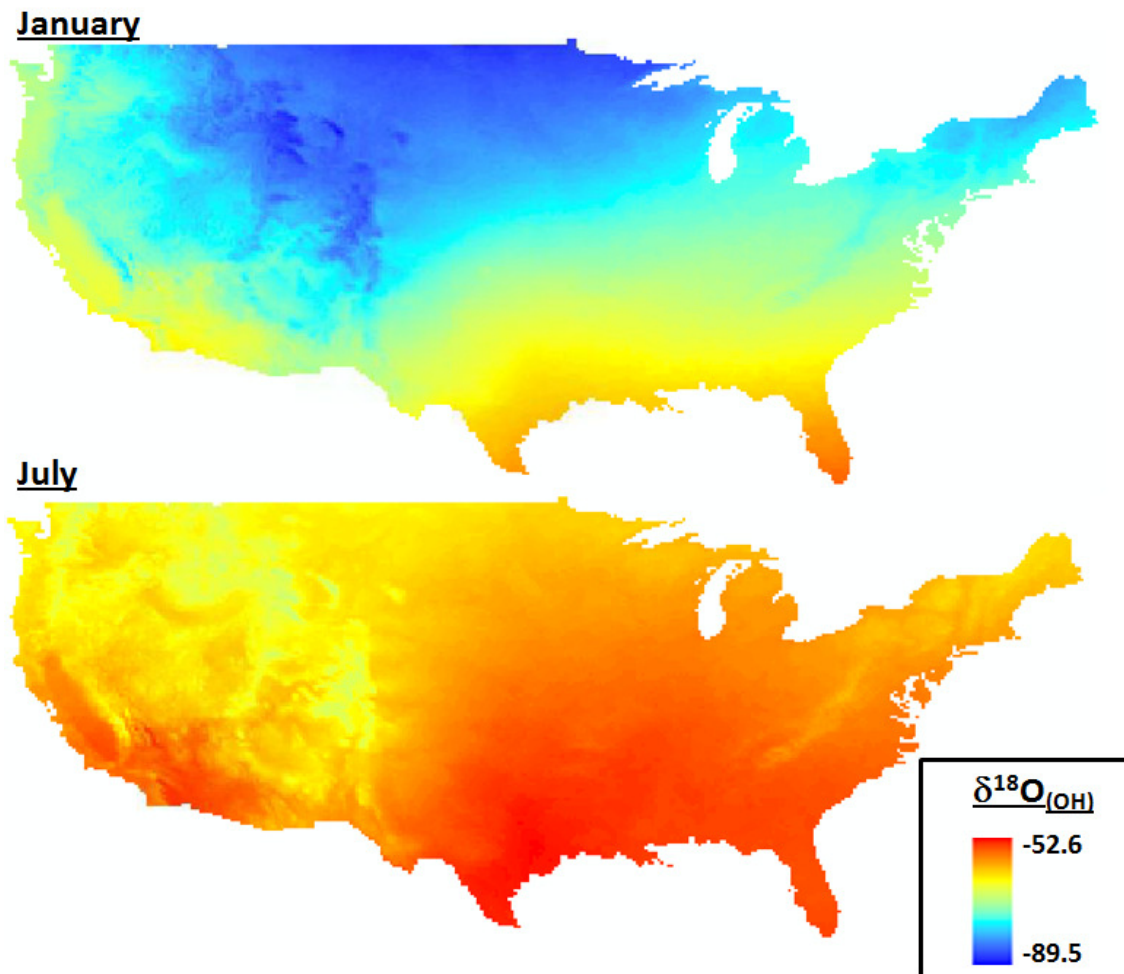


Figure 3.3: Spatial trends of the $\delta^{18}\text{O}_{(\text{OH})}$ dataset for the months of January and July based on equilibrium calculations.

3.4.3. $\delta^{18}\text{O}$ of Tropospheric O_3

As discussed in section 3.2.6, the temperature and pressure equations derived from Morton et al. (1990) do not share a common variable that makes it easy to simplify them into a single equation. However, both temperature and pressure vary with altitude (Figure 3.4). The dry adiabatic lapse rate is used for the variation of temperature with changes in altitude (-6.5 K/km), and the barometric formula (Berberan-Santos et al., 1997) (E3.21) is used for pressure:

$$P=P_b*\{T_b/[T_b+L_b*(h-h_b)]\}^{(g*M/R*L)} \quad (\text{E3.21})$$

where P_b is the static pressure in pascals, T_b is the standard temperature in degrees K (298 for the troposphere), L_b is the dry adiabatic lapse rate (K/m), h is the height above sea level (m), h_b is the height at the bottom of the layer being calculated for (0 m in the troposphere), R is the universal gas constant (N*M/(mol*K)), g is acceleration due to gravity, and M is the molar mass of Earth's air (0.0289644 kg/mol). This equation is used to test the potential range of estimated $\delta^{18}\text{O}$ values for tropospheric O_3 (Figure 3.5).

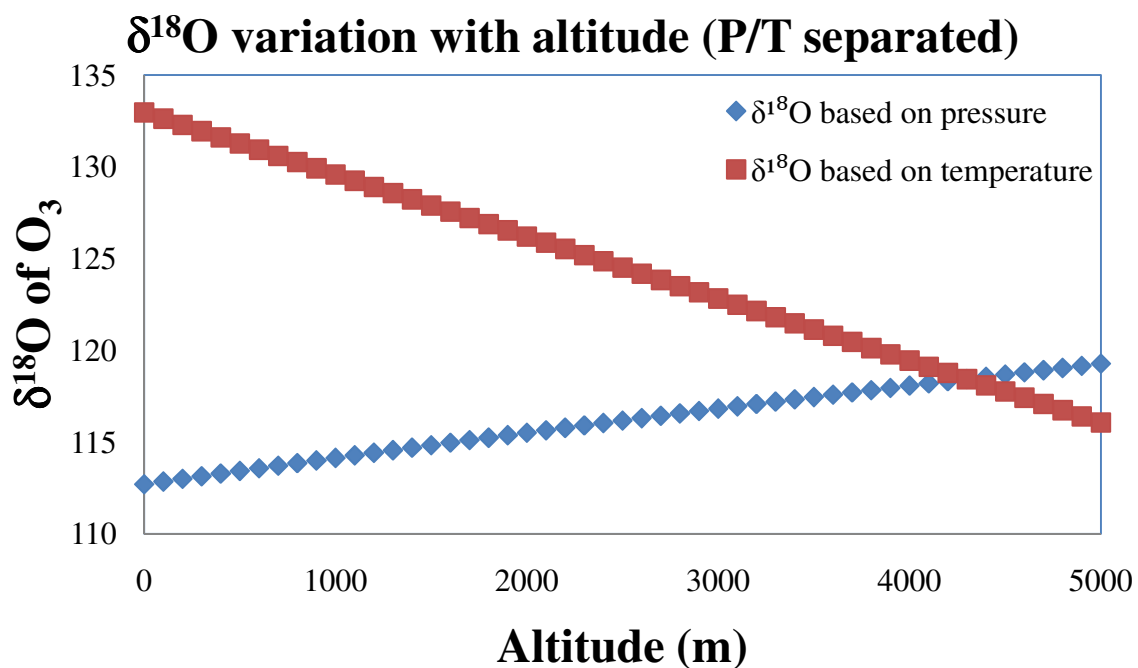


Figure 3.4: Variation of $\delta^{18}\text{O}$ with altitude, with P and T separated.

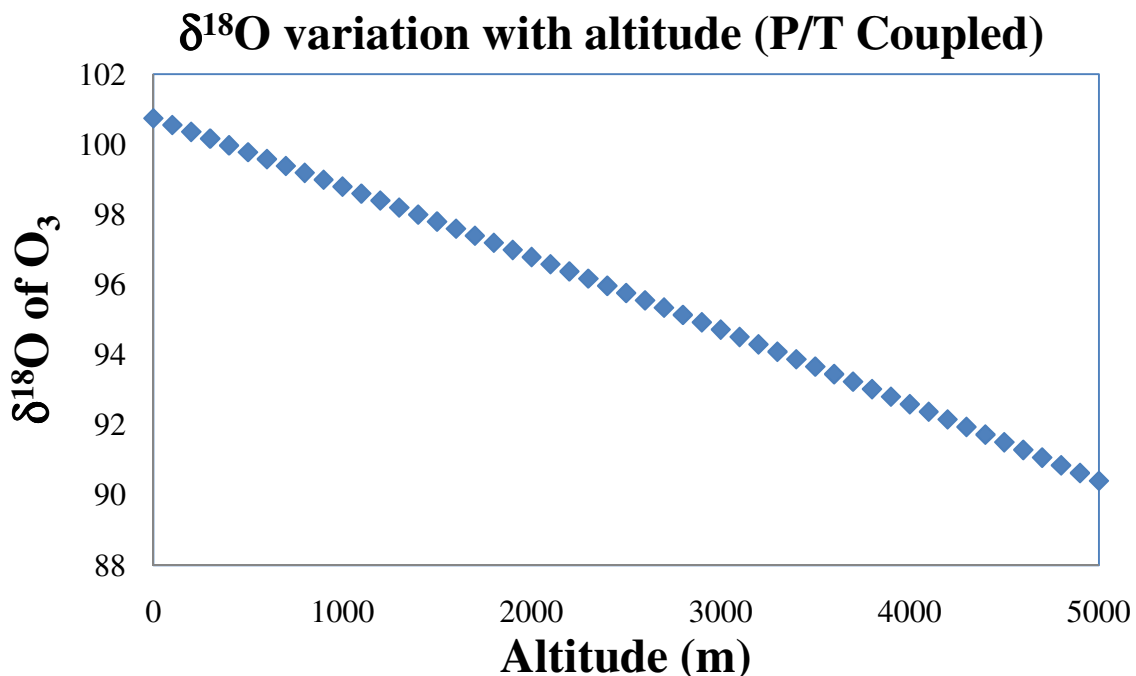


Figure 3.5: Variation of $\delta^{18}\text{O}$ in O_3 with altitude with T and P coupled.

A map showing the predicted spatial distribution of $\delta^{18}\text{O}$ of atmospheric O_3 in the continuous United States is presented in Figure 3.6. While pressure does not change significantly at the surface from day to day, changes in altitude cause significant changes in pressure. As per Equation 3.19, decreases in pressure are reflected in the resulting higher $\delta^{18}\text{O}$ value of O_3 at locations at higher altitudes. At these higher altitudes however, temperature is also lower which has an inverse effect on the $\delta^{18}\text{O}$ values of O_3 at these locations. Despite the negative correlation between pressure and the $\delta^{18}\text{O}$ value of tropospheric O_3 , the effect of temperature on the $\delta^{18}\text{O}$ value of O_3 is much more significant, and as a result even at the highest elevations the corresponding decreases in temperature cause lower $\delta^{18}\text{O}$ values. We see the lowest $\delta^{18}\text{O}$ values of tropospheric O_3 in the Northern United States compared to the Southern United States, as a result of this temperature dependence of the $\delta^{18}\text{O}$ of O_3 .

The value of $\delta^{18}\text{O}$ in ozone changes by approximately .52‰ per degree K, and - 0.0299‰ per torr ($\sim -0.003\%$ /m of altitude), further indicating that temperature is much

more significant in immediate changes to O_3 in the troposphere. The primary variable between seasons is temperature, and the predicted $\delta^{18}O$ values of atmospheric O_3 reflect these temperature changes between seasons, showing a swing in values from approximately +80.4‰ in the winter months to approximately +108.2‰ in the summer months. The changing $\delta^{18}O$ values of atmospheric O_3 greatly affect the $\delta^{18}O$ of atmospheric HNO_3 , as O_3 is very significant in the three HNO_3 production pathways. As a result, $\delta^{18}O$ values of HNO_3 can be correlated with $\delta^{18}O$ values of O_3 in the troposphere.

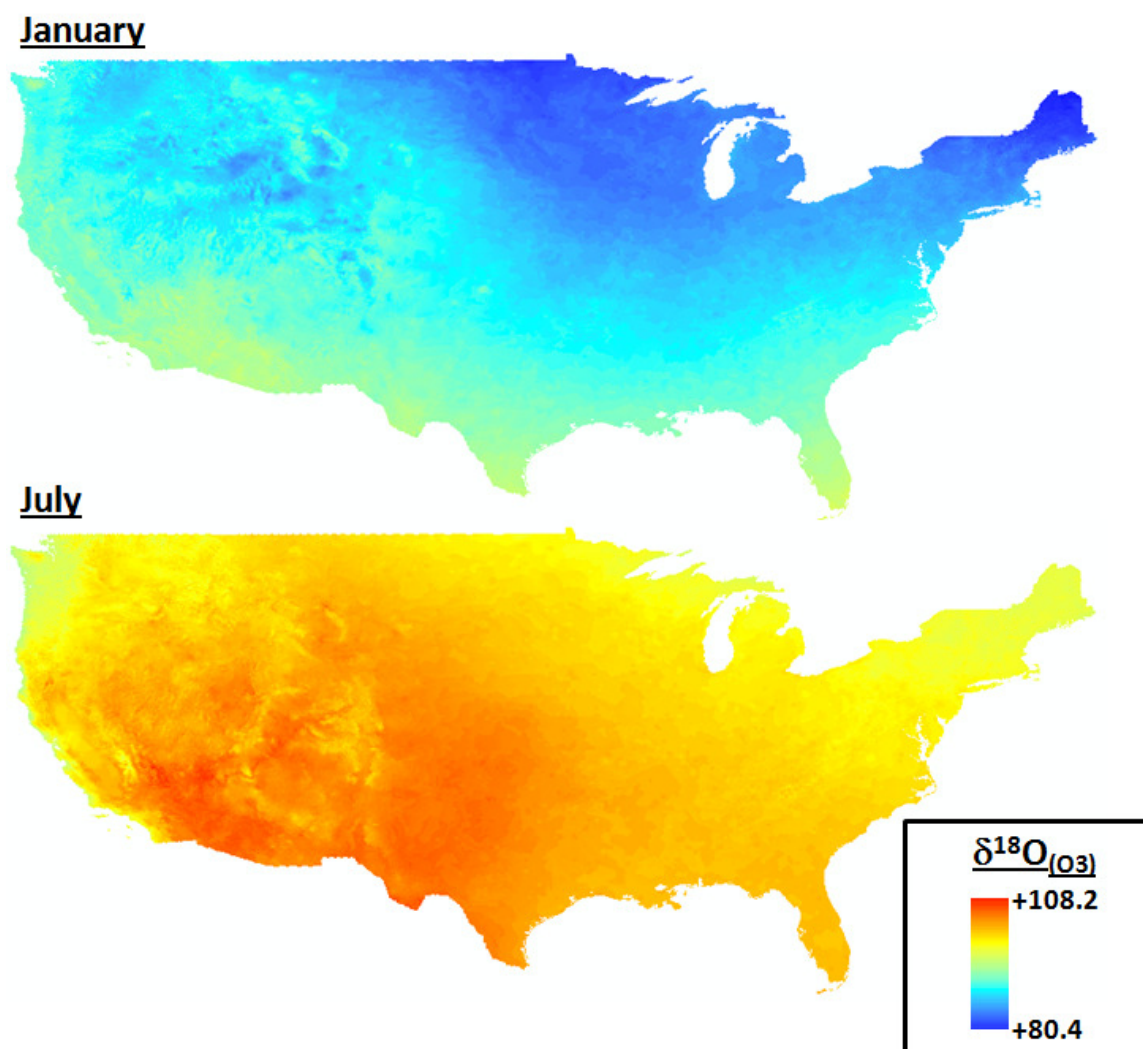


Figure 3.6: Spatial trends of the $\delta^{18}O_{(O_3)}$ dataset for the months of January and July.

The $\delta^{18}\text{O}$ values of O_3 predicted by this model are similar to previously published observations in La Jolla, CA (Johnston and Thiemens, 1997) (Figure 3.7). During the warmer months the predicted and measured values are very similar, however as temperatures change to colder the predicted and measured datasets become increasingly different. It is possible that the $\delta^{18}\text{O}$ of O_3 is underestimated by the model, particularly in the winter months, due to surface reactions and photolysis that are not accounted for in our mass balance scheme. Such processes would cause an enrichment of the $\delta^{18}\text{O}$ values of atmospheric O_3 , to be more similar to those observed in Johnston and Thiemens (1997) in the winter months.

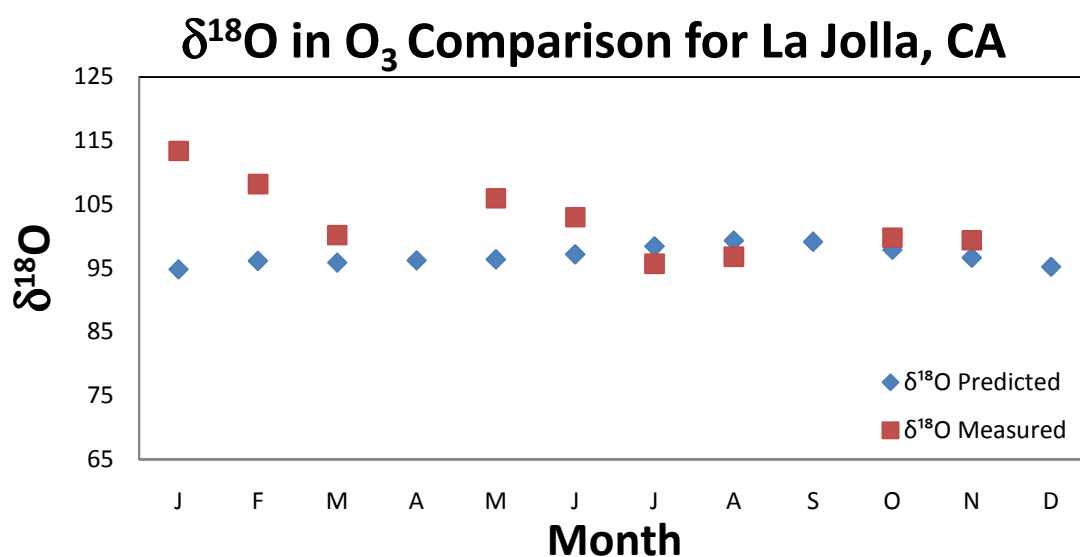


Figure 3.7. Comparison of predicted and observed $\delta^{18}\text{O}$ values for O_3 relative to VSMOW at La Jolla, CA. (data from Johnston and Thiemens, 1997).

3.4.4. Modeling HNO_3 production pathway R3.1

The $\text{NO}_2 + \text{OH} \rightarrow \text{HNO}_3$ pathway is usually the most dominant HNO_3 production pathway (e.g., Finlayson-Pitts and Pitts, 2000). A map showing the predicted spatial distribution of $\delta^{18}\text{O}$ values in HNO_3 produced from this pathway for January is shown in Figure 3.8. The values are very low, due to the equilibrium calculation of values of $\delta^{18}\text{O}$ in the OH radical, discussed above in section 3.3.2. The distribution of $\delta^{18}\text{O}$ values in

HNO₃ produced by this pathway, as it is a result of a mass balance between the $\delta^{18}\text{O}$ values of O₃, atmospheric O₂, and the OH radical, is heavily reliant on the temperature distribution. To a lesser extent, the spatial pressure distribution over the United States also effects the $\delta^{18}\text{O}$ values of HNO₃ produced from this pathway, however since there is only one O₃ component (detailed in E3.8) the pressure contribution is very small compared to that of temperature. The seasonal variations of the $\delta^{18}\text{O}$ values of HNO₃ from the NO₂ + OH \rightarrow HNO₃ pathway range from approximately +10‰ to approximately +25‰, based on equilibrium calculations for $\delta^{18}\text{O}$ of OH in Northwestern Indiana. These calculations use 0.8 for X (the fraction of O₃ contribution in the formation of NO₂).

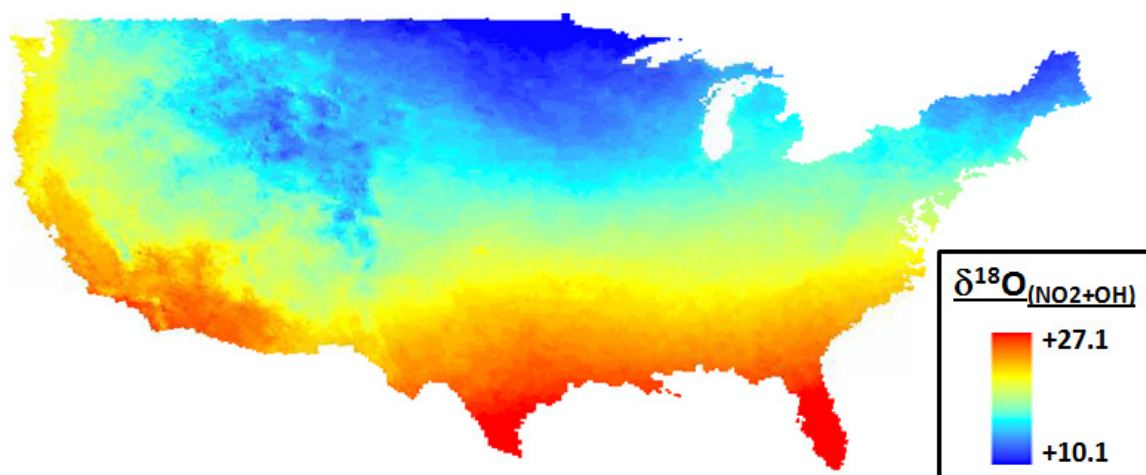


Figure 3.8: Spatial trends of the $\delta^{18}\text{O}_{(\text{NO}_2+\text{OH})}$ dataset for the month of January based purely on equilibrium fractionations for the $\delta^{18}\text{O}$ of OH

3.4.5. Modeling HNO₃ production pathway R3.2

The N₂O₅ + H₂O_(surface) \rightarrow 2HNO₃ pathway tends to be the second most prevalent HNO₃ production pathway (e.g., Finlayson-Pitts and Pitts, 2000). A map showing the predicted spatial distribution of $\delta^{18}\text{O}$ values of HNO₃ produced by this pathway for the continuous United States for January is shown in Figure 3.9. N₂O₅ is the product of NO₂ and NO₃. Both NO₂ and NO₃ have $\delta^{18}\text{O}$ values resulting from the combination of O₃ and

atmospheric O_2 , with NO_3 having a slightly greater contribution of O_3 as NO_2 reacts with O_3 to produce NO_3 in the atmosphere. HNO_3 produced from this pathway has 1/6 of its oxygen come from H_2O on the surface of an aerosol. The addition of H_2O in this mass balance depletes the $\delta^{18}O$ values of HNO_3 predicted from this pathway.

The seasonal variations of $\delta^{18}O$ values of HNO_3 in Northern Indiana from the $N_2O_5 + H_2O_{(surface)} \rightarrow 2HNO_3$ reaction pathway show a range of values between approximately +50‰ in the winter months to approximately +61‰ in the summer months. As with the other seasonal effects shown in this chapter, seasonal variations of $\delta^{18}O$ in HNO_3 produced by this pathway are primarily driven by temperature. The spatial distribution of $\delta^{18}O$ values produced from this pathway shows the highest values in the southern US and the lowest values in the northern US. High elevations, where temperatures are low, show some of the lowest $\delta^{18}O$ values in the US, however these values are generally not as low as the northern Midwest or Northeastern US.

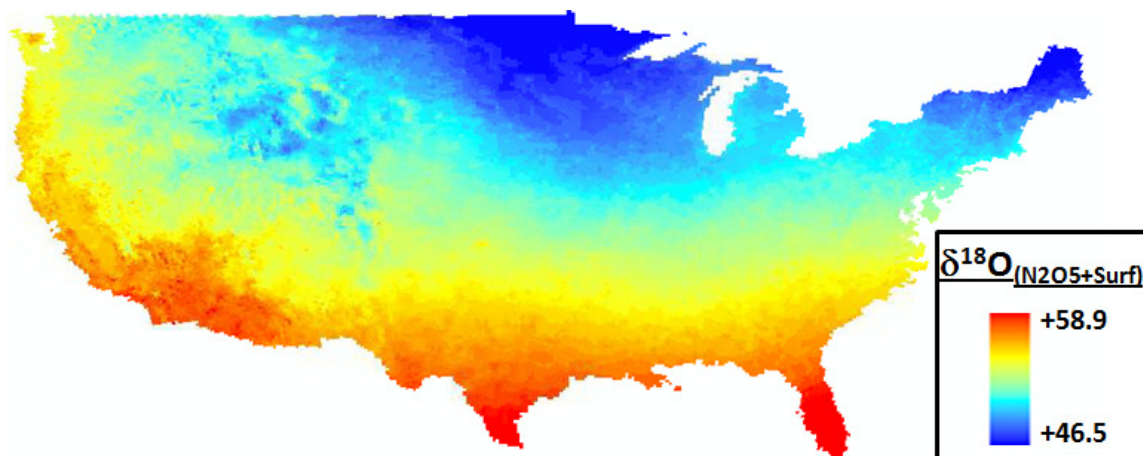


Figure 3.9: Spatial trends of the $\delta^{18}O_{(N_2O_5+surface)}$ dataset for the month of January

3.4.6. Modeling HNO_3 production pathway R3.3

A map showing the predicted spatial distribution of $\delta^{18}O$ of HNO_3 values produced from the $NO_3 + VOC \rightarrow HNO_3$ pathway for the continuous United States in

January is shown in Figure 3.10 as the spatial distribution of the $\delta^{18}\text{O}$ of NO_3 . This is due to the lack of contribution of VOC to the $\delta^{18}\text{O}$ value of HNO_3 produced by this pathway. The $\delta^{18}\text{O}$ values predicted for this pathway are the result of a mass balance between $\delta^{18}\text{O}$ values atmospheric O_3 and $\delta^{18}\text{O}$ values of atmospheric O_2 . As with the other two HNO_3 production pathways, the spatial variation is controlled mostly by temperature, though the role of pressure in these calculations should not be disregarded. Since atmospheric O_3 is the primary component of this mass balance, the pressure effect on the $\delta^{18}\text{O}$ value of atmospheric O_3 is noticeable in mountainous regions where pressure is reduced due to high altitudes.

Seasonal variations of the $\delta^{18}\text{O}$ values of HNO_3 produced by this pathway range from approximately +65‰ in the winter months to approximately +77‰ in the summer months based on predictions for Northwest Indiana. As with the other HNO_3 production pathways, seasonal variations in $\delta^{18}\text{O}$ values for HNO_3 produced from this pathway are primarily the result of changes in temperature from season to season. This results in higher values in the colder months and lower values in the warmer months of the year.

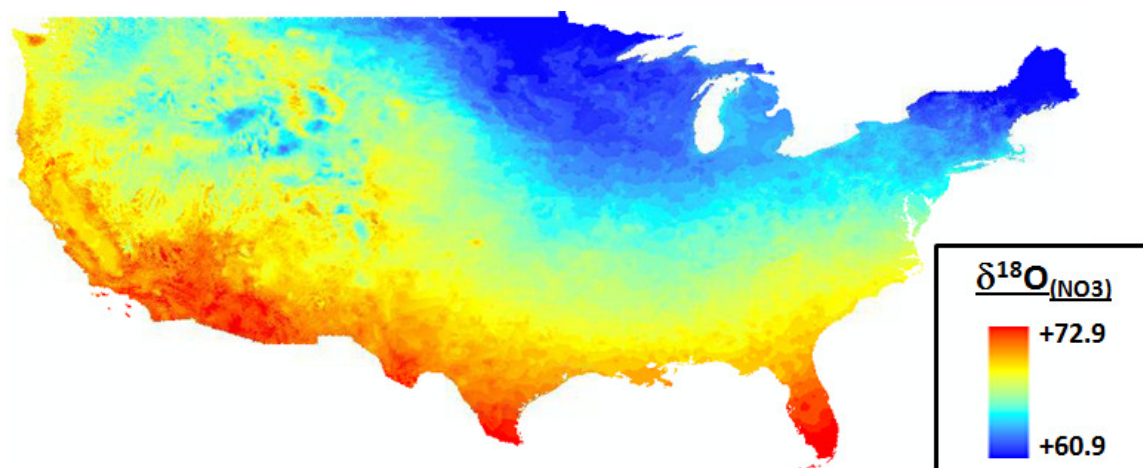


Figure 3.10: Spatial trends of $\delta^{18}\text{O}_{(\text{NO}_3+\text{VOC})}$ shown as the $\delta^{18}\text{O}_{(\text{NO}_3)}$ dataset for the month of January

3.4.7. Total HNO₃

Assumed β , χ , and ζ values of the three HNO₃ production pathways allows for the calculation of a spatial dataset showing the total $\delta^{18}\text{O}$ of HNO₃ resulting from all three of the HNO₃ production pathways reacting simultaneously. Figure 3.11 is a predicted dataset for total HNO₃ across the continuous United States using assumed β , χ , and ζ values of 0.78, 0.2, and 0.02 for the pathways R 4.1, 4.2, and 4.3, respectively. These predicted values are just for the sake of the production of Figure 3.10, and do not necessarily reflect an actual model simulation. During model simulations, values for β , χ , and ζ will be calculated based on the RACM (Stockwell et al., 1997) model of regional atmospheric chemistry.

Figure 3.10 shows low values compared to NO₃⁻ measured in work by other authors, which is likely the result of the predicted $\delta^{18}\text{O}$ values from R3.1. The low values for the $\delta^{18}\text{O}$ of the OH radical in that pathway result in lower than expected $\delta^{18}\text{O}$ values further along in the mass-balance. Applying the correction described above ($\sim +120\%$) (Savarino and Thiemens, 1999) may result in a potentially more ideal value for the $\delta^{18}\text{O}$ of OH to be used in the calculation of $\delta^{18}\text{O}$ of HNO₃.

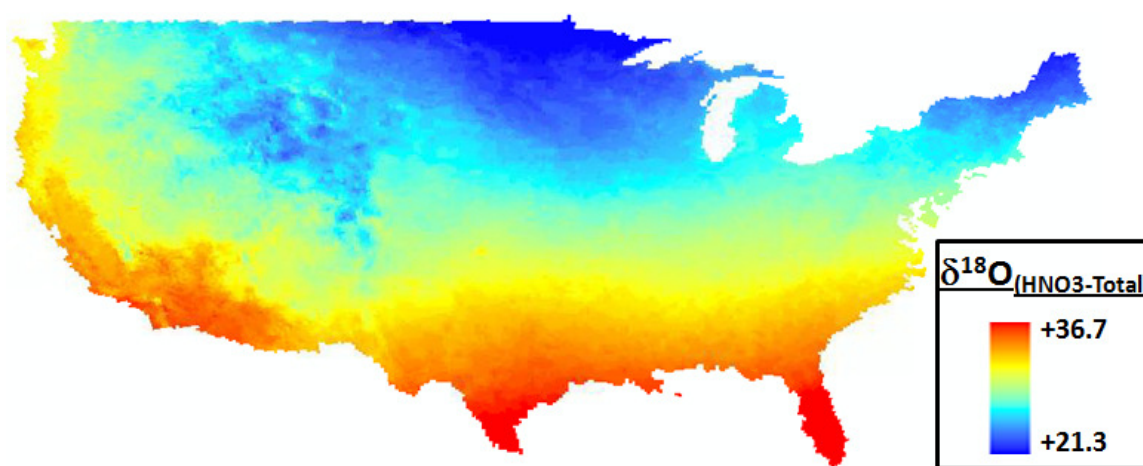


Figure 3.11: Spatial trends of the $\delta^{18}\text{O}_{(\text{total HNO}_3)}$ dataset for the month of January based on equilibrium fractionations for the $\delta^{18}\text{O}$ of OH

3.5. Conclusions and Future Considerations

The first attempt at modeling $\delta^{18}\text{O}$ of atmospheric HNO_3 is shown here. This approach utilizes simple isotopic mass-balance approximations to predict values of $\delta^{18}\text{O}$ in atmospheric HNO_3 . This mass balance is based on the three primary HNO_3 production pathways in the atmosphere: R3.1, 3.2, and 3.3. The primary components of an isotopic mass balance predicting $\delta^{18}\text{O}$ values of HNO_3 are the $\delta^{18}\text{O}$ of atmospheric OH, O_3 , and liquid water. $\delta^{18}\text{O}$ of liquid water is a known dataset, and based on temperature, pressure, and liquid water, the $\delta^{18}\text{O}$ of O_3 and OH are calculated. Presented here are the results of these mass-balance calculations, as well as a detailed description of every component of this mass-balance. Results of this modeling effort utilizing assumed mole fraction values are summarized in figures in section 3.3. This model has been integrated into a web interface (operational by December, 2010), found at <http://michalski.eas.purdue.edu/racm>, which allows for easy location-based $\delta^{18}\text{O}$ of HNO_3 predictions. A comparison of the output of this model with measured results is carried out in Chapter 4 of this thesis. A mass-balance approach such as this one is a powerful tool which can aid in interpretations of $\delta^{18}\text{O}$ measurements of HNO_3 .

One way to improve the model output would be a better handle on the mechanisms controlling the formation of the OH radical in the atmosphere. As an equilibrium approach to the $\delta^{18}\text{O}$ value of the OH radical yields very low results, and a kinetics approach to the $\delta^{18}\text{O}$ value of the OH radical yields very high results, it is difficult currently to calculate the $\delta^{18}\text{O}$ of OH in the atmosphere. Given that oxidation of NO_2 by OH in the atmosphere is one of the most prevalent HNO_3 -producing reactions, it is of the utmost importance that modeling efforts are able to utilize reasonably accurate $\delta^{18}\text{O}$ values of OH. Once the equilibrium/kinetic mechanisms of the OH radical in the atmosphere are clarified, accurate $\delta^{18}\text{O}$ values can be calculated for OH and utilized to produce accurate $\delta^{18}\text{O}$ predictions of HNO_3 in the atmosphere. Despite this lack of understanding, it is possible to apply a correction to the equilibrium $\delta^{18}\text{O}$ of OH based on the $\delta^{18}\text{O}$ value of H_2O_2 measured by Savarino and Thiemens (1999). This correction may bring the $\delta^{18}\text{O}$ values of OH to a more reasonable range for this mass balance modeling

effort, but a better understanding of atmospheric processes and how they relate to the $\delta^{18}\text{O}$ of OH is needed before the application of such a correction can be seen as viable.

Another possible correction to the mass balance approximations described here is an increase in the $\delta^{18}\text{O}$ of O_3 , at least during the winter months. Since previously reported values from Johnston and Thiemens (1997) show O_3 more enriched in the winter months when compared to model predictions, there is reason to believe that either the model is incorrect in its accounting for O_3 during these times, or that the measurements of $\delta^{18}\text{O}$ of O_3 are incorrect. If our model is at fault, this is likely due to photolysis and aerosol surface reactions that are not properly accounted for in the mass balance. A +15‰ correction to the model predictions for the $\delta^{18}\text{O}$ of O_3 in winter brings the values into better agreement with the observed values in La Jolla, CA by (Johnston and Thiemens (1997)).

CHAPTER 4. AN APPLICATION OF THE MODELING APPROACH TO A SITE IN NORTHWESTERN INDIANA

4.1. Technical Note

This chapter details the use of the model described in Chapter 3 at the Indiana Dunes National Lakeshore to predict $\delta^{18}O$ in atmospheric HNO_3 in precipitation. Isotopic analysis of the precipitation at this site is compared with model predictions. Material in this chapter is meant to stand on its own, though the theory behind the model presented in Chapter 3 will help with understanding the data and interpretations described here.

4.2. Introduction

There is growing concern regarding NO_x ($NO+NO_2$) emissions from the widespread use of fossil fuels and their subsequent effects on the environment and human health. NO_x is primarily emitted as a by-product of fossil fuel combustion (Galloway, 1998; Galloway et al., 2004). In addition to fossil fuel combustion, NO_x is emitted through natural processes such as biological metabolism in soil, lightning, and wildfires (Ehhalt et al., 2001). In the atmosphere, NO_x is oxidized in several ways to form atmospheric nitric acid (HNO_3), which can be removed by precipitation (acid rain). This acidifies soils and results in forest and crop damage (e.g., Likens et al., 2000). The increased nitrogen (N) content of precipitation can wash into bodies of water and cause eutrophication (Rabalais, 2002). Excess N deposition can also limit the diversity of terrestrial plant ecosystems (Fenn et al., 2008; Bobbink et al., 2010). Additionally, HNO_3 in the atmosphere can effect aerosol composition and size, which could increase albedo and cause global cooling (Zhang et al., 2000; Seinfeld and Pandis, 2006). These concerns

make it important to better understand NO_x emissions and the chemistry which is responsible for the formation of atmospheric HNO_3 .

Atmospheric HNO_3 is formed through three primary pathways:



NO_2 (R4.1) forms from a reaction of NO with ozone or peroxy radicals in the atmosphere (R4.4-4.8), NO_3 (R4.3) forms from a reaction of NO_2 with O_3 (R4.9), and N_2O_5 forms from a reaction of NO_2 with NO_3 (R4.10).



NO is regenerated when NO_2 is photolyzed by light at wavelengths less than 420nm (R4.7). R4.7 occurs roughly once every three minutes under daytime conditions at mid-latitudes (Seinfeld and Pandis, 2006). This allows for multiple cycles of R4.4, R4.7, and R4.8, which promotes rapid cycling between NO_x and atmospheric O_2 . This rapid cycling causes O_2 to equilibrate with NO_x via reactions R4.5, R4.6, and R4.7.

Key to understanding atmospheric nitrate is the identification of the potential NO_x sources and chemical alterations that can take place in the atmosphere. The stable isotopes of N and oxygen (O) have recently been used for this identification. Stable isotopes of N (^{14}N , ^{15}N) are primarily used for source determination (e.g., Elliott et al.,

2009, Hastings et al., 2003) whereas stable isotopes of O (^{16}O , ^{17}O , ^{18}O) have been used for determination of atmospheric alterations of NO_x (e.g., Michalski et al., 2004; Savarino et al., 2007). Stable isotope values are reported in standard delta (δ) notation in parts per thousand (permil: ‰), with the ratio of heavy to light isotopes in a sample being held relative to that of a globally accepted reference material. The standard reference material for ^{15}N is air N_2 , and for ^{18}O is Vienna Standard Mean Ocean Water (VSMOW). When used together, both ^{15}N and ^{18}O provide a powerful set of tools which can aid in understanding NO_x source and alterations in the atmosphere.

Several previous studies have used isotopes of N and O in the examination of atmospheric NO_3^- from precipitation samples to examine yearly trends. These samples are collected at a variety of geographic locations, altitudes, and climates. $\delta^{15}\text{N}$ values from atmospheric NO_3^- are useful for determining NO_x emission source type (e.g., Elliott et al., 2007; Elliott et al., 2009). The use of $\delta^{18}\text{O}$ in isotopic studies of atmospheric NO_3^- however is less apparent. $\delta^{18}\text{O}$ of atmospheric NO_3^- has been measured in many studies (e.g., Hastings et al., 2003; Elliott et al., 2007; Elliott et al., 2009), but many authors are uncertain regarding interpretation of $\delta^{18}\text{O}$ values from atmospheric NO_3^- (e.g., Hastings et al., 2003). These authors acknowledge that since the production of HNO_3 in the atmosphere is primarily driven by the transfer of oxygen atoms (R4.1-4.3), changes in oxygen isotope values are likely to indicate chemical alteration in the atmosphere rather than source. Beyond this basic understanding however, a quantitative determination of HNO_3 production pathway prevalence is lacking from these studies. Recently a model based on mass-balance relationships of HNO_3 production in the atmosphere has been developed (Chapter 3 of this thesis). Here, the output of the simple mass balance model is compared with measured $\delta^{18}\text{O}$ values from precipitation at a site in Northwest Indiana. The mass balance relationships which drive this model (available at <http://michalski.eas.purdue.edu/racm>; site fully operational by December, 2010), are coupled with the RACM (Stockwell et al., 1997) model for the determination of NO_x oxidation pathway prevalence.

4.3. Methods

4.3.1. Study Location: Indiana Dunes National Lakeshore, IN, USA

Samples in this study were collected near the Indiana Dunes National Lakeshore as part of the National Atmospheric Deposition Program (NADP) network (NADP site IN34). The Indiana Dunes National Lakeshore ($41^{\circ}37'53.40''\text{N}$, $87^{\circ}5'16.99''\text{W}$) is located in Lake, Porter, and Laporte Counties in Northwest Indiana (Figure 4.2). Emissions of pollutants at this site are influenced by three major areas: The Gary, IN/Chicago, IL metropolitan region, Lake Michigan, and the surrounding agricultural in regions in Lake, Porter, and LaPorte counties, Indiana.

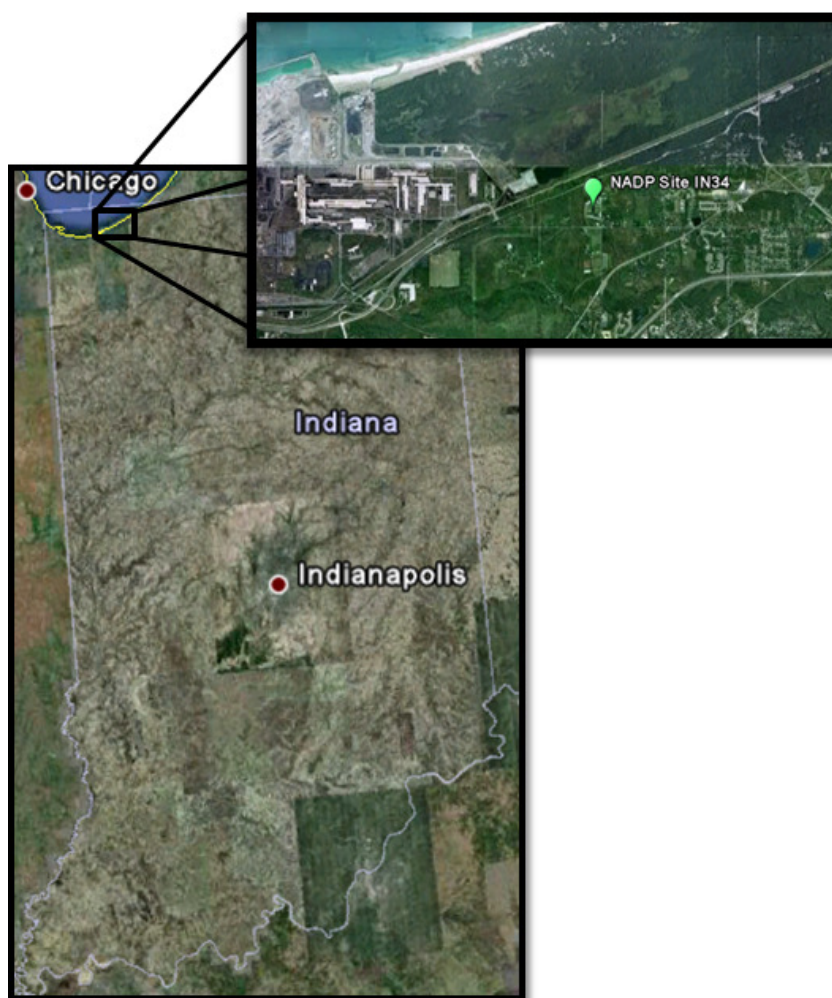


Figure 4.1: Location map of the Indiana Dunes National Lakeshore NADP site IN34

The EPA emissions inventories for this site and the surrounding areas (Table 4.1) show heavy influence of anthropogenic NO_x sources, particularly from the Gary (Lake County, IN) / Chicago (Cook County, IL) metropolitan region. This region's contribution to the atmospheric NO_x budget is primarily due to on-road vehicle emissions from Chicago, IL, although non-road equipment also greatly contributes to NO_x emissions in the area. The third most prevalent NO_x emissions source is general fossil fuel combustion not related to vehicles (Appendix A).

Emissions to the Indiana Dunes National Lakeshore from Lake Michigan are likely a combination of emissions from Chicago, IL, and areas north of Chicago brought to the Indiana Dunes by regional winds. NO_x emissions from agricultural areas, such as LaPorte County, IN, are much lower relative to the more industrialized areas of Lake and Cook counties (IN and IL, respectively). The primary NO_x source in areas such as LaPorte County is electricity generation, with the only other major source of NO_x being vehicle emissions. Anthropogenic NO_x dominate the NO_x inventory when compared to biogenic NO_x emissions at these locations, which is consistent with global trends (Jaegle et al., 2005).

Table 4.1: 2005 EPA emissions inventory for areas near NADP site IN34 (emissions in tons NO_x/year)

Category	Cook County, IL	Lake County, IN	Porter County, IN	LaPorte County, IN
Electricity Generation	4,019	8,258	12,379	5,156
Industrial Processes	2,832	10,377	3,949	30
Fossil Fuel Combustion	26,193	7,253	3,916	563
On-road Vehicles	76,050	9,044	3,567	3,135
Non-road equipment	64,104	7,857	3,359	N/A
Waste Disposal	738	126	67	65
Solvent Use	334	14	14	6
Residential Wood Combustion	42	3	2	5
Miscellaneous	15	2	N/A	N/A

Table 4.1: Continued

Biogenic NO _x	216	290	230	290
Total	174,543	43,224	27,483	9,250

4.3.2. Sample Collection and Preparation

Precipitation samples from the Indiana Dunes National Lakeshore were collected by the NADP over the years 2001-2003. Weekly precipitation samples are collected every Tuesday morning from bucket collectors following NADP protocols (<http://nadp.sws.uiuc.edu/educ/sample.aspx>). These samples are transported to the NADP laboratory for analysis of pH and conductivity, and are then filtered and stored in several (if applicable) 60mL bottles (Nalgene). One 60mL bottle per sample is retained by the NADP for analysis, where the others are archived under refrigeration for up to five years. Analysis by the NADP on the one retained 60mL bottle includes concentration analysis of anions (chloride, sulfate, and nitrate by ion chromatography), cations (calcium, magnesium, sodium and potassium by inductively-coupled plasma-optical emissions spectroscopy), and ammonium and orthophosphate by flow-injection analysis. The NADP employs a rigorous quality assurance process which includes frequent random checking the cleanliness of all equipment in the field and in the laboratory, as well as regular maintenance and calibration of analytical equipment. Data and archived samples for 2001-2003 from the IN34 NADP site were obtained by the Purdue Stable Isotope (PSI) Laboratory for isotopic analysis of NO₃⁻ in these samples. Since samples are taken weekly, the expected number of samples is 156 for the years 2001-2003. However, in some cases it did not rain or rained very little and there was not enough sample to archive. As a result, this study utilizes 98 samples from 2001-2003.

In order to prepare the NADP samples for isotopic analysis of NO₃⁻, the IC instrumentation in the PSI lab was been modified into a preparative instrument which separates the NO₃⁻ fraction from other anions in solution (Chapter 2). The sample pump of the IC is set to 1 mL/min and pumps until the sample volume is depleted (15 or 50mL depending on sample concentration) by 90%. Samples are prepared based on NO₃⁻

concentration data from the NADP to ensure that 300nMol of NO_3^- is present in each sample. As not all NADP samples are the same concentration, the volume required for 300nMol NO_3^- will be different for each sample. Depending on the volume required for 300nMol NO_3^- , the appropriate volume of sample is pipetted into a 15 or 50mL centrifuge tube. For consistency of pumping time across all samples in the same type of tube, samples are segregated based on centrifuge tube size and then diluted to either 15 or 50mL to correspond to the smaller or larger centrifuge tubes, respectively. The sample is pumped directly onto one of two alternating Dionex AS-14A anion exchange columns to separate NO_3^- ions from the rest of the sample. After elution from the column, the NO_3^- fraction is collected in a 5mL centrifuge tube using the Spectrum CF-1 fraction collector. The NO_3^- fraction, containing 300nMol of NO_3^- , is freeze-dried to 3mL to ensure 100nMol/mL NO_3^- . Typically a concern regarding freeze drying NO_3^- is the possible volatilization of acids as H_2O is removed from solution, effectively reducing the viability of isotopic results obtained from those samples. This was not a concern however, as the 0.0018M/0.0017M $\text{NaHCO}_3/\text{Na}_2\text{CO}_3$ mobile phase buffers the NO_3^- fraction so that volatilization does not occur even when dried to completion. The fraction is then taken for isotope analysis.

4.3.3. Isotope Analysis of NO_3^- using the Denitrifier Method

The NO_3^- fraction is prepared for analysis via the denitrifier method (Sigman et al., 2001; Casciotti et al., 2002) interfaced to a Thermo Delta V Isotope Ratio Mass Spectrometer (IRMS). This technique uses *P. aureofaciens* bacteria to convert NO_3^- to $\text{N}_2\text{O}_{(g)}$. The N_2O gas produced is then purified and carried by helium through a continuous flow interface into the IRMS for analysis.

The denitrifier method was modified from that published (Sigman et al., 2001, Casciotti et al. 2002) in two ways. First, Sigman et al. purges their bacteria solution in a vial for 2 hours at 10-20mL N_2/min (to remove atmospheric air from the vial), where our method purges at 40mL He/min . Second, Sigman et al. incubates their samples for an overnight period, where we incubate for only one hour. Tests were completed by Crawley

(2010 *master's thesis*) to show that there is no significant difference in $\delta^{15}\text{N}$ and $\delta^{18}\text{O}$ values for incubation times greater than 1 hour, unless working with samples with over 100ppm NO_3^- . In these cases, incubating the samples for 2 hours is sufficient for complete conversion by the bacteria of NO_3^- to $\text{N}_2\text{O}_{(\text{g})}$. Based on replicated standard analysis of the 5 calibrated working reference standards used in the PSI lab for the denitrifier method, the best precision obtained was $\pm 0.7\text{‰}$ for $\delta^{18}\text{O}$ and 0.6‰ for $\delta^{15}\text{N}$.

The five standards used are “Hoffman-20”, “NCSU”, “Hoffman-10”, “Hoffman-1”, and “NC32”. The Hoffman-20 standard is a Chilean fertilizer KNO_3 that has been calibrated using the USGS35 international reference standard as an intermediate, where the NCSU standard is a KNO_3 that was calibrated at North Carolina State University. The standards used, composition, and isotope values are shown in Table 4.2.

Table 4.2: Isotopic Standard Composition and δ Values (‰)

Standard	Composition	$\delta^{15}\text{N}$ ($\text{N}_2\text{-Air}$)	$\delta^{18}\text{O}$ (VSMOW)
Hoffman-20	100% Hoffman	3.2	54.3
Hoffman-10	50% Hoffman/50% NC32	9.2	17.8
Hoffman-1	5% Hoffman/95% NC32	14.7	-15.2
NC32	93% NCSU/7% USGS32	15.3	-18.8
NCSU	100% NCSU	-2.2	-23.5

Analyses of these standards show that they are linear, making for easy calibration of measured results.

4.3.4. A Simple Mass Balance for the Prediction of $\delta^{18}\text{O}$

Results for $\delta^{18}\text{O}$ of atmospheric NO_3^- in precipitation measured in this study are compared to modeled results from the mass-balance model described in Chapter 3 of this thesis. The model uses several isotopic mass-balance relationships to calculate $\delta^{18}\text{O}$ of several atmospheric species including the OH radical and tropospheric O_3 . These $\delta^{18}\text{O}$ values are coupled with air quality data and through the RACM (Stockwell et al., 1997)

model to compute the total $\delta^{18}\text{O}$ of atmospheric HNO_3 through the three primary HNO_3 producing pathways in the atmosphere (R4.1-4.3).

A mass-balance approximation of $\delta^{18}\text{O}$ in atmospheric NO_3^- is accomplished by reducing the chemical equations responsible for the formation of atmospheric NO_3^- into simple mathematical relationships. These relationships must be based in part on observed data for components that may have an effect the atmospheric HNO_3 production system, such as temperature, pressure, and the initial $\delta^{18}\text{O}$ abundance of liquid water in the atmosphere. Surface temperature and pressure data used in this study for Northwest Indiana is publicly available from the Indiana Department of Environmental Management. $\delta^{18}\text{O}$ of liquid water in the atmosphere is publicly available at <http://www.waterisotopes.org> (Bowen and Ravenaugh, 2003). Temperature is used primarily with the calculation of fractionation factors between $\text{H}_2\text{O}_{(\text{liquid})}$, $\text{H}_2\text{O}_{(\text{gas})}$, and the OH radical. Temperature and pressure are used to calculate the $\delta^{18}\text{O}$ of tropospheric O_3 , as per calculations outlined in Morton (1990), Savarino et al. (2008) and clarified in Chapter 3 of this thesis. The $\delta^{18}\text{O}$ of liquid water is used in calculations of $\delta^{18}\text{O}$ values of $\text{H}_2\text{O}_{(\text{gas})}$ in the atmosphere, which feeds into the calculation of $\delta^{18}\text{O}$ values of the OH radical, as well as in the calculation of the $\delta^{18}\text{O}$ of HNO_3 produced by R4.2. A detailed description of these calculations and the mass-balance model is in Chapter 3 of this thesis.

4.4. Results

4.4.1. Sample Data

Figures 4.2, 4.3, and 4.4 show $\delta^{15}\text{N}$ and $\delta^{18}\text{O}$ values from NO_3^- in precipitation that fell on the Indiana Dunes National Lakeshore during the years 2001 - 2003. Data from these years all share what appear to be noticeable seasonal trends over the course of a year for the measured $\delta^{18}\text{O}$ values. Specifically, the noted trends show an increase in

$\delta^{18}\text{O}$ values during the colder months and a decrease during the warmer months. For $\delta^{15}\text{N}$, however, the trends are far less clear.

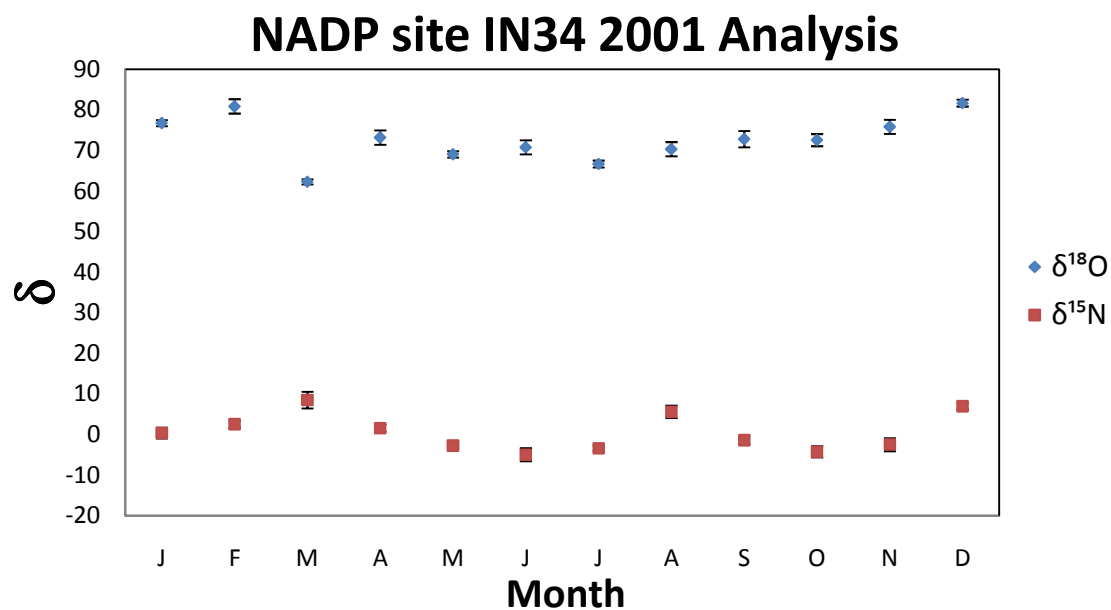


Figure 4.2: Monthly averaged results for NO_3^- in precipitation collected at the Indiana Dunes National Lakeshore in 2001

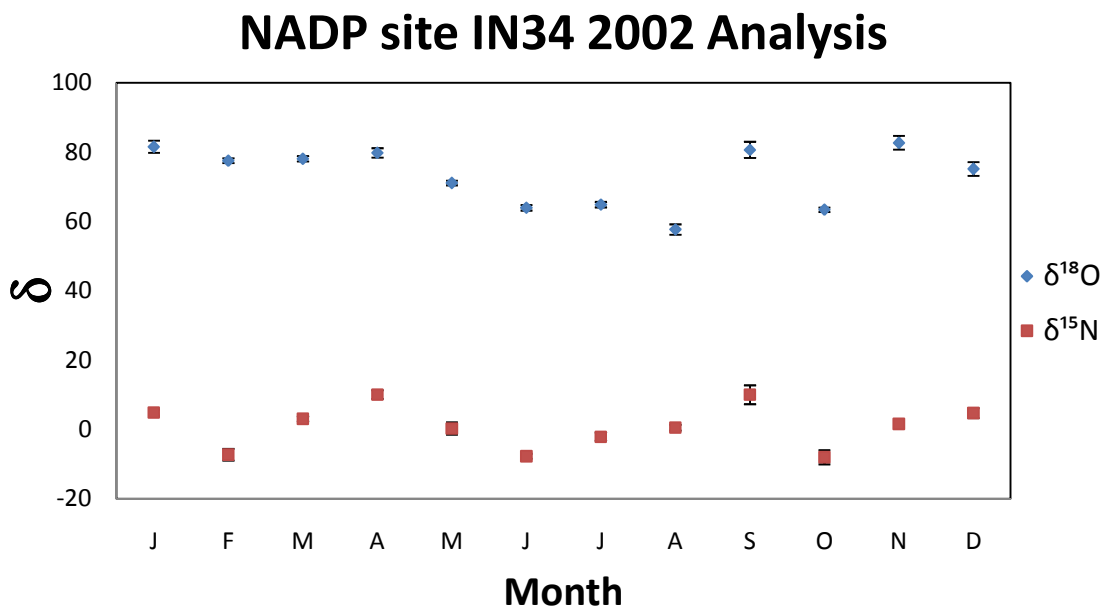


Figure 4.3: Monthly-averaged isotopic results for NO_3^- in precipitation collected at the Indiana Dunes National Lakeshore in 2002

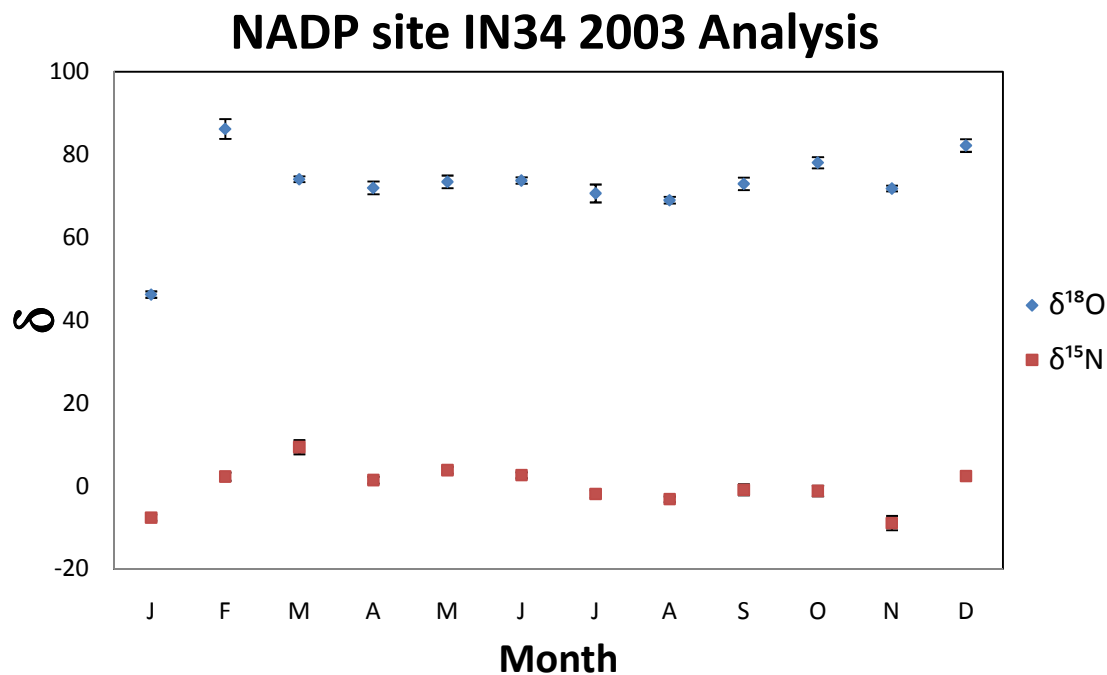


Figure 4.4: Monthly-averaged isotopic results for NO_3^- in precipitation collected at the Indiana Dunes National Lakeshore in 2003

It is difficult to ascertain clear trends with the $\delta^{15}\text{N}$ values measured from this NO_3^- , however there does appear to be undulation over 5-6 month cycles in 2001 and 2002 (an effect less noticeable in 2003). $\delta^{15}\text{N}$ values will consistently rise to approximately +10‰ and fall to approximately -10‰, both of which are within the typical range of $\delta^{15}\text{N}$ values from NO_3^- in precipitation (e.g., Kendall et al., 2008; Russell et al, 1998). Some NO_x source isotope values have been identified by Heaton (1990), showing values of $\delta^{15}\text{N}$ for NO_x from coal combustion between +6 and +9‰, as well as NO_x emitted from automobiles between -13 to +2‰.

Fairly obvious seasonal trends for $\delta^{18}\text{O}$ are shown in the Figures 4.3, 4.4, and 4.5. The general trend of $\delta^{18}\text{O}$ values in this study mimics that of other studies, with $\delta^{18}\text{O}$

values for atmospheric NO_3^- lower in the summer months compared to that of the winter months. All $\delta^{18}\text{O}$ values measured here are within the range of +51 to +87‰ with one exception: January of 2003, a statistical outlier which was included (since $n=1$ for that month).

4.4.2. Model Predictions

The isotopic mass balance model described in Chapter 3 of this thesis coupled with the RACM (Stockwell et al., 1997) model predicts $\delta^{18}\text{O}$ values of several atmospheric compounds, including the OH radical, tropospheric O_3 , and HNO_3 produced by the three major HNO_3 production pathways (R4.1, 4.2, and 4.3). Monthly averages of the predicted values for each of these compounds (OH: Figure 4.5, O_3 : Figure 4.6, HNO_3 pathways: 4.7, 4.8, and 4.9) can help with interpretations of isotope values of NO_3^- measured in precipitation at the Indiana Dunes National Lakeshore.

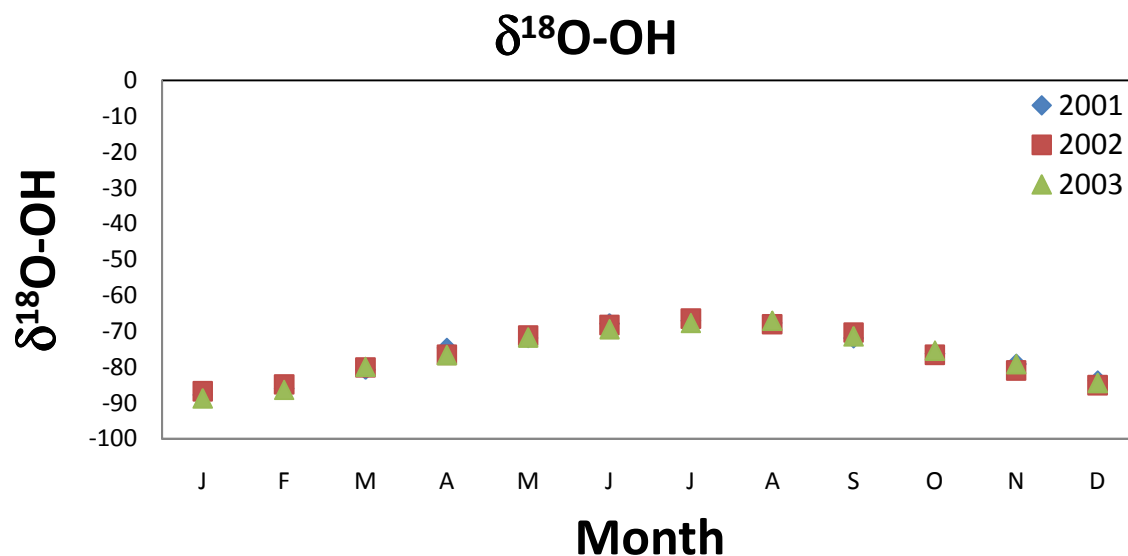


Figure 4.5: Predicted $\delta^{18}\text{O}$ of the OH radical based on equilibrium isotopic fractionation

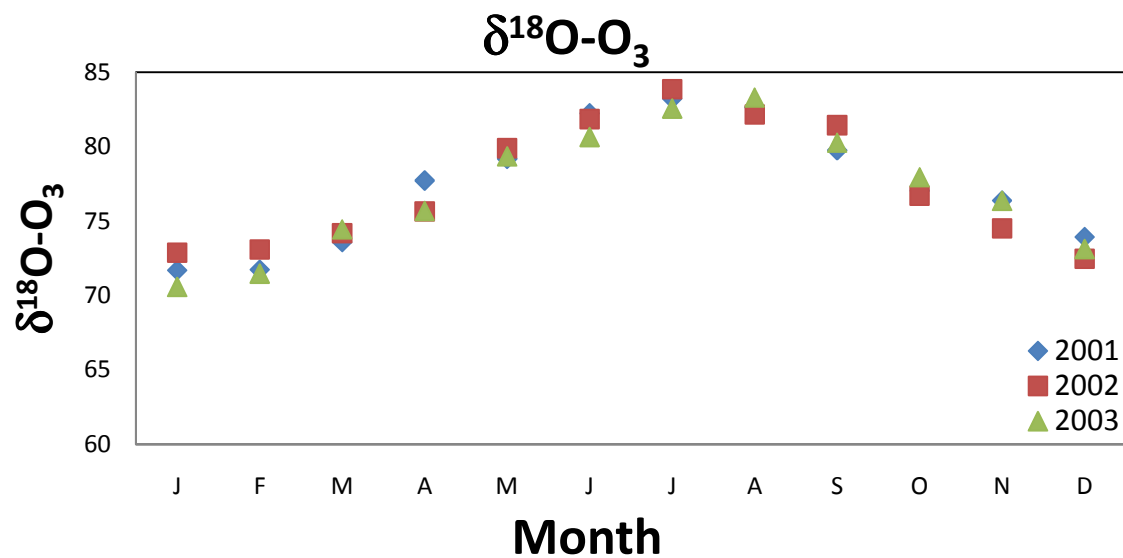


Figure 4.6: Predicted $\delta^{18}\text{O}$ of tropospheric O_3 based on temperature and pressure

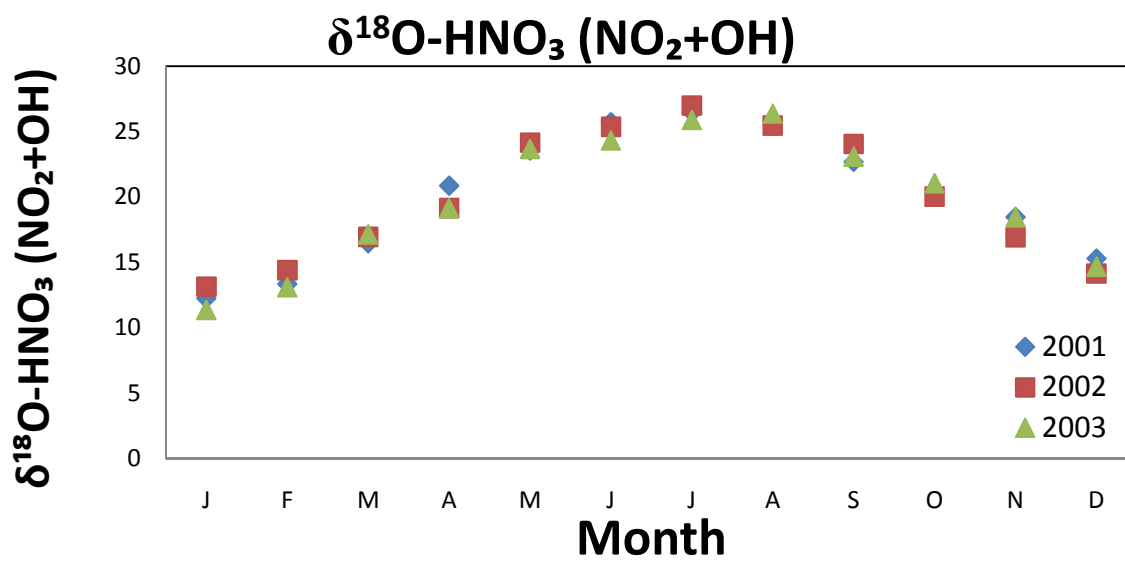


Figure 4.7: Predicted $\delta^{18}\text{O}$ of HNO_3 from HNO_3 production pathway R4.1

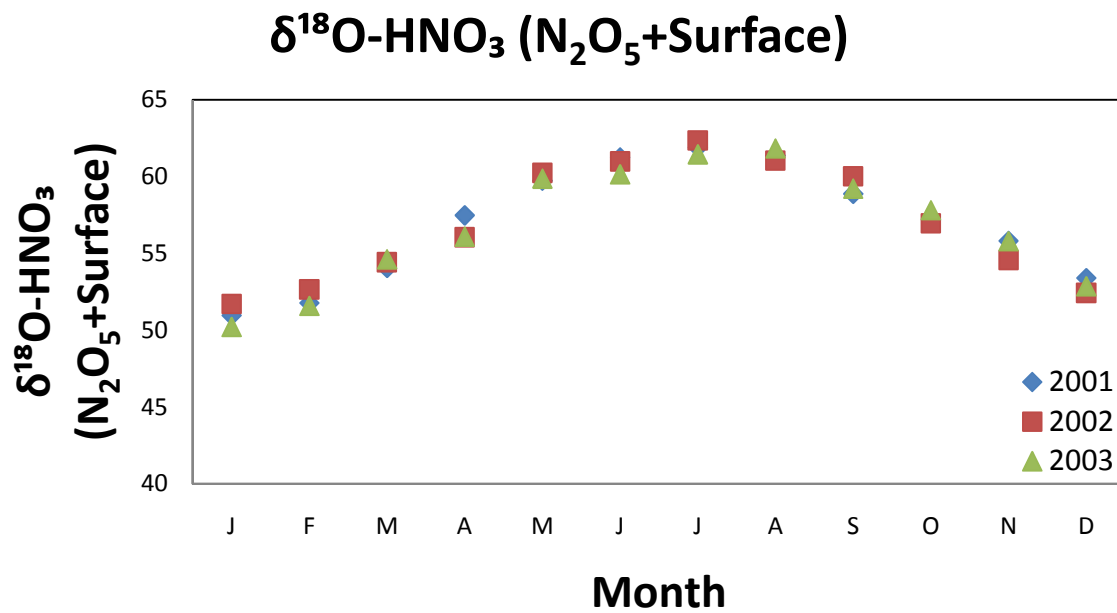


Figure 4.8: Predicted $\delta^{18}\text{O}$ of HNO_3 from HNO_3 production pathway R4.2

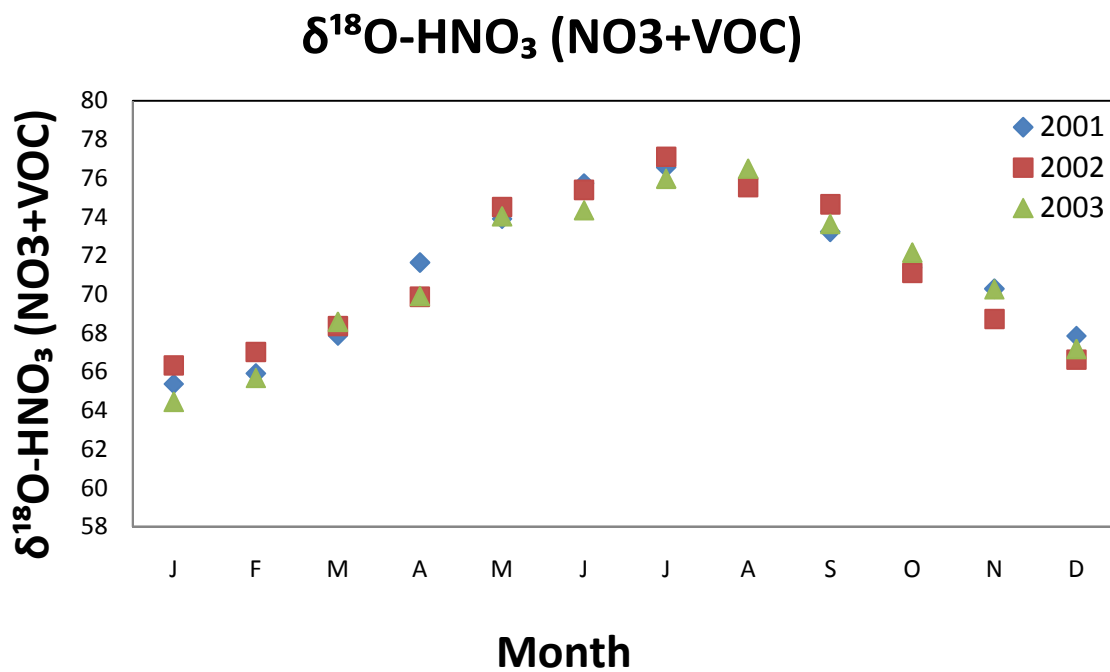


Figure 4.9: Predicted $\delta^{18}\text{O}$ of HNO_3 from HNO_3 production pathway R4.3

The combination of these three pathways takes place after a calculation of the mole fraction of each pathway by RACM (Stockwell et al., 1997) (Figures 4.10, 4.11, and 4.12). This mole fraction is calculated based on 238 chemical reactions which take into account concentrations of several trace compounds in the atmosphere, including NO_x , HNO_3 , O_3 , and VOC based on the Regional Acid Deposition Model (RADM) model for regional air quality modeling (Stockwell et al., 1990).

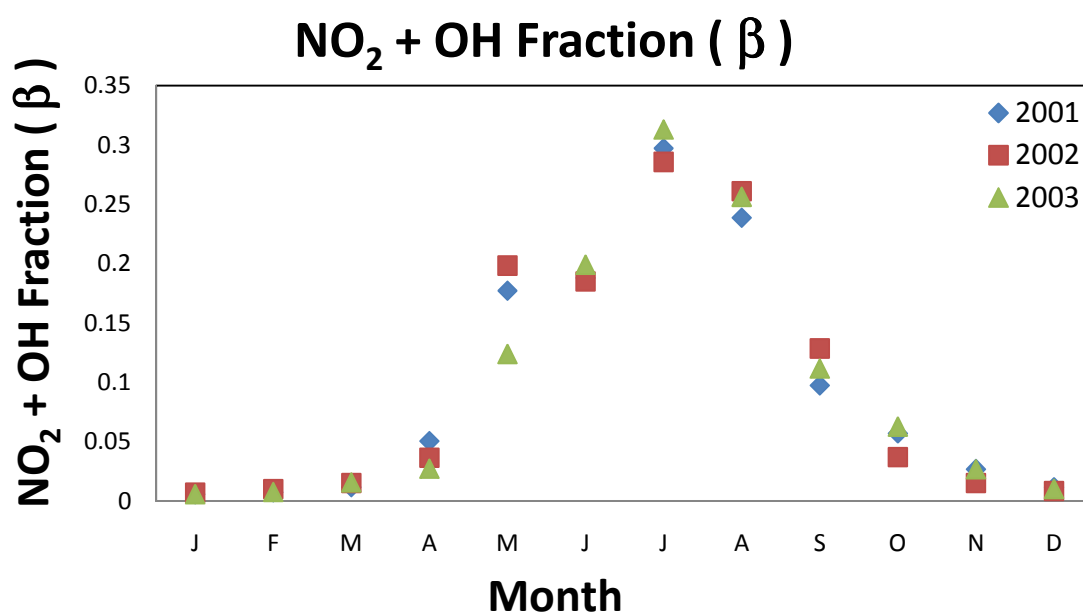


Figure 4.10: Mole fraction of R4.1 for the $\delta^{18}\text{O}$ of total HNO_3

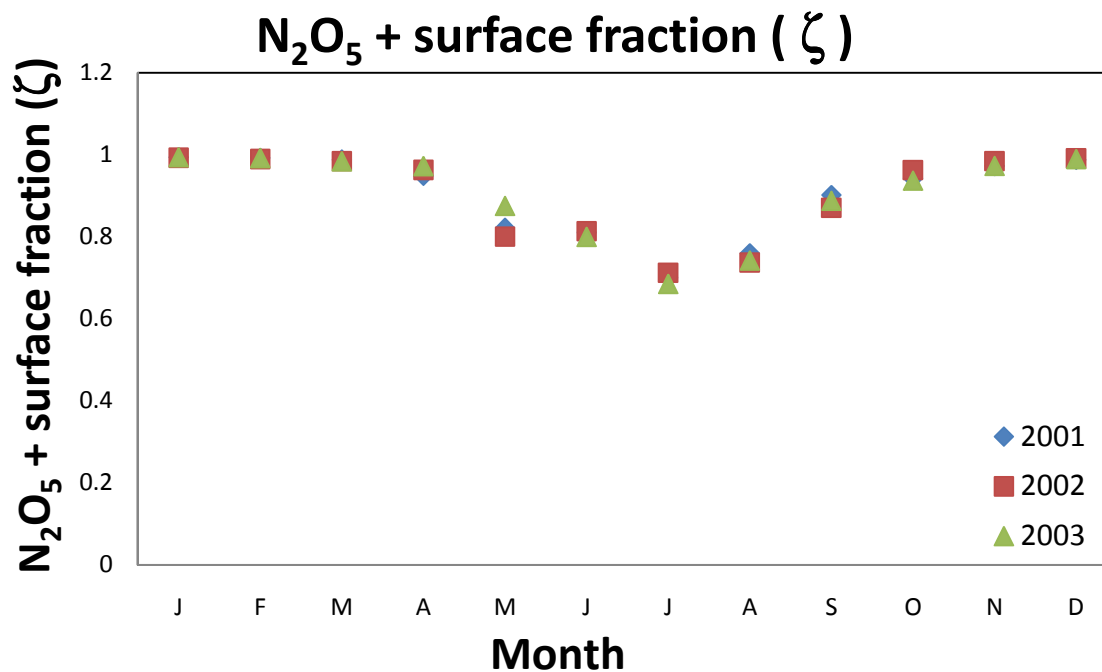


Figure 4.11: Mole fraction of R4.2 for the $\delta^{18}\text{O}$ of total HNO_3

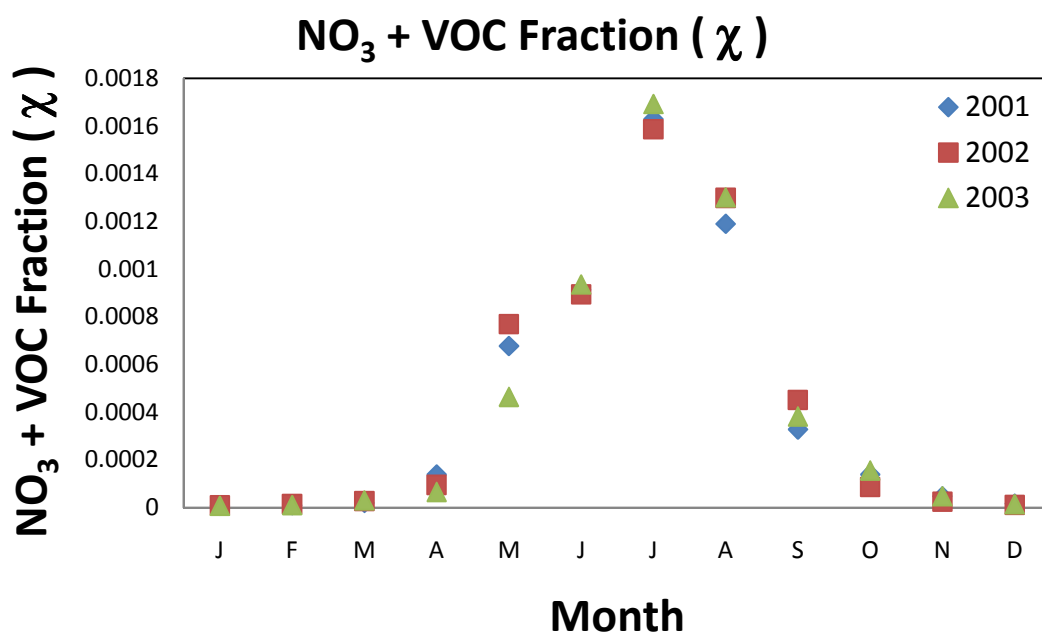


Figure 4.12: Mole fraction of R4.3 for the $\delta^{18}\text{O}$ of total HNO_3

The multiplication of this mole fraction by the $\delta^{18}\text{O}$ value of each pathway for each month allows for the calculation of the $\delta^{18}\text{O}$ of the total HNO_3 (Figure 4.13). The three fractions (Figures 4.10, 4.11, 4.12) show very clear seasonal changes. R4.1 is fairly insignificant during the winter months, however the contribution of this pathway changes steadily to approximately 30% as seasons change to the summer months. R4.2 consistently contributes the most to the $\delta^{18}\text{O}$ of total HNO_3 , with contributions as high as 99% in the winter months and dropping only to 70% in the summer months. The contribution of R4.3 changes significantly (approximately 0% in the winter months to 0.2% in the summer), however its ultimate contribution to the $\delta^{18}\text{O}$ of the total HNO_3 is insignificant relative to the other two pathways.

The total HNO_3 predicted by the mass balance model described in Chapter 3 of this thesis shows similar changes over the course of a year, for each year for the period of 2001-2003. Instead of a gradual change between cold and warm months shown in other predicted datasets described here, the prediction of total HNO_3 shows cyclical changes over 3 or 4 month periods, where predicted $\delta^{18}\text{O}$ values change from approximately +50‰ to +56‰. Over the course of 2001-2003, the highest $\delta^{18}\text{O}$ values predicted for the total HNO_3 are in April (or May in 2003) and October, and the lowest values are in January and July.

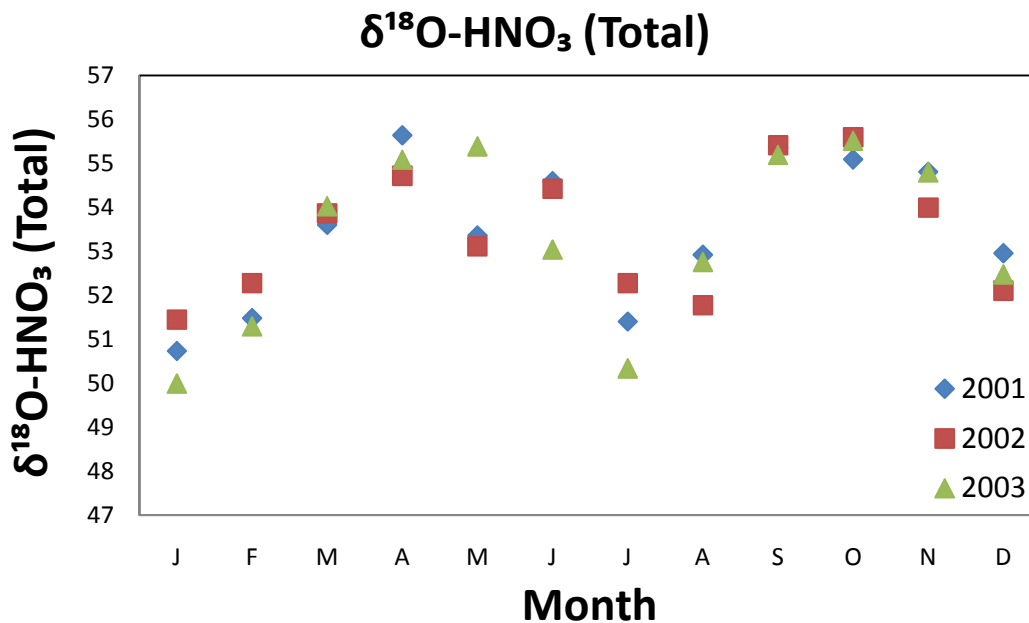


Figure 4.13: Modeled prediction of $\delta^{18}\text{O}$ of total HNO_3

4.5. Discussion

The cyclical nature of changes in $\delta^{15}\text{N}$ values may be indicative of NO_x source changes over 6-month periods, as there is no correlation between the isotope values measured from these samples and concentration of NO_3^- or volume of precipitation. However, the cyclical nature of the $\delta^{15}\text{N}$ variations mimics the cyclical variations of $\delta^{18}\text{O}$ shown with changes in chemistry in Figure 4.13. While Figure 4.13 does not apply directly to $\delta^{15}\text{N}$, the chemistry resulting in these values may help to explain the observed trends. Freyer (1991) suggested that $\delta^{15}\text{N}$ variations can be an indicator of chemical transformations if atmospheric conditions are correct. In cases of high NO_x concentrations, NO and NO_2 are capable of exchanging with each other in the atmosphere, which would change $\delta^{15}\text{N}$ values. $\text{NO}\text{-NO}_2$ reactions occur at different rates dependent on temperature. Conditions seem favorable for these types of reactions to take place at the Indiana Dunes National Lakeshore, which could explain the $\delta^{15}\text{N}$ trends in the data presented here. A potential counterpoint to this is the effect of biogenic NO_x , which has been suggested to cause lower $\delta^{15}\text{N}$ values from atmospheric NO_3^- (e.g., Elliott

et al., 2007; Elliott et al., 2009; Hastings et al., 2003). While this is a valid possibility, biogenic NO_x only contributes ~0.4% to the total atmospheric NO_x budget at this site (Table 4.1) (EPA, 2005). This diminishes the likelihood of biogenic NO_x greatly affecting isotope values measured at this site.

The monthly-averaged $\delta^{18}\text{O}$ values of NO_3^- in precipitation at the Indiana Dunes National Lakeshore show a clear seasonal trend, with lower values in the warmer months and higher values in the colder months. Since it is widely acknowledged that $\delta^{18}\text{O}$ values are generally indicative of atmospheric alterations of NO_x , these seasonal trends are not surprising. The challenge with interpreting $\delta^{18}\text{O}$ results is that while it is useful to recognize a seasonal trend within the data, it is difficult to single out specific causes of seasonal trends. For the purpose of better determining the cause of the seasonal trends of $\delta^{18}\text{O}$ measured at the Indiana Dunes National Lakeshore, the results predicted by the isotopic mass balance model are compared to measured $\delta^{18}\text{O}$ values in NO_3^- from the Indiana Dunes National Lakeshore site. Additionally, back trajectories from the National Oceanic and Atmospheric Administration's (NOAA) Hybrid Single Particle Lagrangian Integrated Trajectory (HYSPLIT) model help to examine the movement of air masses which could explain variations in both $\delta^{15}\text{N}$ and $\delta^{18}\text{O}$ values at this site.

4.5.1. Comparison of Modeled $\delta^{18}\text{O}$ Values to Observed Results

A comparison of model results to observed values for $\delta^{18}\text{O}$ of NO_3^- in this study shows that the two datasets are not particularly correlated (Figures 4.14, 4.15, 4.16).

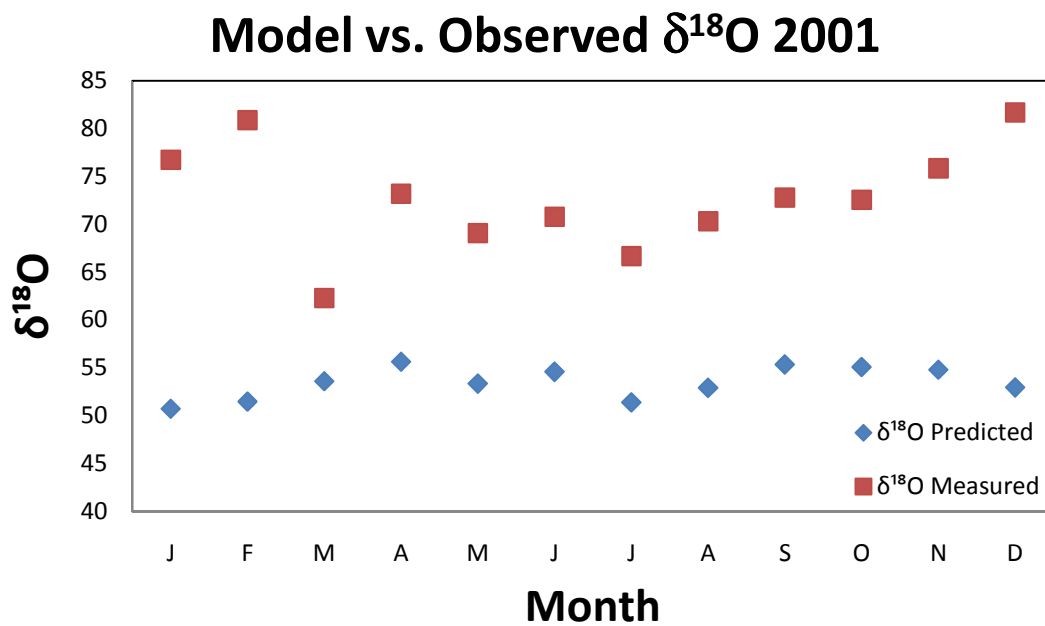


Figure 4.14: Comparison of modeled and observed $\delta^{18}\text{O}$ values in NO_3^- for 2001

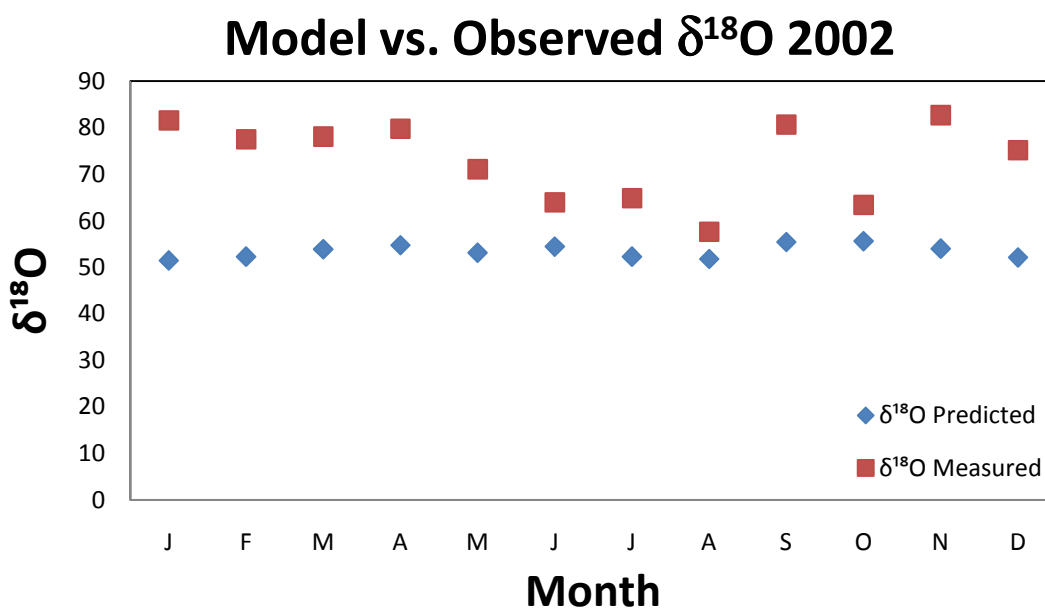


Figure 4.15: Comparison of modeled and observed $\delta^{18}\text{O}$ in NO_3^- values for 2002

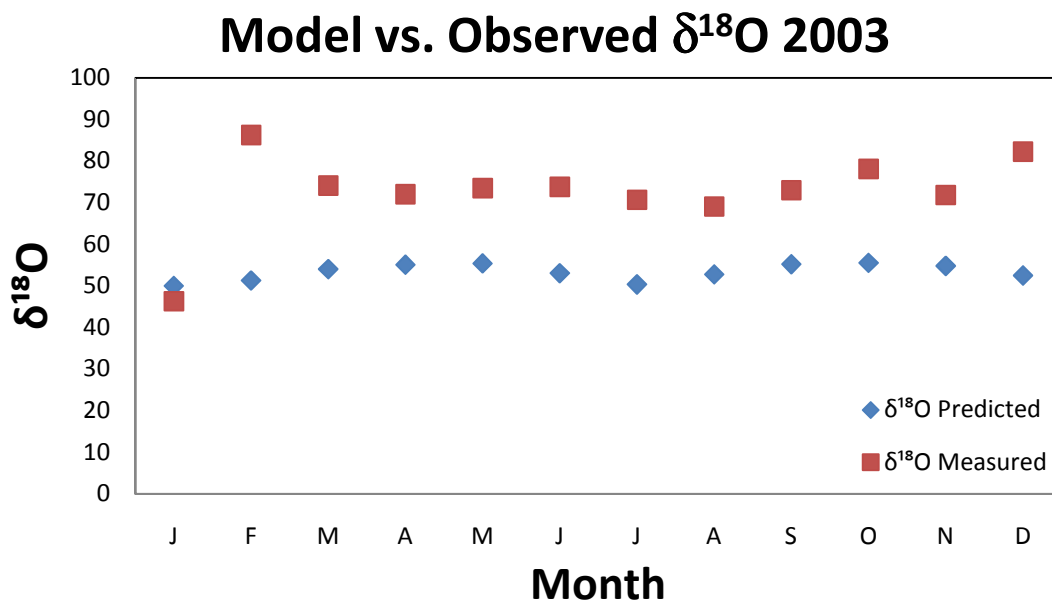


Figure 4.16: Comparison of modeled and observed $\delta^{18}\text{O}$ values in NO_3^- for 2003

Seasonal trends are apparent over the course of a year for the observed $\delta^{18}\text{O}$ values for NO_3^- at the Indian Dunes National Lakeshore, however the trend in the modeled data is not very similar to these observed results. This is likely due to very low values of predicted $\delta^{18}\text{O}$ for OH based on equilibrium fractionation calculations. As discussed in Chapter 3 however, there are also potential kinetic isotope effects which if not accounted for may cause unrealistically low $\delta^{18}\text{O}$ values for the OH radical. The kinetic isotope effect is calculated to be approximately +100‰ (Dubey et al., 1997). As suggested in Chapter 3 of this thesis, a potentially more realistic $\delta^{18}\text{O}$ value of the OH radical would be between the calculated values based on equilibrium and kinetic isotope fractionation. A potential analog for realistic values could be the $\delta^{18}\text{O}$ values measured in H_2O_2 obtained by Savarino and Thiemens (1999). H_2O_2 is formed from the reaction $\text{HO}_x + \text{HO}_x$ in the atmosphere, and HO_x is produced from OH radicals. As a result, applying a correction (+120‰) to the calculated equilibrium $\delta^{18}\text{O}$ values of OH yields a new range of $\delta^{18}\text{O}$ values from +33 to +54 for our study site. Using these new values in

the mass balance approximation of $\delta^{18}\text{O}$ in the atmosphere yields a new range of $\delta^{18}\text{O}$ values for the total HNO_3 from approximately +50‰ to +63‰ (Figures 4.17, 4.18, 4.19).

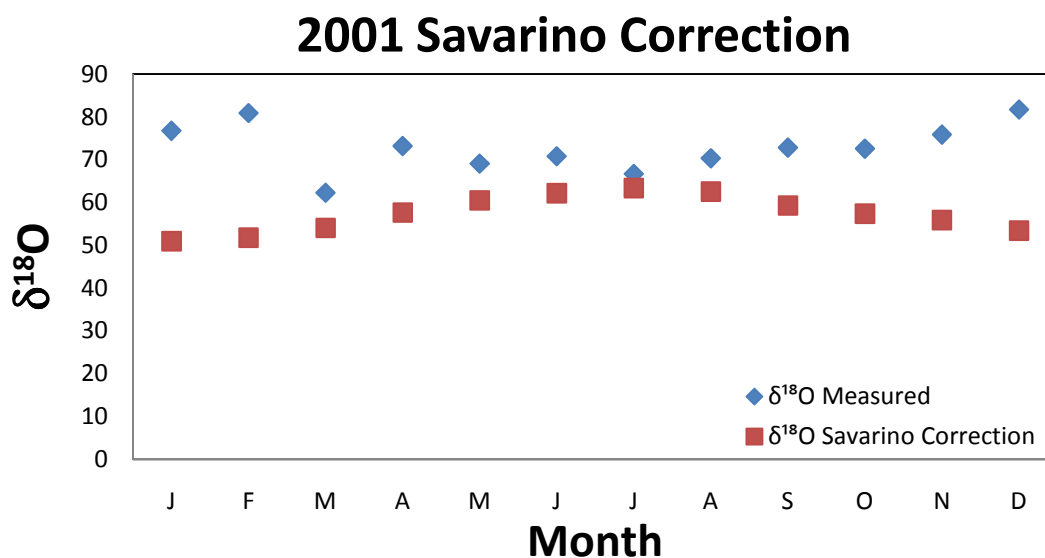


Figure 4.17: $\delta^{18}\text{O}$ values for both measured and predicted NO_3^- in precipitation, utilizing the correction factor calculated from Savarino and Thiemens (1999) for 2001.

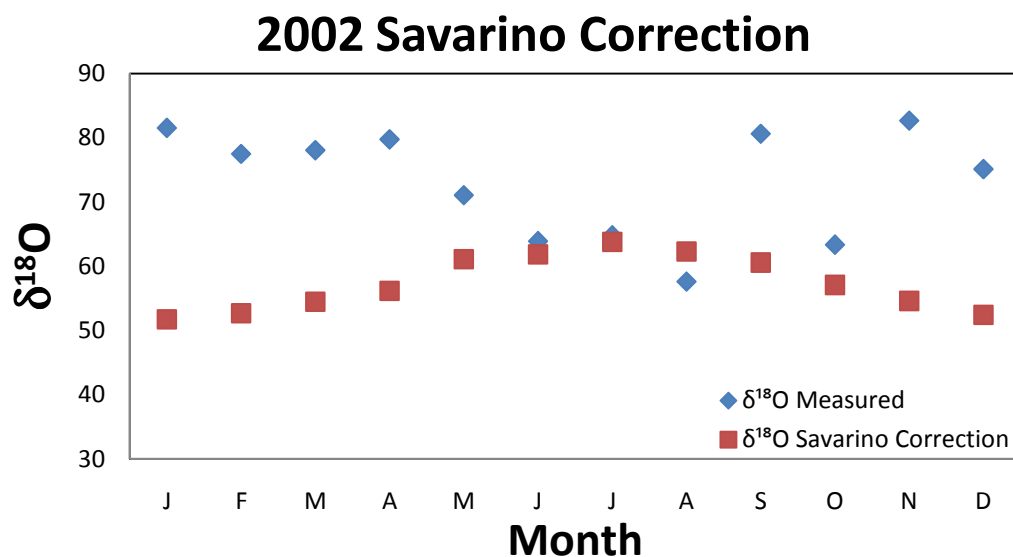


Figure 4.18: $\delta^{18}\text{O}$ values for both measured and predicted NO_3^- in precipitation, utilizing the correction factor calculated from Savarino and Thiemens (1999) for 2002.

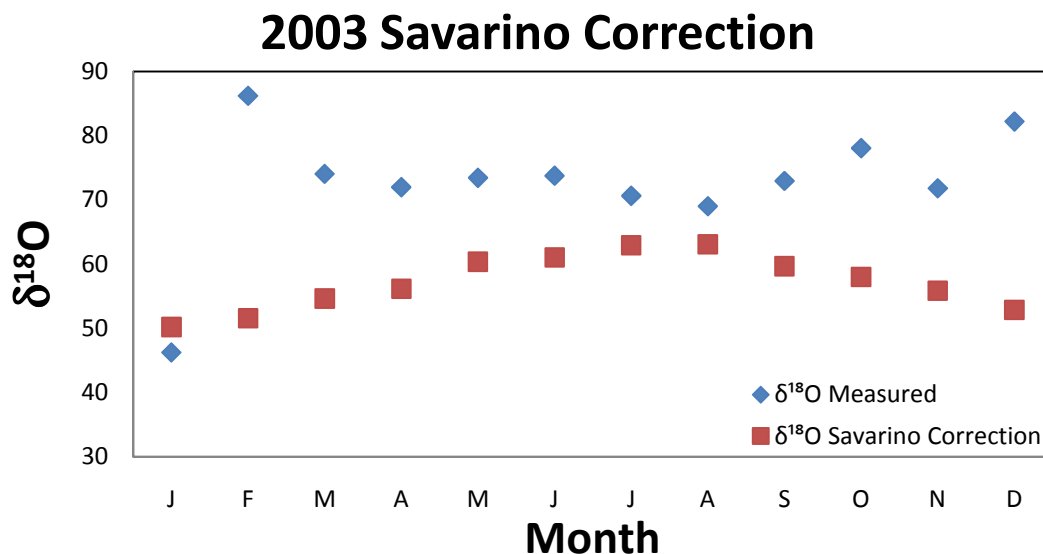


Figure 4.19: $\delta^{18}\text{O}$ values for both measured and predicted NO_3^- in precipitation, utilizing the correction factor calculated from Savarino and Thiemens (1999) for 2003.

These new ‘corrected’ $\delta^{18}\text{O}$ values when the correction are closer to the measured $\delta^{18}\text{O}$ values of NO_3^- in precipitation from the Indiana Dunes National Lakeshore during the summer months. Unfortunately, a seasonal trend which is opposite that of our measured results is shown when utilizing this correction. Assuming the correction calculated from Savarino and Thiemens (1999) is valid, the opposite trends imply that the contribution of $\delta^{18}\text{O}$ of N_2O_5 is not accounted for correctly in the mass-balance model. This could be due to either incorrect calculations for each of the mass balance components due to factors not included in the model, or due to incorrect mole fraction calculations from the RACM (Stockwell et al., 1997) model. As the mole fraction calculations here are similar to fractions reported elsewhere (Dentener and Crutzen, 1993), and the concentrations of species in the atmosphere support the mole fractions calculated by RACM (as the abundance of NO_2 and aerosols at this site drives N_2O_5 formation and subsequent hydrolysis) errors in the mass balance are likely the reason predicted values are lower than expected.

In addition to the OH correction, it is possible that a correction to the $\delta^{18}\text{O}$ of tropospheric O_3 could help yield more accurate predictions of $\delta^{18}\text{O}$ of HNO_3 . Measured

$\delta^{18}\text{O}$ values of O_3 in La Jolla, CA, show a range of approximately +95‰ to +115‰, with the highest values being in the winter and the lowest in the summer (Johnston and Thiemens, 1997). Model predictions show $\delta^{18}\text{O}$ values for La Jolla are between approximately +95‰ and +97‰. As discussed in Chapter 3 of this thesis, the $\delta^{18}\text{O}$ of O_3 is likely effected by photolysis and aerosol surface reactions during the winter which are not accounted for by our model, which only utilizes temperature and pressure to calculate the $\delta^{18}\text{O}$ of atmospheric O_3 . These reactions cause oxygen isotopic exchange, resulting in O_3 with a higher $\delta^{18}\text{O}$ value. In order to account for this in our model we can add a correction factor of 15‰, which brings predictions far more in line with observed values for the $\delta^{18}\text{O}$ of HNO_3 at the Indiana Dunes National Lakeshore (Figure 4.20, 4.21, 4.22) even without the application of the correction for OH calculated from Savarino and Thiemens (1999).

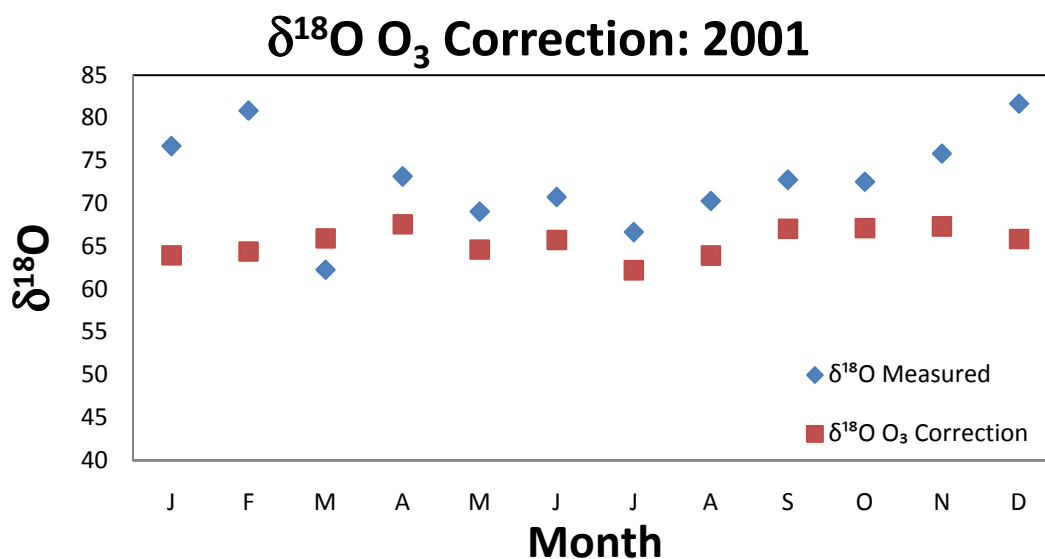


Figure 4.20. Monthly-averaged model calculations for $\delta^{18}\text{O}$ of total HNO_3 in 2001 with the O_3 correction of +15‰ (equilibrium $\delta^{18}\text{O}$ OH values used).

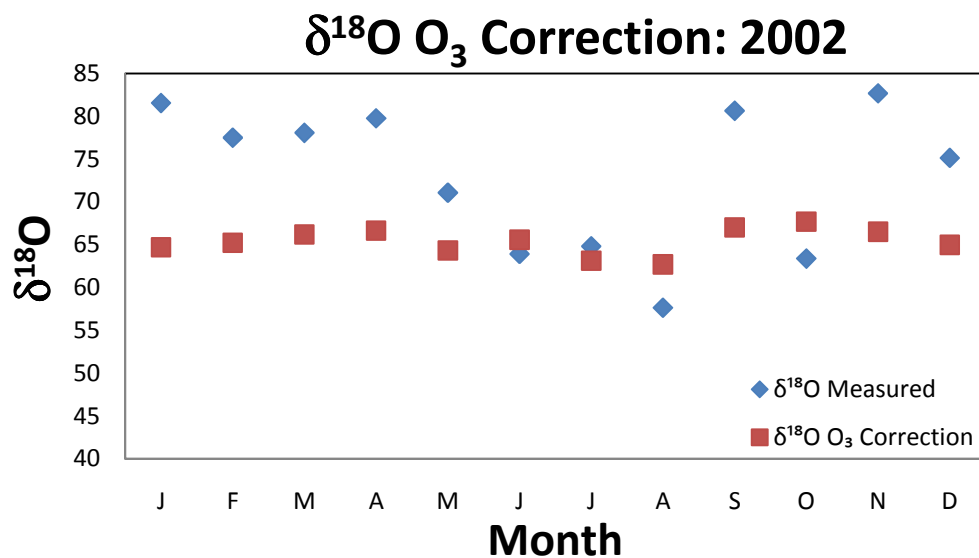


Figure 4.21. Monthly-averaged model calculations for $\delta^{18}\text{O}$ of total HNO_3 in 2002 with the O₃ correction of +15‰ (equilibrium $\delta^{18}\text{O}$ OH values used).

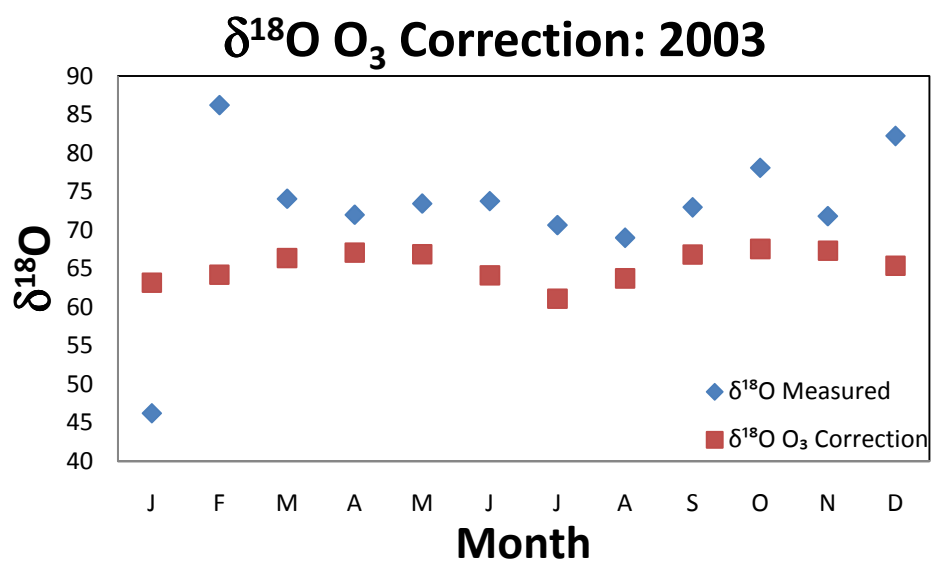


Figure 4.22: Monthly-averaged model calculations for $\delta^{18}\text{O}$ of total HNO_3 in 2003 with the O₃ correction of +15‰ (equilibrium $\delta^{18}\text{O}$ OH values used).

In contrast to the application of the correction calculated from Savarino and Thiemens (1999) for the $\delta^{18}\text{O}$ of OH, the use of the O_3 correction based on Johnston and Thiemens (1997) produces results that are closer to the measured $\delta^{18}\text{O}$ of HNO_3 at the Indiana Dunes National Lakeshore. Further, the predicted data shows seasonal trends which are partially similar to that of the observed data. There are however, two shortcomings of the +15‰ correction to the $\delta^{18}\text{O}$ of O_3 predictions from our mass balance model. The first of these is the discrepancy with the $\delta^{18}\text{O}$ of O_3 data from La Jolla, CA (Johnston and Thiemens, 1997), as the $\delta^{18}\text{O}$ of O_3 predicted is already in decent agreement with the $\delta^{18}\text{O}$ of O_3 measured (except in the winter months). The second of these is that even with the +15‰ correction, the seasonal trends only partially match the observed data. The winter months' trends are still reversed, which is an important issue to overcome in future modifications of this model.

4.5.2. HYSPLIT Analysis

Movement of air masses may also affect the $\delta^{15}\text{N}$ and $\delta^{18}\text{O}$ values of NO_3^- in precipitation collected at the Indiana Dunes National Lakeshore. Back trajectory analysis from the HYSPLIT model traces the path of an air mass over a set period of time to determine the provenance of that air mass. For this study, we traced air masses for each of our samples to see the path of the air mass from 5 days prior to collection. These back trajectory analyses were split into categories depending on the wind direction for each specific trajectory (NW, SW, SE, and NE) with each direction being assigned a number (1, 2, 3, and 4, respectively). These numbers were plotted against the $\delta^{15}\text{N}$ and $\delta^{18}\text{O}$ values measured from the NADP samples to determine any correlations between wind direction and isotope value for both $\delta^{15}\text{N}$ and $\delta^{18}\text{O}$ (Figures 4.23 and 4.24, respectively).

HYSPLIT Back Trajectory at 500m elevation vs. $\delta^{15}\text{N}$ measured at IN34

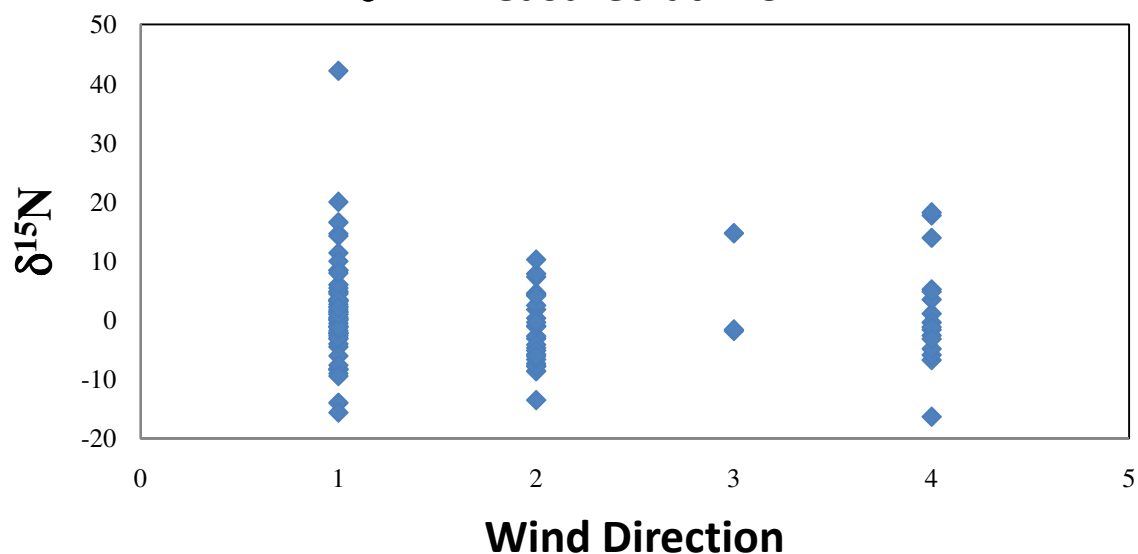


Figure 4.23: HYSPLIT Back Trajectory projected air mass provenance compared to $\delta^{15}\text{N}$ values for precipitation samples collected at the Indiana Dunes National Lakeshore

HYSPLIT Back Trajectory at 500m elevation vs. $\delta^{18}\text{O}$ measured at IN34

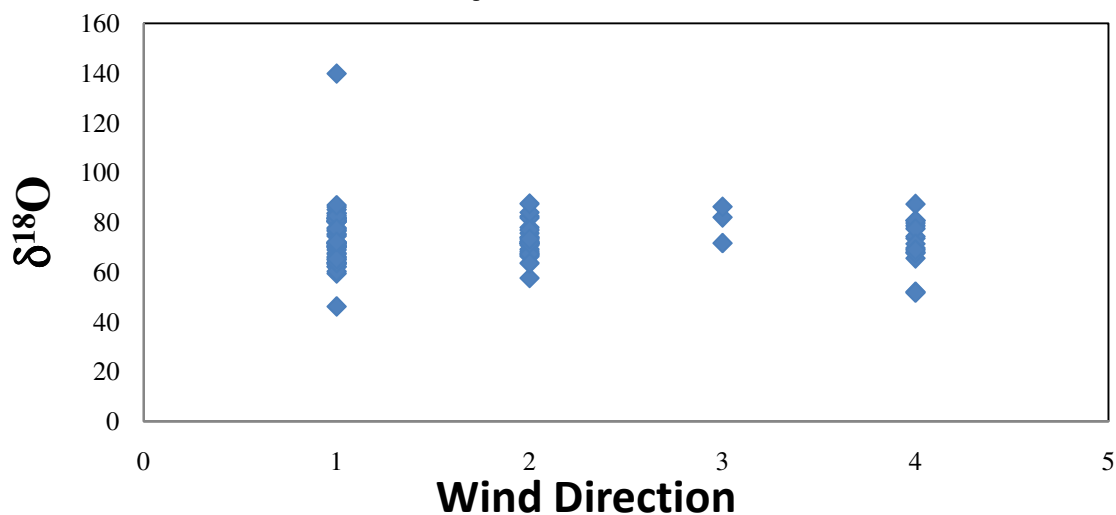


Figure 4.24: HYSPLIT Back Trajectory projected air mass provenance compared to $\delta^{18}\text{O}$ values for precipitation samples collected at the Indiana Dunes National Lakeshore

As shown in Figures 4.23 and 4.24, there does not appear to be a discernable correlation between wind direction and the isotope values of samples of precipitation from the Indiana Dunes National Lakeshore. This is primarily due to the range of overlap between different wind directions. In samples from all wind directions the means were found to be very similar, with the only exception only having three samples (wind direction 3: SE). The lack of difference between these wind directions only implies that the atmosphere is well mixed at around the sample site. Air off of Lake Michigan likely plays a role in the rapid mixing of atmospheric air masses, making it sometimes difficult to discern one source from another in geographic terms. This area consistently shows high NO_x emissions, and a result of atmospheric mixing seems to convolute isotope values when attempting to determine spatial provenance.

4.6. Conclusions and Future Considerations

Precipitation NO_3^- from the NADP Indiana Dunes National Lakeshore site (IN34) for the years 2001-2003 was measured for $\delta^{18}\text{O}$ and $\delta^{15}\text{N}$ in the PSI lab at Purdue University. $\delta^{15}\text{N}$ measurements show interesting trends in all three years of data. While the values fall within the standard range of -16 to +10‰ (Kendall et al., 2008; Russell et al., 1998), the $\delta^{15}\text{N}$ values show a cyclical variation over 5-6 month periods. These variations of $\delta^{15}\text{N}$ values throughout the year at this site may be due to the high concentrations of NO_x in the atmosphere which enable NO-NO_2 exchange and subsequent isotopic fractionation. This is in support of Freyer (1991), where similar pollution levels at sites in Germany were effecting $\delta^{15}\text{N}$ values, likely due to this exchange reaction.

Trends among $\delta^{18}\text{O}$ data consisted of values which are lower in the summer months than in the winter months, which is consistent with analyses of atmospheric NO_3^- at other mid-latitude locations. Initial mass-balance and equilibrium relationships between the species participating in NO_x oxidation predict $\delta^{18}\text{O}$ values which underestimate the measured $\delta^{18}\text{O}$ values in precipitation at the Indiana Dunes National Lakeshore. Applying a correction (+120‰) based on the $\delta^{18}\text{O}$ of H_2O_2 from Savarino and

Thiemens (1999) to the prediction of $\delta^{18}\text{O}$ of OH may be helpful. A correction to the $\delta^{18}\text{O}$ value of O_3 (+15‰) may help to include reactions which are not accounted for in the mass balance model described here. Both of these corrections increase agreement between the model and observed results during the summer months, but in the winter months the values are incorrect and do not follow the appropriate seasonal trends. A detailed study of these two components of the mass balance will be very helpful for optimizing the model.

The RACM model (Stockwell et al., 1997), is used to predict mole fractions for each HNO_3 production pathway. RACM calculates these parameters through the use of air quality data and multiple chemical reactions in the atmosphere. If the air quality data provided to the model is incorrect or imprecise, this will likely affect the mole fraction calculated for each chemical pathway. According to RACM, R4.2 dominates at this site year-round. In general, R4.1 dominates HNO_3 production (e.g., Finlayson-Pitts and Pitts, 2000), however the results from RACM presented here agree with published work on polluted environments (Dentener and Crutzen, 1993). RACM may be underestimating the contribution of R4.3, however the abundance of NO_2 in the atmosphere causes NO_3 to favor reacting to form N_2O_5 , further supporting the results presented here.

While many variables in this modeling approach may be correct, ultimately the $\delta^{18}\text{O}$ of HNO_3 is predicted incorrectly at this Indiana Dunes National Lakeshore site. Corrections to the model predictions may help to improve agreement between modeled and observed results, however these corrections are based on assumptions regarding unknowns in the atmospheric chemical system at this site. To fully optimize this model, a field campaign which collects and analyzes the $\delta^{18}\text{O}$ of tropospheric O_3 and NO_3^- at multiple locations and elevations would be helpful in determining which aspects of this model are working properly and which are not. The $\delta^{18}\text{O}$ of O_3 analyzed at these locations and elevations can help to derive more accurate equations which account for winter changes better than our current estimates. Further, laboratory experiments can be used to determine the $\delta^{18}\text{O}$ of HNO_3 produced by each HNO_3 production reaction. Of particular interest is R4.1, which based on our calculations is predicted to be much lower

than it theoretically should be. Despite these shortcomings however, the use of isotopic mass-balance to predict $\delta^{18}\text{O}$ values in atmospheric HNO_3 can be a valuable tool for the better understanding of $\delta^{18}\text{O}$ values measured from atmospheric NO_3^- . As a first attempt at the prediction of $\delta^{18}\text{O}$ of atmospheric NO_3^- , the model shows tremendous potential. With proper air quality data and mass balance calculations, this model will provide a quantitative tool for the better understanding of $\delta^{18}\text{O}$ values measured from atmospheric NO_3^- .

LIST OF REFERENCES

LIST OF REFERENCES

- Alexander, B., Hastings, M.G., Allman, D.J., Dachs, J., Thornton, J.A., and Kunsasek, S.A. Quantifying atmospheric nitrate formation pathways based on a global model of the oxygen isotopic composition ($\Delta^{17}\text{O}$) of atmospheric nitrate. *Atmos. Chem. Phys.*, 9, 5043-5056, 2009
- Ammann, M., Siegwolf, R., Pichlmayer, F., Suter, M., Saurer, M., Brunold, C. Estimating the uptake of traffic-derived NO_2 from ^{15}N abundance in Norway spruce needles. *Oecologia*, 118, 124-131, 1999
- Anderson D.M. Toxic algal blooms and red tides: A global perspective. In: *Red Tides* (ed. by T. Okaichi. D.M. Anderson & T. Nemoto). pp. 11-16, 1989
- Benkovitz, C.M., Schultz, M.T., Pacnya, J., Tarrason, L., Dignon, J., Voldner, E.C., Spiro, P.A., Logan, J.A., and Graedel, T.E. Global, gridded inventories for anthropogenic emissions of sulfur and nitrogen, *J. Geophys. Res.*, 101, 29239-29253, 1996
- Berberan-Santos, M.N., Bodunov, E.N., and Pogliani, L. On the barometric formula. *Am. J. Phys.*, 65 (5), 404-412. 1997.
- Bey, I., Jacob, D.J., Yantosca, R.M., Logan, J.A., Field, B.D., Fiore, A.M., Li, Q., Liu, H.Y., Mickley, L.J., and Schultz, M.G. Global modeling of tropospheric chemistry with assimilated meteorology: Model description and evaluation, *J. Geophys. Res.*, 106(D19), 23073-23095, 2001
- Böhlke, J. K., Mroczkowski, S. J. and Coplen, T. B. Oxygen isotopes in nitrate: new reference materials for ^{18}O : ^{17}O : ^{16}O measurements and observations on nitrate-water equilibration. *Rapid Communications in Mass Spectrometry*, 17: 1835–1846. doi: 10.1002/rcm.1123. 2003.
- Bowen, G.J., and Wilkinson, B. Spatial distribution of $\delta^{18}\text{O}$ in meteoric precipitation. *Geology*, 30, 4, 315-318. 2002.

- Bowen, G.J, and Ravenaugh, J. Interpolating the isotopic composition of modern meteoric precipitation. *Water Resources Research*. 39:1299, doi:0.1029/2003WR002086. 2003.
- Brothers, L.A., Domingues, G, Fabian, P., and Thiemens, M.G. Using multi-isotope tracer methods to understand the sources of nitrate in aerosols, fog, and river water in Podocarpus Nation Forest, Ecuador, *Eos Trans. AGU*, 89, Abstract A11C—0136, 2008
- Brown, S.S., Dube, W.P., Fuchs, H., Ryerson, T.B., Wollny, A., Brock, C.A., Bahreini, R., Middlebrook, A.M., Neuman, J.A., Atlas, E., Roberts, J.M., Osthoff, H.D. Trainer, M., Fehsenfeld, F.C., and Ravishankara, A.R. Reactive uptake coefficients for N₂O₅ determined from aircraft measurements during the Second Texas Air Quality Study: Comparison to current model parameterizations, *J. Geophys. Res.*, 114, D00F10, 2006
- Buda, A.R. and DeWalle, D.R. Using atmospheric chemistry and storm track information to explain the variation of nitrate stable isotopes in precipitation at a site in Central Pennsylvania, USA. *Atmospheric Environment*. v. 43, 4452-4464, 2009.
- Burns, D.A. and Kendall, C. Analysis of $\delta^{15}\text{N}$ and $\delta^{18}\text{O}$ to differentiate NO_3^- sources in runoff at two watersheds in the Catskill Mountains of New York. *Water Resources Research*, v. 38, no. 1051, 11pp, 2002.
- Campbell, D.H., Kendall, C., Chang, C.C.Y., Silva, S. R., and Tonnessen, T.A. Pathways for nitrate release from an alpine watershed: Determination using $\delta^{15}\text{N}$ and $\delta^{18}\text{O}$. *Water Resources Research*, v. 38, no. 5, 2002.
- Casciotti, K. L.; Sigman, D. M.; Hastings, M. G.; Böhlke, J. K.; Hilkert, A. Measurement of the oxygen isotopic composition of nitrate in seawater and freshwater using the denitrifier method. *Anal. Chem.*, 74 (19), 4905-4912. 2002.
- Casciotti, K.L., Böhlke, J.K., McIlvin, M.R., Mroczkowski, S.J., and Hannon, J.E. Oxygen isotopes in nitrate: analysis, calibration, and equilibration. *Analytical Chemistry*, 79 (6), 2427-2436, 2007.
- Choppin, G., Rydberg, J., and Liljenzin, J.O. Radiochemistry and Nuclear Chemistry, Butterworth-Heinemann, Oxford, 1995.
- Crawley, L. Nitrogen and oxygen isotope ratio analysis of nitrate by the denitrifier method using continuous flow isotope ratio mass spectrometry. Purdue University Master's Thesis. 2010.

- Criss, R.E. *Principles of Stable Isotope Distribution*. Oxford University Press. 1999. 254pp.
- Davis, J.M., Bhave, P.V., and Foley, K.M., Parameterization of N₂O₅ reaction probabilities on the surface of particles containing ammonium, sulfate, and nitrate, *Atmos. Chem. Phys.*, 8, 5295-5311, 2008
- Dentener, F.J., and Crutzen, P.J. Reaction of N₂O₅ on tropospheric aerosols: Impact on the global distribution of NO_x, O₃, and OH. *J. Geophys. Res.*, 98 (D4), 7149-7163. 1993.
- Dubey, M.K, Mohrschladt, R., Donahue, N.M., and Anderson, J.G. Isotope-specific kinetics of hydroxyl radical (OH) with water (H₂O) : Testing models of reactivity and atmospheric fractionation, *J. Phys. Chem. A.*, 101, 1494-1500, 1997
- Ehhalt, D., Prather, M., Dentener, F., Derwent, R., Dlugokencky, E., Holland, E, Isaken, I, Katima, J, Kirtchhoff, V., Matson, P., Midgley, P., Wang, M. Atmosphere chemistry and greenhouse gasses. In *Climate Change 2001: The scientific basis. Contribution of Working Group I to the Third Assessment Report of the Intergovernmental Panel on Climate Change*; Houghton, J.T., Ding, Y, Greggs, D.J., Noguer, M, van der Linden, P.J., Dai, K., Maskell, K., Johnson, C.A., Eds. Cambridge University Press: New York, 2001
- Elliott, E.M., Kendall, C., Wankel, S.D., Burns, D.A., Boyer, E.W., Harlin, K., Bain, D.J., and Butler, T.J., Nitrogen isotopes as indicators of NO_x source contributions to atmospheric nitrate deposition across the Midwestern and Northeastern United States. *Environ. Sci. Technol.*, 41, 7661-7667, 2007.
- Elliott, E.M., Kendall, C., Boyer, E.W., Burns, D.A., Lear, G.G., Golden, H.E., Harlin, K., Bytnerowicz, A., Butler, T.J., and Glatz, R. Dual nitrate isotopes in dry deposition: Utility for partitioning NO_x source contribution to landscape nitrogen deposition. *J. Geophys. Res.*, 114, G04020, doi:10.1029/2008JG000889, 2009.
- Fenn, M.E., Jovan, S., Yuan, F., Geiser, L., Meixner, T., and Gimeno, B.S. Empirical and simulated critical loads for nitrogen deposition in California mixed conifer forests. *Environmental Pollution*, 155, 492-511, 2008.
- Finlayson-Pitts, B.J. and Pitts, J.N. *Chemistry of the Upper and Lower Atmosphere*. Academic Press. 969 pp., 2000.
- Freyer, H.D., Seasonal variation of ¹⁵N/¹⁴N ratios in atmospheric nitrate species. *Tellus*, 43, 30-44, 1991.

- Freyer, H.D., Kobel, K., Delmas, R.J., Kley, D., Legrand, M.R., First results of $^{15}\text{N}/^{14}\text{N}$ ratios in nitrate from alpine and polar ice cores. *Tellus* 48, 93-105, 1996
- Galloway, J.N., Dentener, F., Capone, D., Boyer, E., Howarth, R., Seitzinger, S., Asner, G., Cleveland, C., Green, P., Holland, E., Karl, D., Michaels, A., Porter, J., Townsend, A., Vorosmarty, C., Nitrogen cycles: Past, present, and future. *Biogeochemistry*, 70, 153-226, 2004
- Galloway, N., J., Townsend, R., A., Erisman, Willem, J., Bekunda, Mateete, Cai, Zucong, Freney, R., J., Martinelli, A., L., Seitzinger, P., S., Sutton, and A., M.: Transformation of the Nitrogen Cycle: Recent Trends, Questions, and Potential Solutions, *Science*, 320, 889–892, doi:10.1126/science.1136674, 2008
- Hales, H.C., Ross, D.S., and Lini, A. Isotopic signature of nitrate in two contrasting watersheds of Brush Brook, Vermont, USA. *Biogeochemistry*. v. 84, no. 1, 51-66, 2007.
- Hastings, M. G., Sigman, D. M., and Lipschultz, F.: Isotopic evidence for source changes of nitrate in rain at Bermuda, *J. Geophys. Res.*, 108, 4790, doi:10.1029/2003JD003789, 2003.
- Hastings, M.G., Sigman, D.M., and Steig, E.J., Glacial/interglacial changes in the isotopes of nitrate from the Greenland Ice Sheet Project 2 (GISP2) ice core. *Global Biogeochem. Chcycles*, 19, GB4034, 2005.
- Heaton, T. H. E. $^{15}\text{N}/^{14}\text{N}$ ratios of NO_x from vehicle engines and coal-fired power stations. *Tellus*, 42, 304-307 1990
- Hoering, T. The Isotopic composition of ammonia and nitrate ion in rain. *Geochim. Cosmochim. Acta*, 12, 97-102. 1957
- Jaegle, L.; Steinberger, L.; Martin, R. V.; Chance, K. Global partitioning of NO_x sources using satellite observations: Relative roles of fossil fuel combustion, biomass burning, and soil emissions. *Faraday Discuss.*, 130, 407-423. 2005
- Janssen, C., Guenther, J., and Krankowsky, D.: Relative formation rates of $^{50}\text{O}_3$ and $^{52}\text{O}_3$ in ^{16}O – ^{18}O mixtures, *J. Chem. Phys.*, 111, 7179–7182, 1999.
- Johnston, J. C. and Thiemens, M. H.: The isotopic composition of tropospheric ozone in three environments, *J. Geophys. Res.*, 102, 25395–25404, 1997.

- Kaiser, J., Hastings, M. G., Houlton, B. Z., Rockmann, T., and Sigman, D. M.: Triple Oxygen Isotope Analysis of Nitrate Using the Denitrifier Method and Thermal Decomposition of N₂O, *Anal. Chem.*, 79, 599–607, 2007.
- Kendall, C., Elliott, E. M. and Wankel, S. D. Tracing Anthropogenic Inputs of Nitrogen to Ecosystems, in *Stable Isotopes in Ecology and Environmental Science, Second Edition* (eds R. Michener and K. Lajtha), Blackwell Publishing Ltd, Oxford, UK. doi: 10.1002/9780470691854.ch12. 2008.
- Kiga, T.; Watanabe, S.; Yoshikawa, K.; Asano, K.; Okitsu, S.; Tsunogai, U.; Narukawa, K. In *Evaluation of NO_x Formation in Pulverized Coal Firing by Use of Nitrogen Isotope Ratios*, ASME 2000 International Joint Power Generation Conference, Miami Beach, FL, July 23-26, 2000; ASME: Miami Beach, FL, 2000.
- Krankowsky, D., Bartecki, F., Klees, G. G., Mauersberger, K., Schellenback, K., and Stehr, J.: Measurement of heavy isotope enrichment in tropospheric ozone, *Geophys. Res. Lett.*, 22, 1713–1716, 1995.
- Kunasek, A., S., Alexander, B., Hastings, M. G., Steig, E. J., Gleason, D. J., and Jarvis, J. C.: Measurements and modeling of ¹¹⁷O of nitrate in a snowpit from Summit, Greenland, *J. Geophys. Res.*, 113, D24302, doi:10.1029/2008JD010103, 2008.
- Likens, G.E., Driscoll, C.T., and Buso, D.C. Long-term effect of acid rain: response and recovery of a forest ecosystem. *Science*, 272, 5259, 244-246, 1996.
- Lyons, J. R.: Transfer of mass-independent fractionation on ozone to other oxygen-containing molecules in the atmosphere, *Geophys. Res. Lett.*, 28, 3231–3234, 2001.
- Mauersberger, K., Erbacher, B., Krankowsky, D., Gunther, J., and Nickel, R.: Ozone isotope enrichment: Isotopomer-specific rate coefficients, *Science*, 283, 370–372, 1999.
- McCabe, J. R., Thiemens, M. H., and Savarino, J.: A record of ozone variability in South Pole Antarctic snow: Role of nitrate oxygen isotopes, *J. Geophys. Res.*, 112, D12303, doi:10.1029/2006JD007822, 2007.
- McNeill, V. F., Patterson, J., Wolfe, G. M., and Thornton, J.: The Effect of Varying levels of Surfactant on the Reactive Uptake of N₂O₅ to Submicron Aqueous Aerosol, *Atm. Chem. Phys.*, 6, 1635–1644, 2006.

- Michalski, G., Savarino, J., Böhlke, J.K., and Thiemens, M.: Determination of the total oxygen isotopic composition of nitrate and the calibration of a $\Delta^{17}\text{O}$ nitrate reference material, *Anal. Chem.* 74, 4989-4993, 2002.
- Michalski, G. M., Scott, Z., Kabling, M., and Thiemens, M. H.: First measurements and modeling of ^{17}O in atmospheric nitrate, *Geophys. Res. Lett.*, 30, 1870, doi:1810.1029/2003GL017015, 2003.
- Michalski, G., Kasem, M., Rech, J. A., Adieu, S., Showers, W. S., Genna, B. and Thiemens, M. Uncertainties in the oxygen isotopic composition of barium sulfate induced by coprecipitation of nitrate. *Rapid Communications in Mass Spectrometry*, 22: 2971–2976. doi: 10.1002/rcm.3687. 2008.
- Michalski, G. and Bhattacharya, S. K.: The role of symmetry in the mass independent isotope effect in ozone, *Proc. Natl. Acad. Sci.*, 106, 5493–5496, 2009.
- Moore, H. The isotopic composition of ammonia, nitrogen dioxide, and nitrate in the atmosphere. *Atmos. Environ.*, 11, 1239-1243. 1977
- Moravec, B. G., Keller, C. K., Smith, J. L., Allen-King, R. M., Goodwin, A. J., Fairley, J. P. and Larson, P. B., Oxygen-18 dynamics in precipitation and streamflow in a semi-arid agricultural watershed, Eastern Washington, USA. *Hydrological Processes*, 24: 446–460. 2010.
- Morin, S., Savarino, J., Bekki, S., Gong, S., and Bottenheim, J. W.: Signature of Arctic surface ozone depletion events in the isotope anomaly (^{17}O) of atmospheric nitrate, *Atmos. Chem. Phys.*, 6, 6255–6297, 2007
- Morin, S., Savarino, J., Frey, M., M., Yan, N., Bekki, S., Bottenheim, W. J., and Martins, F. J. M.: Tracing the Origin and Fate of NO_x in the Arctic Atmosphere Using Stable Isotopes in Nitrate, *Science*, 322, 730–732, doi:10.1126/science.1161910, 2008.
- Morton, J., Barnes, J., Schueler, B., and Mauersberger, K.: Laboratory studies of heavy ozone, *J. Geophys. Res.*, 95, 901–907, 1990.
- Paerl, H.W., Boynton, W.R., Dennis, R.L., Driscoll, C.T., Greening, H. S., Kremer, J.N., Rabalais, N.N., Seitzinger, S.P.: Atmospheric Deposition of Nitrogen in Coastal Waters: Biogeochemical and Ecological Implications. Pp. 11-52, In , R. Valigura et al., *Nitrogen Deposition in Coastal Waters, Coastal and Estuarine Studies* No. 57. American Geophysical Union Press, Washington, DC. 2000.

- Paerl, H. W.; Dennis, R. L.; Whitall, D. R. Atmospheric deposition of nitrogen: Implications for nutrient over-enrichment of coastal waters. *Estuaries*, 25, 677-693. 2002
- Park, R.J., Jacob, D. J., Field, B. D., Yantosca, R. M., and Chin, M.: Natural and transboundary pollution influences on sulfate-nitrate-ammonium aerosols in the United States: implications for policy, *J. Geophys. Res.*, 109, D15204, doi:10.1029/2003JD004473, 2004.
- Pearson, J.; Wells, D. M.; Seller, K. J.; Bennett, A.; Soares, A.; Woodall, J.; Ingrouille, M. J. Traffic exposure increases natural ^{15}N and heavy metal concentrations in mosses. *New Phytol.*, 147, 317-326. 2000
- Rodhe, H., Dentener, F., and Schulz, M. The global distribution of acidifying wet deposition. *Environ. Sci. Technol.* 36, 4382-4288. 2002.
- Rabalais, N.N., Turner, R.E., and Wiseman, W.J. Gulf of Mexico hypoxia, A.K.A., “The Dead Zone.” *Annu. Rev. Ecol. Syst.* 33, 235-263. 2002.
- Russell, K. M.; Galloway, J. N.; Macko, S. A.; Moody, J. L.; Scudlark, J. R. Sources of nitrogen in wet deposition to the Chesapeake Bay region. *Atmos. Environ.*, 32, 2453-2465. 1998
- Savarino, J. and Thiemens, M. H.: Mass-independent oxygen isotope (^{16}O , ^{17}O , ^{18}O) fractionation found in Hx, Ox reactions, *J. Phys. Chem.*, 103, 9221–9229, 1999a
- Savarino, J. and Thiemens, M. H.: Analytical procedure to determine both $\delta^{18}\text{O}$ and $\Delta^{17}\text{O}$ of H_2O_2 in natural water and first measurements, *Atmos. Env.*, 33, 3683–3690, 1999b.
- Savarino, J., Kaiser, J., Morin, S., Sigman, D. M., and Thiemens, M. H.: Nitrogen and oxygen isotopic constraints on the origin of atmospheric nitrate in coastal Antarctica, *Atmos. Chem. Phys.*, 7, 1925–1945, 2007.
- Savarino, J., Bhattacharya, S. K., Morin, S., Baroni, M., and Doussin, J.-F.: The $\text{NO}+\text{O}_3$ reaction: A triple oxygen isotope perspective on the reaction dynamics and atmospheric implications for the transfer of the ozone isotope anomaly, *J. Chem. Phys.*, 128(19), 194303, doi:10.1063/1.2917581, 2008.
- Seinfeld, J.H., Pandis, S.N. *Atmospheric Chemistry and Physics – From Air Pollution to Climate Change* (2nd ed.). John Wiley & Sons. 1203 pp. 2006.

- Sigman, D. M.; Casciotti, K. L.; Andreani, M.; Barford, C.; Galanter, M.; Böhlke, J.K. A Bacterial Method for the Nitrogen Isotopic Analysis of Nitrate in Seawater and Freshwater. *Anal. Chem.* 73 (17), 4145-4153. 2001.
- Silva, S.R., Kendall, C., Wilkison, D.H., Ziegler, A.C., Chang, C.C.Y., and Avanzino, R.J.: A new method for collection of nitrate from fresh water and the analysis of nitrogen and oxygen isotope ratios. *J. Hydro.*, 228, 22-36, 2000.
- Spoelstra, J., Schiff, S.L., Elgood, R.J., Semkin, R.G., and Jeffries, D.S. Tracing the sources of exported nitrate in the Turkey Lakes Watershed using $^{15}\text{N}/^{14}\text{N}$ and $^{18}\text{O}/^{16}\text{O}$ isotopic ratios. *Ecosystems*, v. 4, no. 6, 536-544, 2001.
- Stockwell, W.R., Middleton, P., Chang, J.S., and Tang, X. The second generation regional acid deposition model chemical mechanism for regional air quality modeling. *J. Geophys. Res.*, v. 95, no. D10, 16343-16367.
- Stockwell, W. R., F. Kirchner, M. Kuhn, and S. Seefeld. A new mechanism for regional atmospheric chemistry modeling, *J. Geophys. Res.*, 102(D22), 25,847–25,879, doi:10.1029/97JD00849. 1997.
- Theimens, M., and Heidenreich, J. The mass-independent fractionation of oxygen: a novel isotope effect and its possible cosmochemical implications. *Science* 219, 4588, 1073 – 1075 1983.
- Thiemens, M., and Jackson, T. Pressure dependency for heavy isotope enhancement of ozone. *Geophysical Research Letters*. 17 (6), 717-719. 1990.
- Urey, H.C. Thermodynamic properties of isotopic substances. *J. Chem. Soc.*, 562-581, 1947.
- Xue, D., De Baets, B., Botte, J., Vermeulen, J., Van Cleemput, O. and Boeckx, P. Comparison of the silver nitrate and bacterial denitrification methods for the determination of nitrogen and oxygen isotope ratios of nitrate in surface water. *Rapid Communications in Mass Spectrometry*, 24: 833–840. doi: 10.1002/rcm.4445. 2010.
- Yienger, J.J, and H. Levy, Empirical model of global soil-biogenic NO_x emissions, *J. Geophys. Res.*, 100, D6, 11,447-11464, June 20, 1995
- Zhang, R. Y.; Tie, X. X.; Bond, D. W. Impacts of anthropogenic and natural NO_x sources over the U.S. on tropospheric chemistry. *Proc. Natl. Acad. Sci. U.S.A.*, 100, 1505-1509. 2003

APPENDICES

Appendix A.

Table A.1: EPA Source Sector Descriptions

<u>12 Major Source Sectors</u>	<u>Detailed Category Names</u>
Fertilizer & Livestock	Livestock Waste
	Fertilizer Application
Electricity Generation	Fuel Combustion - Electric Utilities
Fossil Fuel Combustion	Fuel Combustion - Industrial Boilers, Internal Combustion Engines
	Fuel Combustion - Commercial/Institutional
	Fuel Combustion - Residential Fossil
Residential Wood Combustion	Fuel Combustion - Residential Fireplaces
	Fuel Combustion - Residential Woodstoves
Waste Disposal	Waste Disposal
	Waste Disposal - Open Burning
Fires	Wildfires
	Prescribed Fires
	Agricultural Field Burning
	Logging Slash Burning
Industrial Processes	Industrial Process - NEC
	Commercial Cooking
	Industrial Process - Metals
	Industrial Process - Chemical Manufacturing
	Industrial Process - Storage & Transfer
	Industrial Process - Petroleum Refineries
	Industrial Process - Oil & Gas Production
	Industrial Process - Pulp & Paper
Industrial Process - Cement Manufacturing	
On-Road Vehicles	On-Road Vehicles - Gasoline
	On-Road Vehicles - Diesel
Non-Road equipment	Non-Road Equipment - Gasoline
	Non-Road Equipment - Diesel
	Planes, Trains, & Ships
Road Dust	Unpaved Roads
	Paved Roads
Solvent Use	Solvent - Non-industrial
	Surface Coating - Industrial
	Degreasing

Solvent Use	Surface Coating - Architectural
	Graphic Arts
	Solvent - Not Classified Elsewhere
	Dry Cleaning
Miscellaneous	Agriculture - Crop Tilling & Livestock Dust
	Construction
	Gas Stations
	Bulk Gasoline Terminals
	Other Miscellaneous Sources

Appendix B.

Detailed Ion Chromatography Instrumentation Description

B.1. Analytical Ion Chromatography (IC)

Standard analytical operation of the IC in the PSI lab starts with the injection of a sample into a 100 μ L sample loop (Alltech) by an Alltech Model 426 sample pump. This sample is then pushed through a Dionex AS14 anion exchange column (4x250mm; resin affinities Figure B.1) with a carbonate ($\text{Na}_2\text{CO}_3/\text{NaHCO}_3$) mobile phase solution via an Alltech Model 626 eluant pump. Signal is suppressed by an Alltech Model 641 electronic suppressor, and conductivity is detected by an Alltech Model 650 conductivity detector. A 6-port Alltech ProSelect electronic-actuation valve controls the alternation of flow from sample loop to analytical column. As with the preparative separation setup, the entire chromatography system is controlled by the SRI PeakSimple Model 202 relay board and software package.

Counterion	Relative Selectivity for AG 1 and AG MP-1 Resins
OH^-	1.0
Benzene sulfonate	500
Salicylate	450
Citrate	220
I^-	175
Phenate	110
HSO_4^-	85
ClO_3^-	74
NO_3^-	65
Br^-	50
CN^-	28
HSO_3^-	27
BrO_3^-	27
NO_2^-	24
Cl^-	22
HCO_3^-	6.0
IO_3^-	5.5
HPO_4^-	5.0
Formate	4.6
Acetate	3.2
Propionate	2.6
F^-	1.6

Figure B.1: Example anion resin affinities for specific anions (from Bio-Rad AG1 Resin Manual).

B.2. Preparative Separation Instrumentation

The separation device used in the study described by this thesis is a Spectrum Chromatography CF-1 (Figure 2.1), and has several modes of operation. The first attempt at operating this device was through its peak detection capability. Once attached to the conductivity detector, the CF-1 fraction collector can detect when changes in conductivity pass a certain threshold (set by the user), and open a valve to collect the 'peak'. Similar to this method is the 'slope detection' method, which allows the device to detect sudden changes in conductivity (effectively, the slope of the leading and tailing edges of the peaks), and begin collection after detection of a slope of a certain value.

Delay time is a very important aspect of specific anion collection, and is calculated based on the equation, $time_{(delay)} = 5.07 * d^2 * (lf)$ where d is the tubing inner diameter (ID) in inches, l is the tube length in cm, and f is the flow rate in mL/min. The '5.07' parameter is a conversion factor used for consistency between inches and cm. The result of this equation is a time, in minutes, which corresponds to the time it will take for fluid to flow through the tube whose ID and length were used in the calculation. Assuming this delay time is calculated correctly, the previously mentioned methods are effective for peak separation so long as the machine operates consistently with low background conductivity. If these two situations are not the case however, two other methods are potentially more reliable: manual separation and 2) timing-based separation.

B.3. Manual Separation

Manual separation is the manual operation of the instrument by the user. This consists of the operation of a button that switches the valve from waste to collection, and then back again once the anion of interest is finished eluting. While tedious, this method is usually best for the most accurate peak separation. In order to manually separate a sample, a user monitors the output from the computer detection software for when an anion is detected. At the beginning of the anion detection, the output shows a peak beginning to take shape. The user must then wait the calculated delay time (about 2

minutes for our setup) and press the button labeled “manual valve” on the CF-1 fraction collector to open the valve and collect the peak. Once the peak is finished eluting, as indicated by the tail end of an anion peak on the computer software, the user must again wait the delay time and again press the “manual valve” button to divert flow back from collection to waste.

There are multiple downsides to using the manual separation, not the least of which is tedium. Depending on the anions of interest, manual separation will take a significantly large amount of time and attention per anion to be separated. While this is not necessarily a problem, when tasked with an abundance of samples to be separated over a short period of time, a user may have difficulty managing to complete the separation of samples in the time allotted. An alternative, automatic separation based on time, alleviates the time constraints imposed by manual separation without sacrificing sound data collection and management.

B.4. Time-Based Separation

The CF-1 fraction collector can separate based on the elution times of different anions from a column. Barring any significant chemical contamination, a column’s elution times will remain consistent across multiple sample runs. Therefore, the CF-1 fraction collector can be programmed to collect a fraction based on the time an anion elutes through the conductivity detector. This is possible through the use of time windows, programmed through the fraction collector’s user interface (UI). These windows are programmed based on the options to set up the time, as well the choice to either collect or skip sample for that specific time window. By running standards of a desired concentration for the anions of interest and examining the anion elution times through the software interface, the user can determine the necessary peak elution times to program into the fraction collector. Once this programming is completed, the instrument will automatically collect peaks at the programmed times and advance collection vessels when necessary. These timings need to be closely coupled with any automatic sampling

equipment. For our specific uses, the timing of events over a typical 15mL sample run is shown in Table B.1.

Table B.1: Events and times for timed fraction collection

Event	Time (Minutes)	Purpose
Fraction Collector On	0.015	Power on Fraction Collector
Fraction Collector Off	0.08	Turn off fraction collector relay-Collector stays on
Sample Pump On	0.2	Begin Pumping Sample
Sample Pump Off	13.6	Stop Pumping Sample
Autosampler On	13.8	Move needle from sample to wash bottle
Autosampler Off	13.82	Turn off autosampler relay-needle stays in wash bottle
Sample Pump On	14.2	Pump from wash bottle
Sample Pump Off	15.2	Stop pumping from wash bottle
10-Port valve switch	29.75	Switch 10-port valve to begin next sample run
Autosampler On	29.8	Move needle from wash bottle to sample
Autosampler Off	29.82	Turn off autosampler relay - needle stays in next sample

Unfortunately, downsides of this method include the possibility of unforeseen changes in column chemistry as well as the possibility of missed fraction collections due to too closely spaced collection times. For this reason it is appropriate for the user of the instrument to regularly observe the operation of the instrument to ensure their samples are being separated properly. Usually if there is an issue with the device it is easily

noticed and can be corrected before any further problems develop. After the first sample is eluted and its fractions collected properly, issues rarely arise which may cause problems with the sample separation and collection for the remaining samples. A second potential downside to this method is the somewhat limited number of samples that can be set up to be run and separated in one continuous run. Since the timed fraction collection described here causes one fraction vial to remain empty between each sample (Figure B.2), and there are only 174 vials available on the rotating rack of the CF-1 fraction collector, this method is limited to only running 25 samples at a time. Despite these downsides, this method allows for the relatively rapid separation and collection of anion fractions from multiple samples. The usefulness of timed fraction collection is apparent in situations where a user has an abundance of samples to run and does not wish to manually separate each sample as described above. This method provides a relatively easy and time-saving way to separate and collect multiple anions from an abundance of solutions.

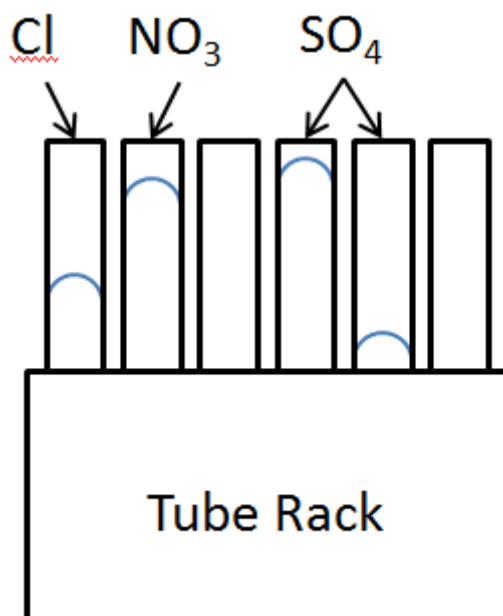


Figure B.2: Schematic of Tube Rack used with CF-1 Collector
Tube volume is 5mL. Approximate collected fraction volume shown.

B.5. Specific Alteration of IC Equipment for this Study

For the purposes of the study described in this thesis, the CF-1 Separation Instrument (Spectrum Chromatography) was chosen to accurately separate precipitation samples into individual fractions for Cl^- , NO_3^- , and SO_4^{2-} . In order to interface the existing IC instrumentation with the CF-1 instrument, several changes needed to be made. The first of these was the attachment of an electronically actuated 3-port controller valve to the waste output from the conductivity detector. This enables the diversion of mobile phase from waste (after the conductivity detector) to the CF-1 Fraction Collector. The valve can be controlled either manually (valve buttons on CF-1 instrument) or scripted to run automatically through our relay board (SRI PeakSimple Model 202).

In 'analytical mode,' as mentioned above, an electronic suppressor (Alltech) is used to suppress the background signal from the mobile phase. The accuracy of this instrument comes at a cost however, as 30-40% of the sample is lost in the suppression process to keep the electrolytic suppression reactions occurring. Therefore, in order to maximize sample retention for samples which have very small concentrations of NO_3^- , a suppressor which does not remove sample during the suppression process is useful. In order to best achieve this, a micromembrane chemical suppressor (Dionex AMMS-300) was selected. This suppressor uses a membrane which is regenerated by H_2SO_4 , supplied from two pressurized 2L tanks. This H^+ charged membrane exchanges H^+ with the carbonates present in the mobile phase to lower the background conductivity. This suppression method unfortunately does not suppress the background conductivity as well as the electronic suppressor ($\sim 22\mu\text{S}$ compared to $\sim 2\mu\text{S}$, respectively) but the additional sample retention for preparative purposes is necessary and therefore well worth the reduced accuracy.

The addition of a second Dionex AS14 column for preparative separation IC purposes is made necessary by the removal of the 100 μL sample loop. Instead of 100 μL of the sample being pumped into the sample loop and then pushed through a column via the mobile phase as with the analytical IC setup, the entire sample (15mL to 50mL depending on volume required for 300nmol NO_3^-) is pumped directly onto a Dionex

AS14 anion exchange column. This change makes the limiting factor on the ability to work with small samples the volume of the sample, rather than the concentration. The reason a second column is added is to increase the efficiency of sample runs. To adequately pump an entire sample volume onto an analytical column and push it through that column to separate the species takes between 30 to 45 minutes depending on the volume. Two columns help to speed this process.

To control the dual-column system, an Alltech SelectPro 10-Port, 2-position valve is used (positions: Figure B.3). Once a sample is pumped onto a column, the valve is switched to its second position causing the mobile phase to push the sample through that column. While this is occurring, the second column is receiving the next sample on the autosampler rack. This methodology allows for each sample run to take much less time, depending on volume. We find that a sample of 15mL takes ~30 minutes to pump and analyze, where a 50mL sample takes ~45 minutes to pump and analyze. The scaling of sample sizes is like this due to the time required to analyze the sample in the case of the 15mL size, and the time required to pump the sample in the case of the 50mL size.

Both the dual-column (for separation) and single-column (analytical) IC setups are required to coexist for different purposes in our lab. To make this possible, the installation of several valves allowing a user to switch fluid flow to either 'mode' of the instrument is necessary. To control mobile phase flow (and the high pressures associated with it) between the analytical and separation sides of the instrument, a 6-port Valco Cheminert manually actuated valve was installed. This valve is connected to the mobile phase output as well as the output of the columns to the two different suppressors. In its initial position, the valve is completely dedicated to controlling the direction of flow for the purposes of the analytical mode of the instrument, and in the second position, the valve is completely dedicated to controlling the direction of flow for the purposes of the preparative mode.

A second valve was installed to control the sample flow between the analytical and preparative setups. Since sample flow is usually at pressures significantly less than that of the mobile phase, a less-rigorous valve is needed. For these purposes the chosen

valve is air actuated (Dionex), and controlled by a solenoid valve connected to a Dionex pressure control panel. This module controls gas pressure to not only the air-actuated sample control valve, but also to the tanks of H_2SO_4 required for the regeneration of the Dionex AMMS-300 micromembrane suppressor.

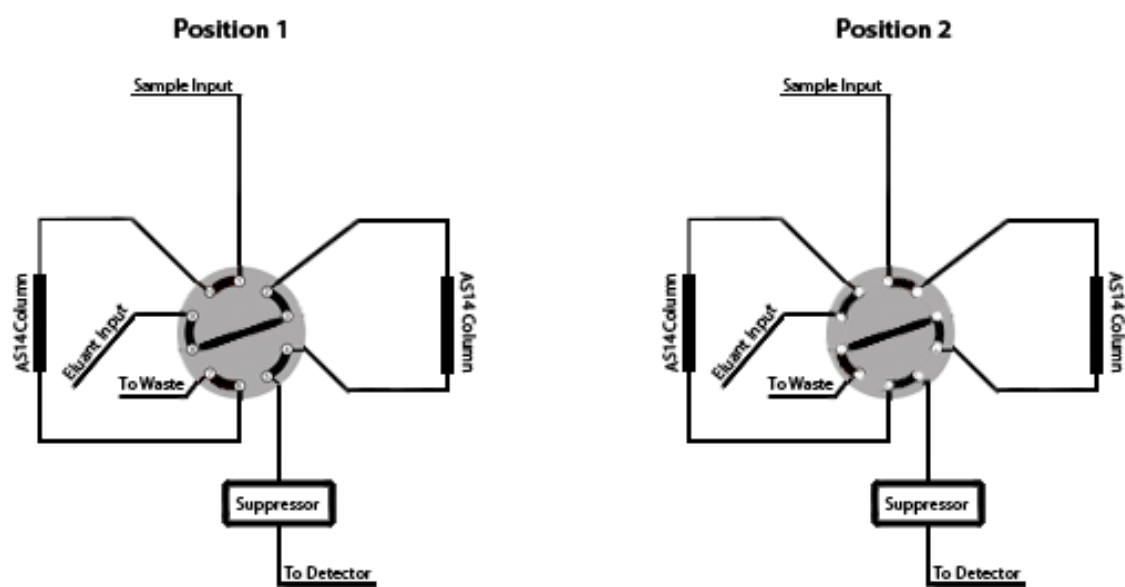


Figure B.3: Schematic of 10-port Alltech SelectPro Valve as set up with our preparative IC system

B.6. Standard Operating Conditions

B.6.1. Analytical Use of IC

When using the analytical capabilities of this instrument, the mobile phase pump is set to run at ~3.0 mL/min. This flow rate produces internal pressures of ~2000 psi, which is within the optimal range for the equipment described here. The sample pump is set to pump at ~1 mL/min. The conductivity detector has a wide range of detection sensitivities (0.01 – 5000 μ S), and these can be changed by the user on the fly. Generally the conductivity detector is set to run at 10 μ S, but this is changed occasionally for samples with lower or higher concentrations than what is usually measured. Beside pump flow rates and detection sensitivity, no other hardware item is adjusted to ensure an optimal run. The mobile phase used is a sodium carbonate/bicarbonate solution ($\text{NaHCO}_3/\text{Na}_2\text{CO}_3$) with concentrations of 0.0017M for NaHCO_3 , and 0.0018M for Na_2CO_3 .

The autosampler (Gilson) is set up with space for four sample racks, and has been programmed to sample from either 15mL or 50mL sample tubes. This allows for a total of 176 15mL samples or 56 50mL samples to be run at the same time. Since each sample in analytical mode takes 15 minutes to run, a full set of 15mL samples (176) would take 44 hours to run. A full set (56) of 50mL samples would take 14 hours to run.

B.6.2. Separation Use of IC

To use the IC in preparative mode, some settings need to be adjusted from what is standard in the analytical setup. The mobile phase flow rate is lowered to ~2.0 mL/min, while the sample flow remains at ~1 mL/min. The lower mobile phase flow rate allows for a more effective suppression of background conductivity (giving the mobile phase more time to react with the membrane), as well as keeping the pressure below the failure threshold of the suppressor membranes. The mobile phase concentration is the same as that used with the analytical methods of the IC. Pressure settings need to be adjusted to ensure appropriate background conductivity suppression. The Dionex Eluant Degas

Module has a pressure regulator which has been fitted to adjust the pressure controlling the regenerant H₂SO₄ flow rate. The pressure on this gauge is usually set to roughly 1psi, allowing for a regenerant flow rate of ~2.4 mL/min). As with the eluant flow rate, it is important to keep the regenerant flow rate below the failure threshold for the membranes unless irreversible damage may occur.

B.6.3. IC Separation Instructions

Step 1: Preparation of the Acid Delivery System for chemical suppression

- A. Set the pressure regulator on the argon tank (to the right of the IC setup) to ~90psi for sufficient valve control and acid tank pressurization, and open tank valve (Figure B.4). Flow of argon will stop at a small black solenoid valve controlled by the PeakSimple software.



Figure B.4. Pressure regulator for argon tank

- B. Flip switch on left side of IC labeled “On/Off” to off (if not already in the off position). Ideally acid bottles should both be full (4L each) of H₂SO₄. If one is

empty (or both tanks can be combined to empty one), the empty tank can be refilled by adding 4L of 25 mN H₂SO₄ to the empty bottles (wear gloves!).

- C. In the PeakSimple program, click on the 'F' relay (Figure B.5), which controls the solenoid valve mentioned in step 'A'.

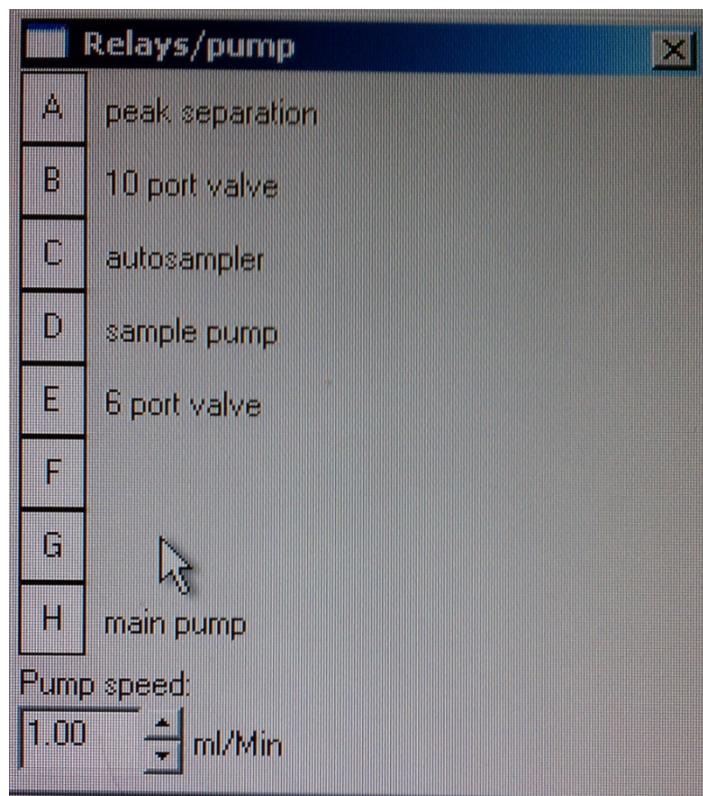


Figure B.5: Relay selection in the PeakSimple (SRI) software

- D. Flip the switch in step 'B' to on to pressurize the acid bottles and begin acid flow to the Dionex AMMS-300 chemical suppressor.

Step 2: Equilibration of system with Mobile Phase

- A. Fill each 2L mobile phase bottle with a solution of 0.0018M/0.0017 Na₂CO₃/NaHCO₃.

- B. Siphon two eluant bottles together utilizing a syringe with one of the tubes threaded through the luer ports on the bottle caps. The filtered tube is the direct line to the IC and a siphon should not be attempted with it.
- C. Set eluant pump to pump at 2mL/min if it is not already set to pump at that rate.
- D. Turn manual Valco 6-port valve to 'separation' to direct mobile phase flow to the appropriate analytical columns (Figure B.6).



Figure B.6: Valco 6-port valve (manual)

- E. If all connections are tight, turn on the mobile phase pump (model 626). It will take approximately 30 minutes to equilibrate the system on one analytical column, although this time could vary depending on the time since the last use of the IC and environmental factors.
- F. After one column is equilibrated (conductivity detector reading has stabilized), click the “B” relay labeled “10-port valve” to change flow to the second column. Equilibration for this column will take another 30 minutes (approximately),

although this time could vary depending on the time since the last use of the IC and random environmental factors.

Step 3: Purging injection line of air, setup of autosampler, and setup of sampling interface.

- A. The Gilson autosampler used with this IC instrumentation is already programmed to operate with two different kinds of sample racks: 15mL (44 samples/rack) and 50mL (14 samples/rack). Select the appropriate program using the autosampler interface (on right side of IC computer desk; Figure B.7) by pressing “Edit/File/Save” until the appropriate file comes up, and then “Enter” to confirm rack type followed by another “Enter” to lock in the appropriate file. If the appropriate program is not present in the autosampler, it is possible to program one by following the instructions in step 5 of this appendix.



Figure B.7: Gilson Autosampler controller

- B. To purge the injection line of air and possible contaminants, the injection needle can be lowered (by pressing start on the autosampler controller) into either a centrifuge tube with deionized water, or into the needle wash cup (filled with

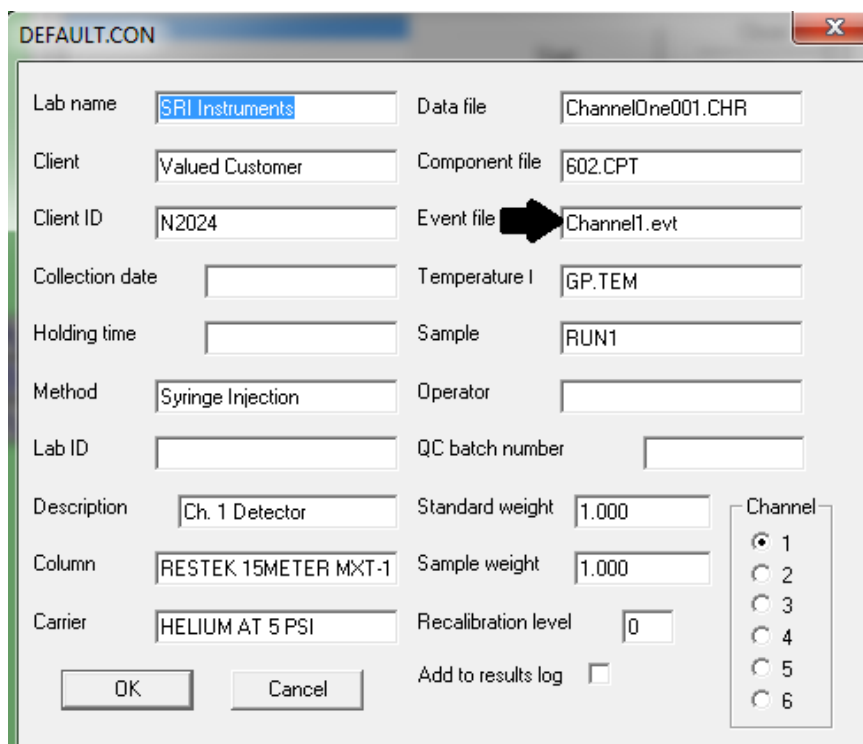
fresh deionized water). Once the needle is submerged, a syringe is used in the sample pump (model 426) pump to pull water through the needle and into the injection.

- C. Find the appropriate control file set on the IC computer (found on the Desktop in the 'Control Files' folder) and copy the content of the appropriate control file set to a folder made specifically for this sample run.
- D. Access the PeakSimple software interface to begin setting up the sample run by clicking on View>Autosampler. In the autosampler popup window, click 'Add...' and navigate to the folder that was created for this sample run. Add the 'DEFAULT.CON' file to the autosampler window.
- E. Click 'Edit All' and add copies of DEFAULT.CON so that the number of files exceeds the number of samples by one (Figure B.8), ensuring that the "increment file name" box is checked.

Num	Control file	Component file	Collection date	Method	Data file
1	DEFAULT.CON	602.CPT		Syringe Injection	5A.CHR
2	DEFAULT1.CON	602.CPT		Syringe Injection	10A.CHR
3	DEFAULT2.CON	602.CPT		Syringe Injection	25A.CHR
4	DEFAULT3.CON	602.CPT		Syringe Injection	50A.CHR
5	DEFAULT4.CON	602.CPT		Syringe Injection	741524.CHR
6	DEFAULT5.CON	602.CPT		Syringe Injection	741525.CHR
7	DEFAULT6.CON	602.CPT		Syringe Injection	750932.CHR
8	DEFAULT7.CON	602.CPT		Syringe Injection	750933.CHR
9	DEFAULT8.CON	602.CPT		Syringe Injection	701115.CHR
10	DEFAULT9.CON	602.CPT		Syringe Injection	701116.CHR
11	DEFAULT10.CON	602.CPT		Syringe Injection	701117.CHR
12	DEFAULT11.CON	602.CPT		Syringe Injection	701118.CHR
13	DEFAULT12.CON	602.CPT		Syringe Injection	701119.CHR
14	DEFAULT13.CON	602.CPT		Syringe Injection	701120.CHR
15	DEFAULT14.CON	602.CPT		Syringe Injection	5B.CHR
16	DEFAULT15.CON	602.CPT		Syringe Injection	10B.CHR
17	DEFAULT16.CON	602.CPT		Syringe Injection	25B.CHR

Figure B.8: Autosampler Queue with multiple samples in PeakSimple

- F. Rename the first file to VOID by highlighting the contents of the “Data file” field for the first entry and typing over it. After VOID, proceed to rename each file to whatever seems fit for the samples being run (numbers, sample names, descriptors, etc.).
- G. Click “Update Control Files” when finished renaming files, close the autosampler queue window, and then click ‘Edit All’ again to make the software locate the newly created control files. After closing this new Autosampler queue window, all new control files will be listed in the main autosampler window.
- H. The event files referenced for each control file need to be changed so that the instrument switches between the two analytical columns used for separation. Starting with the first control file (DEFAULT.CON), alternate between auto1.evt and auto2.evt in the ‘Event File’ space (Figure B.9).



The screenshot shows the 'DEFAULT.CON' dialog box in PeakSimple software. It contains the following fields and values:

Lab name	SFI Instruments	Data file	ChannelOne001.CHR
Client	Valued Customer	Component file	602.CPT
Client ID	N2024	Event file	Channel1.evt
Collection date		Temperature I	GP.TEM
Holding time		Sample	RUN1
Method	Syringe Injection	Operator	
Lab ID		QC batch number	
Description	Ch. 1 Detector	Standard weight	1.000
Column	RESTEK 15METER MXT-1	Sample weight	1.000
Carrier	HELIUM AT 5 PSI	Recalibration level	0

At the bottom, there are 'OK' and 'Cancel' buttons, and an 'Add to results log' checkbox which is unchecked. On the right side, there is a 'Channel' selection list with radio buttons for channels 1 through 6. Channel 1 is selected.

Figure B.9: Edit file window in PeakSimple software. Event file space is marked.

- I. Add the endrun.con control file to the autosampler window by clicking 'Add...' in the autosampler window. Navigate to the 'endrun.con' file and click OK to add it to the autosampler. This end control file turns off the eluant pump and depressurizes the acid bottles at the end of a run. Save the autosampler file by clicking 'Save' on the autosampler window.

Step 4: Sample Preparation and Beginning the Run

- A. Make sure samples are prepared and in their appropriate positions on the sample rack bracket.
- B. Ensure that the CF-1 fraction collector is on, but do not start it (it will start automatically when the sample run begins).
- C. If not already done, make sure the injection needle is in the first sample.
- D. Click the large 'Start' button on the Autosampler window in the PeakSimple software.

Step 5 (OPTIONAL): Programming the Gilson Autosampler

FILE IDENTIFICATION

File 1: 15-mL vials

File 2: 50-mL vials

File 3: Culture Tube

INSTRUCTIONS and TEMPLATE FOR FILE PROGRAMMING

To begin, press "Edit/File/Save" and enter the number of an unoccupied file.

Enter the following commands, being careful to change the variables as indicated below:

- 1) 1 For A=1/3 (Sets the A variable to the number of racks. 1/3 is default.)

- 2) 2 Rack Code ?/A (Replace ? with the number printed on the side of the sample rack. This tells the autosampler which rack it's sampling from.)
- 3) 3 For B=1/? (Replace ? with the number of columns present in the rack. This sets the variable B to the number of columns.)
- 4) 4 For C=1/? (Replace ? with the number of rows present in the rack. This sets the variable C to the number of rows.)
- 5) 5 Tube B/C/A (Tells the autosampler that tubes are present in rack A, column B, row C)
- 6) 6 Height -32 (Sets the height of the needle to go into the vial, measured from the bottom, in mm. Negatives indicate mm below the bottom (machine does not actually measure from the bottom of the vials, so negatives may be necessary for adequate sample injection.)
- 7) 7 Wait /3/0 (Wait command)
- 8) 8 Rack Code 24/5 (Inputs the location of the DI wash bottle.)
- 9) 9 Tube 1/6/5 (Further pinpoints DI wash location.)
- 10) 10 Height -32 (Height from bottom to dip into DI wash.)
- 11) 11 Wait /3/0 (Wait Command)
- 12) 12 Next C
- 13) 13 Next B
- 14) 14 Next A
- 15) 15 Home

HOW TO LOAD FILES ONCE PROGRAMMED

- 1) Push "Edit/File/Save" until the file number is shown.
- 2) Press "Enter" until "File Stored" is shown.
- 3) Press "Start."

HOW TO RETURN THE NEEDLE TO THE “HOME” POSITION

- 1) Press “Pause.”
- 2) Press “Home.”

Appendix C.

Operation of ArcGIS (ESRI) for Purposes of Producing Maps Shown in this Thesis

Step 1: Obtain necessary data

For the purposes of the work described in this thesis, the data required was temperature, pressure, and the $\delta^{18}\text{O}$ of liquid water for N. America. Temperature and Pressure data is freely available from the North American Regional Reanalysis (NARR) dataset, and the $\delta^{18}\text{O}$ of liquid water is available from <http://www.waterisotopes.org> (maintained by Gabe Bowen at Purdue University).

Issues associated with using this data as is are that the NARR data is a Lambert Conformal Conic projection, and the $\delta^{18}\text{O}$ of liquid water is a WGS 1984 projection. Luckily, ArcGIS makes it easy to convert from one projection to another on the fly, though if multiple datasets are loaded into the same Arc document, the first dataset becomes the default projection, and the subsequent datasets are usually morphed to fit that same projection.

If a dataset is in an incorrect projection for the purposes of a project, by right clicking on the data layer and going to properties (the coordinate system tab) the projection can easily be changed to fit either the projection of another dataset, or one of several projections built into the Arc software suite (Figure C.1).

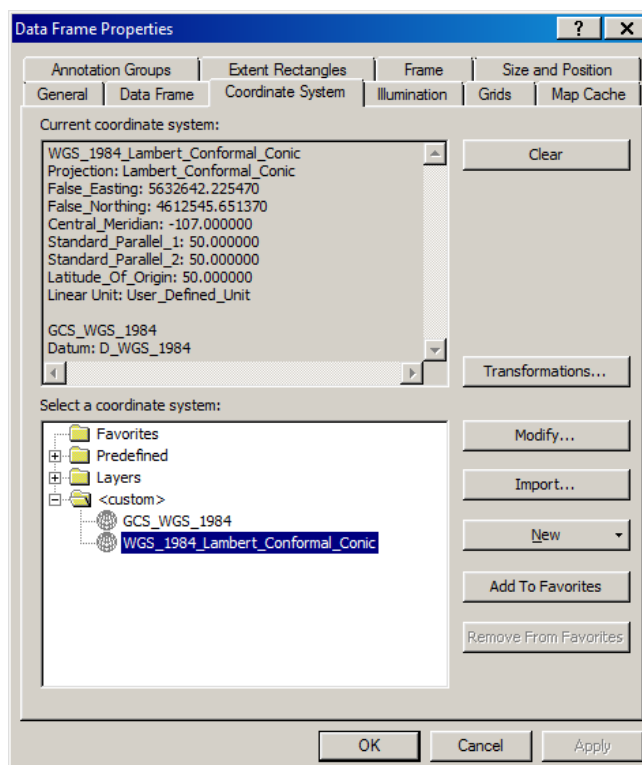


Figure C.1: Coordinate System Tab in ArcMap

Step 2: Creating a shapefile meant to be used as a data crop outline

Once all data is in the same coordinate system, it may become necessary to crop some data out for the purposes of a study. For the purposes of the work described in this thesis, data was cropped to fit the continuous United States. In order to accomplish this, an Arc shapefile needed to be produced in the shape of the continuous United States. To create a shapefile, ArcCatalog is used. Select File> New> Shapefile... in ArcCatalog to produce a new generic shape file. When selected, a 'Create New Shapefile' box pops up requesting that the shapefile be defined and given a Coordinate system (Figure C2). In the 'Name:' field the name of the shapefile is entered, and in the 'Feature Type:' field the type of shapefile is entered. For our purposes the 'Feature Type' was selected as 'Polygon.'

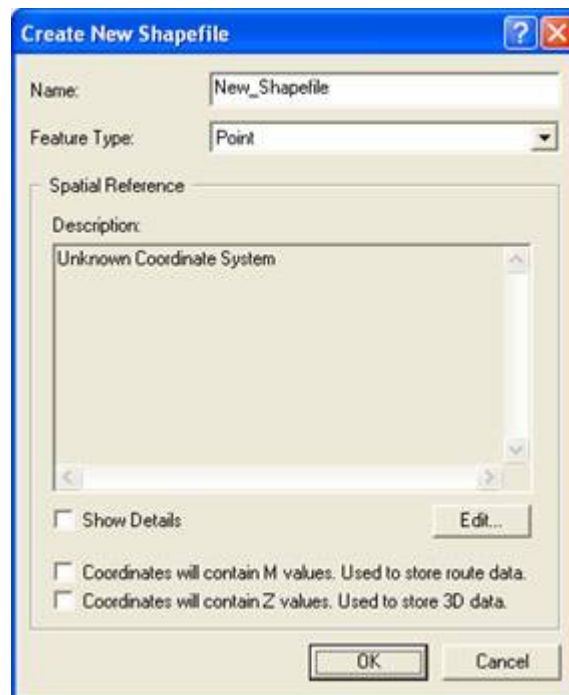


Figure C.2: Create New Shapefile popup window (image from <http://www.u-s-c.org>)

Specify the coordinate system by clicking ‘Edit...’ and selecting a new coordinate system (from either the built-in coordinate systems, or by clicking on a dataset that’s already in the coordinate system needed).

After the creation of the shapefile, load the shapefile into ArcMap. Here is where the generic shapefile will be cut into a specific shape which will be used for cropping datasets. Activate the editor toolbar by clicking View>Toolbars>Editor. From the Editor drop down menu, select ‘Start Editing.’ Then select the ‘Sketch Tool’ and begin connecting vertices into a shape that matches the data to remain after the dataset is cropped. For the purposes of the work described here, the continuous United States was traced from a built-in ArcMap template superimposed on to the shapefile. Once the desired shape is traced, select ‘Save Edits’ from the editor dropdown menu to save the edits to the shapefile.

Step 3: Extracting data within a shapefile

Once a shapefile of the appropriate shape and size is created, it is easy to extract the data in a dataset that fits within that shape (Figure C.3).



Figure C.3: Shapefile laid over a dataset for all of N. America. When extracted, the data beneath the shapefile will be preserved as a new dataset.

Select Tools>Extensions and check 'Spatial Analyst,' which enables the use of the Spatial Analyst tools. Next, open the Arc Toolbox and select Spatial Analyst Tools>Extraction>Extract by Mask. Click the folder on the right side of the blank entry boxes (Figure C4) to navigate to and select the 'Input raster' (the raster that you are editing), and the 'Input raster or feature mask data' (the shapefile that was just created). The output raster will be filled in automatically, but this box can be used to change the name of the data when the new raster is saved. Click 'OK' and the new raster will be created in the location specified in the 'Output raster' box.

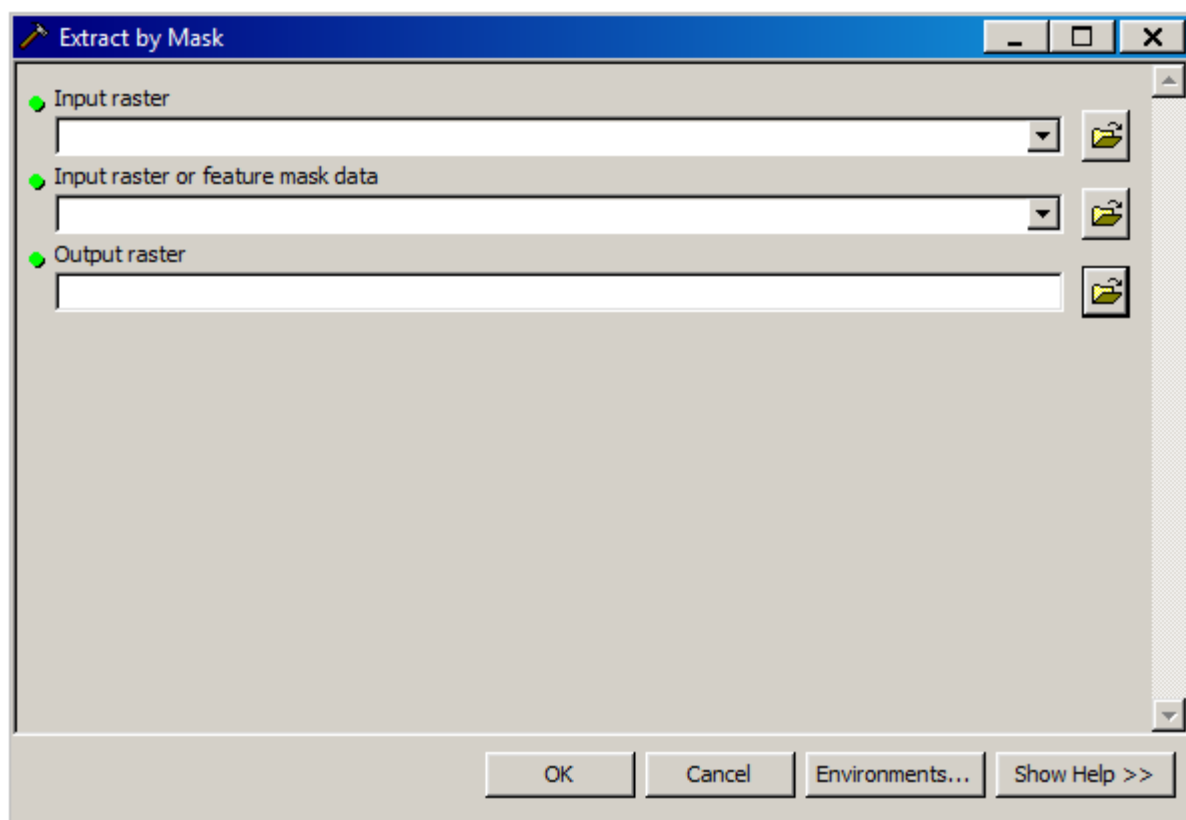


Figure C.4: 'Extract by Mask' input box